

Aus dem Bereich Theoretische Medizin und Biowissenschaften
der Medizinischen Fakultät der Universität des Saarlandes,
Homburg/Saar

**Electroencephalographic Responses to Frictional Stimuli:
Measurement Setup and Processing Pipeline**

*Dissertation zur Erlangung des Grades eines
Doktors der Theoretischen Medizin*
**der Medizinischen Fakultät
der UNIVERSITÄT DES SAARLANDES**
2018

vorgelegt von:
Novaf Özgün, M.Sc.
geb. am: 01 Januar 1982 in Midyat-Türkei

Dekan: Prof. Dr. med. Michael D. Menger

Referent: Prof. Dr. rer. nat. Dr. rer. med. Daniel J. Strauss

Korreferent:

Tag der mündlichen Prüfung:

Meiner Familie
Ji bo malbata min (kurdisch)

Eidesstattliche Erklärung

Hiermit erkläre ich an Eides statt, dass ich die vorliegende Arbeit ohne unzulässige Hilfe Dritter und ohne Benutzung anderer als der angegebenen Hilfsmittel angefertigt habe. Die aus anderen Quellen direkt oder indirekt übernommenen Daten und Konzepte sind unter Angabe der Quelle gekennzeichnet.

Bei der Auswahl und Auswertung folgenden Materials haben mir die nachstehend aufgeführten Personen in der jeweils beschriebenen Weise unentgeltlich/entgeltlich geholfen:

- Alle die in der Danksagung erwähnten Personen haben mir in der dort beschriebenen Weise unentgeltlich geholfen.

Weitere Personen waren an der inhaltlich-materiellen Erstellung der vorliegenden Arbeit nicht beteiligt. Insbesondere habe ich nicht die entgeltliche Hilfe von Vermittlungs- bzw. Beratungsdiensten (Promotionsberater/innen oder anderer Personen) in Anspruch genommen. Au ßer den Angegebenen hat niemand von mir unmittelbar oder mittelbar geldwerte Leistungen für Arbeiten erhalten, die im Zusammenhang mit dem Inhalt der vorgelegten Dissertation stehen.

Die Arbeit wurde bisher weder im Inland noch im Ausland in gleicher oder ähnlicher Form in einem anderen Verfahren zur Erlangung des Doktorgrades einer anderen Prüfungsbehörde vorgelegt.

Ich versichere an Eides statt, dass ich nach bestem Wissen die Wahrheit gesagt und nichts verschwiegen habe.

Vor Aufnahme der vorstehenden Versicherung an Eides Statt wurde ich über die Bedeutung einer eidesstattlichen Versicherung und die strafrechtlichen Folgen einer unrichtigen oder unvollständigen eidesstattlichen Versicherung belehrt.

Beckingen, den 02.07.2018

Novaf Özgün, M.Sc.

Abstract

Tactility is a key sense in the human interaction with the environment. The understanding of tactile perception has become an exciting area in industrial, medical and scientific research with an emphasis on the development of new haptic technologies. Surprisingly, the quantification of tactile perception has, compared to other senses, only recently become a field of scientific investigation. The overall goal of this emerging scientific discipline is an understanding of the causal chain from the contact of the skin with materials to the brain dynamics representing recognition of and emotional reaction to the materials. Each link in this chain depends on individual and environmental factors ranging from the influence of humidity on contact formation to the role of attention for the perception of touch.

This thesis reports on the research of neural correlates to the frictional stimulation of the human fingertip. Event-related electroencephalographic potentials (ERPs) upon the change in fingertip friction are measured and studied, when pins of a programmable Braille-display were brought into skin contact. In order to contribute to the understanding of the causal chain mentioned above, this work combines two research areas which are usually not connected to each other, namely tribology and neuroscience. The goal of the study is to evaluate contributions of friction to the process of haptic perception. Key contributions of this thesis are:

- 1) Development of a setup to simultaneously record physical forces and ERPs upon tactile stimulation.
- 2) Implementation of a dedicated signal processing pipeline for the statistical analysis of ERP -amplitudes, -latencies and -instantaneous phases.
- 3) Interpretation of skin friction data and extraction of neural correlates with respect to varying friction intensities.

The tactile stimulation of the fingertip upon raising and lowering of different lines of Braille-pins (one, three and five) caused pronounced N50 and P100 components in the event-related ERP-sequences, which is in line with the current literature. Friction between the fingertip and the Braille-system exhibited a characteristic temporal development which is attributed to viscoelastic skin relaxation. Although the force stimuli varied by a factor of two between the different Braille-patterns, no significant differences were observed between the amplitudes and latencies of ERPs after standard across-trial averaging. Thus, for the first time a phase measure for estimating single-trial interactions of somatosensory potentials is proposed. Results show that instantaneous phase coherency is evoked by friction, and that higher friction induces stronger and more time-localized phase coherency.

Zusammenfassung

Die Taktilität ist ein zentraler Sinn in der Interaktion mit unserer Umwelt. Das Bestreben, fundierte Erkenntnisse hinsichtlich der taktilen Wahrnehmung zu gewinnen erhält großen Zuspruch in der industriellen, medizinischen und wissenschaftlichen Forschung, meist mit einem Fokus auf der Entwicklung von haptischen Technologien. Erstaunlicherweise ist jedoch die wissenschaftliche Quantifizierung der taktilen Wahrnehmung, verglichen mit anderen Sinnesmodalitäten, erst seit kurzem ein sich entwickelnder Forschungsbereich. Fokus dieser Disziplin ist es, die kognitive und emotionale Reaktion nach physischem Kontakt mit Materialien zu beschreiben, und die kausale Wirkungskette von der Berührung bis zur Reaktion zu verstehen. Dabei unterliegen die einzelnen Faktoren dieser Kette sowohl individuellen als auch externen Einflüssen, welche von der Luftfeuchtigkeit während des Kontaktes bis hin zur Rolle der Aufmerksamkeit für die Wahrnehmung reichen.

Die vorliegende Arbeit beschäftigt sich mit der Untersuchung von neuronalen Korrelaten nach Reibungsstimulation des menschlichen Fingers. Dazu wurden Reibungsänderungen, welche durch den Kontakt der menschlichen Fingerspitze mit schaltbaren Stiften eines Braille-Display erzeugt wurden, untersucht und die entsprechenden neuronalen Korrelate aufgezeichnet. Um zu dem Verständnis der oben erwähnten Wirkungskette beizutragen, werden Ansätze aus zwei für gewöhnlich nicht zusammenhängenden Forschungsbereichen, nämlich der Tribologie und der Neurowissenschaft, kombiniert. Folgende Beiträge sind Hauptbestandteile dieser Arbeit:

- 1) Realisierung einer Messumgebung zur simultanen Ableitung von Kräften und ereigniskorrelierten Potentialen nach taktiler Stimulation der Fingerspitze.
- 2) Aufbau einer speziellen Signalverarbeitungskette zur statistischen Analyse von stimulationsabhängigen EEG -Amplituden, -Latenzen und -instantanen Phasen.
- 3) Interpretation der erhobenen Reibungsdaten und Extraktion neuronaler Korrelate hinsichtlich variierender Stimulationsintensitäten.

Unsere Resultate zeigen, dass die taktile Stimulation der Fingerspitze nach Anheben und Senken von Braille-Stiften zu signifikanten N50 und P100 Komponenten in den ereigniskorrelierten Potentialen führt, im Einklang mit der aktuellen Literatur. Die Reibung zwischen der Fingerspitze und dem Braille-System zeigte einen charakteristischen Signalverlauf, welcher auf viskoelastische Hautrelaxation zurückzuführen ist. Trotz der um einen Faktor zwei verschiedenen Intensitätsunterschiede zwischen den Stimulationsmustern zeigten sich keine signifikanten Unterschiede zwischen den einfach gemittelten Amplituden der evozierten Potentialen. Erstmals wurde ein Phasen-Maß zur Identifizierung von Unterschieden zwischen somatosensorischen *"single-trial"* Interaktionen angewandt. Diese Phasenanalyse zeigte, im Gegensatz zur Amplituden- und Latenzanalyse, deutlichere und signifikantere Unterschiede zwischen den Stimulationsparadigmen. Es wird gefolgert, dass Kohärenz zwischen den Momentanphasen durch Reibungsereignisse herbeigeführt wird und dass durch stärkere Reibung diese Kohärenz, im zeitlichen Verlauf, stärker und lokalisierter wird.

Abbreviations

ANOVA	analysis of variance
ASs	assistive systems
APs	action potentials
BA	brodmann area
CNS	central nervous system
CoF	coefficient of friction
CTRA	consecutive trial resolving analysis
E	Young's modulus
EEG	electroencephalography
ERP	event-related potential
f	frequency
Hz	hertz
ISI	interstimulus interval
LPDa	first part of the late positive deflection
LPDb	second part of the late positive deflection
LSP	late somatosensory potential
MMI	man machine interface
mN	milli newton
μ	micro
ms	milli seconds
n	number of subjects
NLM	nonlocal means
Ω	ohm
PC	personal computer
RA	rapid adapting
s	seconds
S	signal
SA	slow adapting
SNR	signal-to-noise-ratio
SoT	sense of touch
SS	somatosensory system
WPSS	wavelet phase synchronisation stability

Contents

1	Introduction	1
1.1	Application Areas for Haptics	5
1.1.1	Communication and Gaming	5
1.1.2	Virtual, Assistive and Educational Systems in Medicine . . .	8
1.1.3	Virtual Reality	10
1.2	Tactual System - Somatosensory System	11
1.2.1	The Skin - The Outer Shell of the Body	11
1.2.2	Somatosensory System	14
1.3	Mechanical Properties of the Skin	16
1.4	Contact Mechanics and Friction	20
1.5	State of the Art	24
1.6	Contribution of this Work - Motivation	34
2	Materials and Methods	37
2.1	Participants and Inclusion Criteria	37
2.2	Experimental Design and Stimulus Material	39
2.3	Measurement Setup	42
2.4	Data Processing Pipeline	44
2.4.1	Preparation and Segmentation of the Data	44
2.4.2	Step Intensity Calculation	48
2.4.3	Wavelet Phase Synchronisation Stability (WPSS)	49
2.4.4	Denoising of ERP-images	52
3	Results	59
3.1	Part A: Experiments - Structured Surface	59
3.1.1	Tribology of the Structured Surface	59
3.1.2	Electrophysiological (EEG) Activity	61
3.2	Part B: Experiments - Braille-display	63
3.2.1	Tribology of the Braille-display	63
3.2.2	Electrophysiological (EEG) Activity	70
3.2.3	Wavelet Phase Synchronization Stability (WPSS)	76

4	Discussion	83
4.1	Tribology of Fingertip	83
4.2	Neurological Responses	89
4.3	Physical Stimuli and Neural Correlates	92
4.4	Limitations and Future Work	97
5	Conclusions	101
	Bibliography	103
	Own Publications	115
	Acknowledgements	

1 Introduction

Haptic perception is of great importance in our daily life. It is a modality with a high impact on almost every interaction and therefore inevitable for understanding the world surrounding us. According to the English Oxford Dictionaries, *haptic* (from the Greek word *haptesthai*, meaning "to touch") entered English in the late 19th century as a medical synonym for *tactile* (Dictionary, 2008). From the developmental point of view, it is the first sense developed in the human fetus and thus also referred to as to be the origin where awareness begins to form (see Gallace and Spence (2010) and references therein). Since recent years haptic is an emerging field in science bridging the gap between materials properties on the one hand and grip and feel upon touch on the other hand.

Hearing, seeing, smelling, tasting and feeling are the five traditional senses. Each has its fundamental role in providing the human being with crucial information where the relevant receptors transduce information into neural impulses and transmit via their associated nerve fibers to the brain. Depending on the innervated sense modality a mapping to the respective brain area after centrally processed results in a conscious perception (Pleger and Villringer, 2013). This signal transduction or bottom up process happens in a causal way substantiating the importance of our senses. The input information can either arise from an external (exteroceptive), an internal (interoceptive, i.e. feedback on the internal status of the body) or a proprioceptive (movements and posture of the body) source. In addition, there exist few more subsenses outside the above mentioned, namely the senses of pressure, temperature, pain and kinesthetic (i.e. motion). Those submodalities are also important as they are working along with the senses in a mutual and coordinate manner to give accurate knowledge about the physical condition of the body and the world surrounding us (LeConte, 1885; Ayres and Robbins, 2005).

But, is there a sense which can be regarded as the ultimate one? Is there a kind of hierarchical ordering senses are ranked to? Aristoteles, one of the greatest philosopher and scientist of ancient Greece (384 BC - 322 BC) stated out that the sense of vision is the noblest of senses because of being eidetic, i.e, sight allows for an adhoc distinction between the changing and the unchanging (Wolfe, 2009). More than two thousand years later most attention is focusing on sight and hearing (Loomis and Lederman, 1986). Just few years ago research has started on the olfactory and

smell sense with a strong growth in knowledge about how the system functions as a whole (see Shepherd (2009) and references therein). It soon became evident by the food industry that taste and smell are very important while at the same time are easily accessible. For example just by releasing of ambient scents, such as the smell of fresh coffee in a coffee house, using electric fragrance diffuser is enough to mask the olfactory sense, changing both the buying habits as well as the duration spent in those locations (Spence, 2015).

The last missing sense and object of this work, which in many instances appears to have fallen into oblivion is the *sense of touch* (SoT). Among all senses the SoT has the highest amount of sensory organs. The cone of sensory innervation, i.e the spatial location of the respective receptor fields is omnipresent through the whole body. Information enters the nervous system from every single part of the body. In contrast, for the other senses the fields are more restricted, namely eyes are used for vision, ears for hearing, nose for smelling and the tongue for tasting. We can survive or live relatively normal without our senses, meaning that a loss of sight, hearing, taste or smell can be compensated either by restoration (e.g., visual or auditory implants) or by a sensory substitution or reorganization of the loss (Striem-Amit et al., 2012). It is known that the remaining senses enhance their capacities as a function increasing cross-modal plasticity to replace the lost inputs to some extent (Lessard et al., 1998; Mao and Pallas, 2013). Blind people are more sensitive in audition or the SoT than people not affected from a loss (Kolarik et al., 2013; Goldreich and Kanics, 2003), even when they are not blind from birth (Norman and Bartholomew, 2011). Without touch the probability of a mental breakdown is high, since there is a need for touch whether by means of social-emotionally or physical-environmentally interactions (Siewe, 2004).

However, reports on a missing of the SoT from birth with a corresponding preservation by other modalities can be hardly found. Just Robles-De-La-Torre (2006) report two cases, but with the occurrence of the loss arising from health issues. One is the case of *Mr. I. Waterman*, who had the loss due to destroyed nerve fibers resulting from a viral infection. Documented in Robles-De-La-Torre (2006), Mr. Waterman was not able to feel his body and to sense body position, as needed for example in grasping an object, which changed his life in major ways. It therefore appears that the SoT may be the most interesting, important and necessary sense of the human (Siewe, 2004).

There are two subchannels underlying touch, namely affective and discriminative

touch. Affective touch, also called emotional touch, can be defined as the interpersonal touch related communication (e.g. handshake). Discriminative touch gives the ability to feel differences between things while sensing pressure, shape, texture, vibration, and slip and thus gives information on handled objects (McGlone et al., 2014). Those differences can be perceived at nanoscale in an exploratory process, i.e. in a dynamic or active scanning of a surface, whereby for a static condition with no movement of the fingertip the minimum feature size for a discrimination lies in the micrometer-range (Skedung et al., 2013). Thus, discriminative touch, also referred to as cutaneous, tactile or as a collective term haptic perception can be seen as the physical contact of the somatosensory system with the outer world.

In tactile sensing, this physical contact is formed by physical quantities (see section 1.4) acting between the skin and objects or surfaces, which collectively contribute to the percept. The SoT and its physical finger - surface interaction includes a complex chain of processes. Attributes of the contacted matter strongly vary depending on deformations and viscoelastic changes of the skin, changes in shape-, material- and topography of the counterpart, mechanical vibrations due to sliding of the fingertip and frictional forces acting at the interface (Skedung et al., 2013). *Tribology* (from the Greek word *tribos* and the suffix *ology*, meaning the "study" of "rubbing"), is the science of friction, wear and lubrication with respect to surfaces moving relative to one another (Bhushan, 2013). Aside its historical background concerning scientists since the time of Aristotle, tribology was first coined in 1966 in Great Britain by H.P. Jost. (Tzanakis et al., 2012). Tribology is of great importance and relevance in our daily life, involving an extensive range of natural tissues, such as cartilage, blood vessels, tendons, and skin. In the framework of haptic perception the frictional contribution due to a sliding contact between the fingertip and a surface is believed to be a key feature. The perceptual interpretation depends on the activation of distinct mechanoreceptors (see section 1.2) and the amount of the physical transmission of strains and stresses to those receptors.

An important technique for the evaluation of sensory and cognitive processes is the use of the electroencephalogram (EEG) which was discovered by Hans Berger, a German psychiatrist, in 1929. This breakthrough technique made it possible to measure brain activity non-invasively with a quite impressive time resolution and thus was and still is a highly attractive technique (Strauss et al., 2013; Blackwood and Muir, 1990), especially for the recording of so called event related potentials

(ERPs). ERPs are neural correlates, i.e., brain responses (small voltages) with waveforms representing both, endogenous and exogenous factors which are evoked by specific external stimuli such as visual, auditory or somatosensory (Strauss et al., 2013; Sur and Sinha, 2009). From a scientific point of view and with respect to the ERP-method, the auditory and visual modalities are best investigated. For the tactile sense, however, the scientific quantification and the understanding of the mentioned processing chain are not well investigated.

1.1 Application Areas for Haptics

Haptic or tactile perception is playing a crucial role in our daily life. It is a modality with a high impact on almost every interaction and therefore inevitable for understanding the world surrounding us. Given that haptic is a relatively new research field, it is expected to turn into a very central area of future-oriented research. This chapter serves as a literature survey including on the one hand a review on application areas, and on the other hand a summary of the physical as well as psychophysical-neurophysiological studies.

Haptic perception is derived from mechanoreceptors providing information to the central nervous system. Those mechanoreceptors are spread all over the human body (most located in the skin) and can sense pressure, vibration, and skin stretch (see section 1.2). On this basis the sense of touch is quite attractive for a selective stimulation purpose. As a starting point haptic devices or haptic man-machine interfaces can be described as a technology which incorporates touch and force. There are a bundle of systems based on skin perception and sensation, where the source is a vibrating feedback to the user. The most noticeable fields are the communication and the gaming section. Other recent application fields where haptic is more and more present and important are the virtual and telepresence/teleoperation environment, especially for medical purposes.

1.1.1 Communication and Gaming

At a very early stage it was realized that tactile channels are attractive to retain the gamer's attention. In 1976, the company *Sega* developed an arcade racing video game called *Fonz*, where the general task was to steer a motor-bike as fast as possible across a curvy road. What made this game so famous and successful was the integration of a feature mimicking a realistic gaming-environment. Whenever the bike was veering off the road, or a crash occurred the handlebar vibrated and thereby offered the gamer a feeling of driving the bike in real. Meanwhile this tactile feedback is an integral part of almost every modern gaming console and has become indispensable to this field.

To enable visually impaired individuals to take part in games, interactions with a special focus on audio or haptic cues are implemented, which is nothing less

than a technical way of a sensory substitution of the missing sense. For example, the group of Yuan and Folmer (2008) modified the game *Guitar Hero* (from Red Octane), which provides a guitar shaped device including colored buttons being pressed following visual cues appearing on a screen. To include haptic cues they exchanged the visual ones by providing the information to the fingertips of the user using small pager motors integrated in a glove (see Figure 1.1, a). The study showed that the accuracy of the performance in following the music scenario was higher for the blind people than for the control group of sighted people. At the same time the reaction time for the tactile scenario was shorter, independent of whether the operator was handicapped or not.

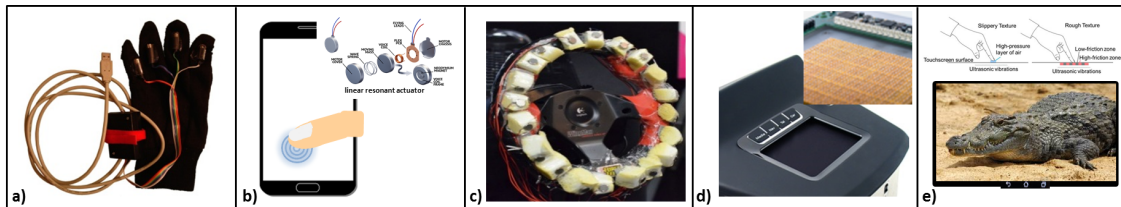


Figure 1.1: Haptic in the communication and gaming branch. a) Wearable glove for tactual games (from Yuan and Folmer (2008)). b) Vibrational feedback using resonant actuator (from *Somatic Labs*) in modern smartphones. c) Rotationally vibrating steering wheel prototype for route guidance (from *AT&T*). d) MMI Haptic Touchpad in car for navigation purpose (from *Audi*). e) Haptic display (from *Fujitsu Siemens*)

As a flagship-area, the mobile phone area is including tactile cues since years. The integration is quite simple but nevertheless exciting a high demand and a considerable impact. In contrast to visual or audio features, the tactile channel is predestined in ensuring that information is just exposed to the person for whom it is intended, fulfilling the aspect of discreteness. Modern handsets and smartphones provide basic tactile feedback (see Figure 1.1, b) when touching the display, for example for messaging, or in general when a virtual button is pressed to retrieve information.

The automotive industry, as a younger application field, is highly interested in integrating cues with respect to the sense of touch. The status of a car is changing from initially being conceived for the transport of people or items, to an highly advanced technological headquarter providing any kind of information about the car itself, the human as operator and the surrounding world. However, these improvements may also lead to a cognitive overload and distract the driver. The integration of

haptic features as a new and more intuitive channel for information transfer could reduce the overload of information. First applications took place in the provision of car warning systems. One main attribute of driving is to operate the car via the steering wheel, which requires a permanent physical contact of the driver with it. Thus, companies like *Audi* and *BMW* already use vibrating steering wheels or vibrations in the seat to warn drivers when for instance the vehicle is about to drift out of the lane (Norén, 2008; Shaout et al., 2011). The *American Telephone and Telegraph Company* (AT&T) recently build a steering wheel prototype, where tactile cues are used for guiding the driver over a route (see Figure 1.1, c). A rotationally motion (either clockwise or counterclockwise) is presented to the driver, using vibrating motors installed close to each other in the steering wheel, to indicate the route tactually (Kim et al., 2012).

Car information-, communication- and navigation-systems are common features in vehicles. The operation and selection of the different functions is done via menu items visually provided on a screen to the driver, which may increase the risk of distraction during driving. To minimize the visual effort in choosing from the menu on the screen, the automotive company *Audi* recently introduced a tactile display driven by piezoelectric elements. Figure 1.1 (d) depicts the man-machine interface (MMI) which allows for intuitive navigation solely by palpating the distinct patterns of the menu structure to enter the specific menu entry (Spies et al., 2009, 2010).

To feel for example a crocodiles texture, Fujitsu Siemens 's research lab developed a tablet which enables to do so (see Figure 1.1, e). For this, the haptic display applies high speed ultrasonic vibrations to its surface resulting in a high pressure layer of air at the interface. These spots are of low friction mimicking smooth areas. In that way any kind of textures can be presented as a function of the sense of reduced or enhanced frictional resistance.

As an excellent communication and information channel for visually impaired people the tactile sense can play a crucial role in daily life interactions. As depicted in Figure 1.2 (a), (b), and (c) devices like smartphones, tablets or watches are developed to compensate the loss of vision. Thereby the devices are based on Braille-characters and patterns which are generated by dots that can be tactually deciphered. For example, the smartphone from Samsung (see Figure 1.2, a) features an electric active plastic surface which has the ability to raise pins underneath the surface, resulting in patterns providing the actual time.

For the sake of completeness, Figure 1.2 (d) and (e) show tactile cues which are

integrated in the environment. These kind of applications are not necessarily just aimed for handicapped people. For example, the special road paving in Figure 1.2 (d) presents protrusions which feel different from the normal paving. Thus, pedestrians who may not pay attention to the road can be kept again to an attentive stage due to the sudden change they feel under the soles of their feet.



Figure 1.2: Haptic application for visually impaired people. a) Braille phone from *Samsung*. b) Refreshable Braille Kindle from *University of Michigan*. c) Dot Watch from *Dotincorp* d) Macroscopic Braille paving. e) Vibrating traffic light push buttons.

1.1.2 Virtual, Assistive and Educational Systems in Medicine

Assistive systems (ASs) maintain, improve or enhance the capability of individuals with disabilities (Scherer, 2002). The spectrum of ASs ranges from simple functional objects (such as walkers) to complex technologies for the compensation of a sensory loss, e.g. hearing aids. The success of a surgery depends not only strongly on the quality of technical devices, assistance and associates, but also on the knowledge and skills of the surgeon - as the acting hand. It remains ultimately a subjective assessment how tight for example a laparoscopic instrument can be pressed without damaging tissue or arteria. The subjective judgment always relies strongly on sight, so that the addition of another modality can only be of benefit. In recent years a variety of systems, as depicted in Figure 1.3 have been investigated providing a force feedback to the tactile channel of the operator. Figure 1.3 (a) depicts the daVinci surgical system from *Intuitive Surgical*. This system, with the whole bundle of instruments, has its control unit away from the surgical table and is based on two modalities which mutually complement each other, namely vision and tactility. For visual inspection, the spot of interest is localized by an eye tracking system and presented to the surgeon by a high resolution imaging system. The control of the instruments and tools is realized with manipulators (see Figure 1.3,

1.1 Application Areas for Haptics

b), which provide a tactile feedback in order to present the exact applied forces during instrumental use.

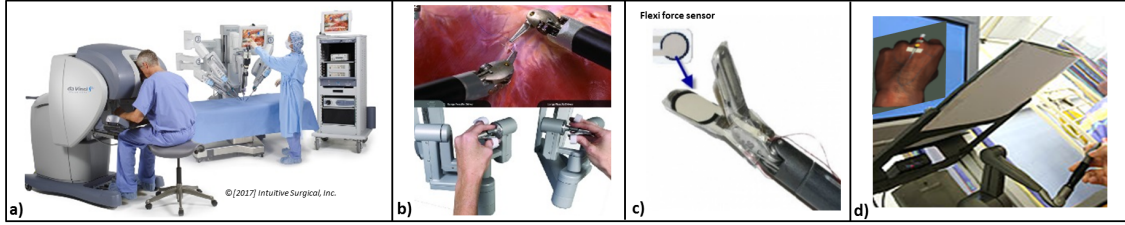


Figure 1.3: Haptic application in medicine. a) daVinci S surgical system (from *Intuitive Surgical*). b) Tactile manipulators. c) Grasping system with Flexi-Force (from *Center for Advanced Surgical and Interventional Technology (CASIT)*). d) Medical training simulator for practising the insertion of cannulae into a vein (from *Geomagicclub*).

In this framework, and to validate whether an unimodal (just vision) or a multimodal (vision plus tactility) scenario is offering more benefits in strengthening the dexterity of the operator, Bethea et al. (2004) proposed a study where they evaluated the knot tying of suture material with respect to breakage. They concluded that in the case of a multimodal scenario the number of breakages was significantly lower than in the just vision based case. Other studies show that multimodality is even contributing towards minimization of, both, the duration of a surgical intervention (Nitsch and Färber, 2013) as well as errors that may occur (Wagner et al., 2002; Tholey et al., 2005), while at the same time increasing the safety of patients. Apart from those complex surgical robot-like devices, also just simple instruments like grasping tools (see Figure 1.3, c) are extended with a tactile feedback. A thin flexible pressure sensor measures the force acting between the gripper and the object while informing the operator via a haptic interface. Due to the accurate response, the user is capable of fine-adjust the applied forces and prevent suture damages, for instance. Tactile-feedback systems are predestined as training tools mimicking realistic conditions and scenarios. Figure 1.3 (d) shows a system for practicing the insertion of a cannulae into a hand vein. The model itself is operated via an haptic device (*Touch X* from *Geomagic*), where a mechanical feedback (using actuators) is given in a realistic way. This invention, making it possible to practice surgery before entering the clinical environment is a major breakthrough in medicine, and has revolutionized medical education to a large extent (Kapoor et al., 2014).

1.1.3 Virtual Reality

Virtual reality (VR) is a technology that makes it possible to replicate experiences obtained through the ways we sense the world surrounding us. Three keywords also known as the I³ - immersion-interaction-imagination - define VR (Burdea, 1999). The beginning of VR is based on vision (VR-headsets or glasses) and audition (binaural headphones) which together can give an illusion of a real life situation. Of vital importance to communicate with the physical world is the tactile sense. This is where haptics and VR met to consequently complete the illusion. Figure 1.4 shows applications where the tactile sense is explicitly addressed in VR scenarios.



Figure 1.4: Haptic in virtual environments (VR). a) Ultrasonic display (from *Ultrahaptics*). b) Bimanual haptic device HUG (from *DLR*). c) Full body haptic suit (from *Teslasuit*).

The ultrasonic display from *Ultrahaptics* (see Figure 1.4, a) enables the perception and manipulation of 3D shapes and blocks. The display uses ultrasound transducers and a tracking camera (captures the location of the hand) to exert an acoustic radiation force on the hand in mid-air (Carter et al., 2013; Subramanian et al., 2016). It may find implementation in the dashboard of a car, for instance in for controlling virtual buttons or knobs just by gestures. Figure 1.4 (b) shows the six-DoF telemanipulating HUG system from the german aerospace centre *DLR*. Due to telemanipulation the system makes it possible to work at a remote workplace (Korondi et al., 2005, Sec. 4 p60). HUG consists of two arms providing dynamic interaction forces to the human finger and hand when operating for instance a humanoid robot (Sagardia et al., 2016). In Figure 1.4 (c) the skintight tactile full body *Teslasuit* is depicted. The suit is integrated with electro muscular stimulation as well as temperature units, enabling the wearer to feel sensations in the virtual world at any part of the skin ranging from a wind breeze on the skin to immediate temperature changes.

1.2 Tactual System - Somatosensory System

The tactile sense can be subdivided into two categories, namely discriminative and affective touch, where the properties are mediated on the one hand by fast conducting $A\beta$ fibers for discrimination and on the other hand by unmyelinated peripheral CT-afferents (C-tactile) for the affective function (McGlone et al., 2007, 2014). The scope of this thesis is the electrophysiological evaluation of the human tactile sense due to the use of frictional stimuli exposed to the glabrous fingertip. Since the glabrous skin does not incorporate CT-afferents (McGlone et al. (2007)) and affective touch describes mainly the interpersonal touch related communication, focus is laid on the discriminative rather than the affective category.

The following section introduces the two main systems which are responsible for tactile perception. First, an overview is given about the skin, its natural structure and the specialized receptors that receive and transmit external physical information. Subsequently, the somatosensory system which is the processing unit will be described together with its pathway in more detail.

1.2.1 The Skin - The Outer Shell of the Body

The skin is the largest sensory organ of the human covering an area of approximately $1.5\text{-}2\text{m}^2$. Serving as the outer shell of the body, the main functions of the skin include protection (from external physical, chemical and biological), regulation (temperature, excretion, endocrine - synthesis of Vitamin D) and sensation (sensory nerve cells). There are two kind of skin types, namely the hairy and the glabrous (hairless) skin. Figure 1.5 (a) shows the glabrous skin of the fingertip which consists of three layers. The epidermis is the top layer which varies in thickness from thinner (0.05mm - eyelids) to thicker areas (1.5mm - sole of the foot) and is mainly responsible for the cell regeneration and the protection against pathogens. The dermis is a thicker layer of the skin (1.5-4mm) and incorporates blood vessels, sweat glands and cells for sensation. The third layer (not seen in the figure) is the thickest layer and named subcutis. It is composed of fat and collagen, serving insulation and energy storage purposes with a strongly varying thickness between individuals and bodyparts (Agache and Humbert, 2004).

There are a bundle of distinct subsystems that comprises sensation. Those subsystems or sensory receptors differ in their specialized nerve endings and are capable

of detecting different external stimuli.

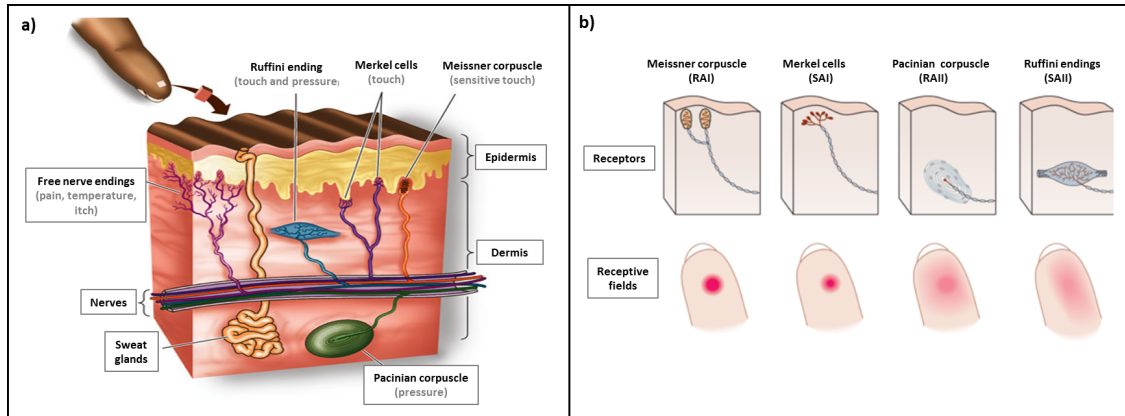


Figure 1.5: The glabrous skin of the fingertip. a) The Skin layer and the location of mechanoreceptors (Sadava et al., 2008). b) Receptive fields of the involved mechanoreceptors (Kandel et al., 2000, Ch. 22-23).

The skin incorporates three kinds of nerve cells, namely thermoreceptors, nociceptors and mechanoreceptors. The latter ones form the basis of the tactile sense. Figure 1.5 (b) shows the four types of mechanoreceptors and their respective receptive fields. The receptive fields are larger for deeper lying receptors and thus provide a lower spatial resolution. Table 1.1 lists the main characteristics for the mechanoreceptors.

Table 1.1: Mechanoreceptors of the tactile sense.

Receptor type	Density (units/cm ²)	Adaptation	Sensation	Frequency
Merkel cells	70	SA I	Touch, pressure texture perception (static force)	0.3 – 3Hz
Meissner corpuscle	140	RA I	Touch, pressure, skin deformation stretch (dynamic force)	3 – 40Hz
Ruffini endings	10	SA II	tangential forces skin stretch stretch (dynamic force)	15 – 400Hz
Pacinian corpuscle	20	RA II	Deep pressure, vibration	10 – 500Hz

They differ in their location in the compound of skin layers, their ability in perceiving different stimuli, the frequency range (due to their biomechanical structures) they respond to, their physical features and the size of their receptive fields, and in

temporal properties like adaptation.

Each sensory system has its fundamental role in perceiving, transforming and processing information. Usually, stimulation of the sensory system results in a change of the membrane potential and cause action potentials (APs) to propagate along an axon to the central nervous system (CNS). Adaptation is depending on the stimulus intensity. Adaptation is the ability of the nervous system to regulate the threshold of sensitivity with respect to the intensity of the stimuli. Mechanoreceptors react in two ways to persisting constant stimuli, either in a slow adapting (SA) or a fast/rapid adapting (RA) manner. Meissner and Pacinian corpuscles (RA-receptors) respond to the beginning and to the end of a stimulation, i.e. to sudden changes of the physical property (for instance pressure), while Merkel cells and Ruffini endings (SA-receptors) signal as long as the stimuli is present. Because of their high sensitivity to mechanical stimulation mechanoreceptors are referred to as low threshold receptors (LTMs) with large myelinated ($A\beta$) afferents (Bourane et al., 2009). SA and RA adapting nerve cells are marked with an suffix, either *I* (indicating a small receptive field with sharp borders) or *II* (indicating a large receptive field with diffuse borders). The spatial density of the receptors is lower for deeper lying SA II and RA II receptors and higher for near surface receptors especially in the fingertips (Johansson and Vallbo, 1979), (Kern, 2009, Chap. 2 p33). Kern and Hatzfeld describe that the overall amount of receptors is similar between individuals which implies that small hands are more sensitive than large ones (Kern, 2009, Chap. 2 p34).

There are approximately 10^6 touch receptors located in our skin – $250/cm^2$ in a fingertip with stimuli frequencies in the range from 0.3 -500Hz (Johansson and Vallbo, 1979). The spatial acuity of the tactile sense varies depending on the interaction - either in a passive or active manner. Skedung et al. (Skedung et al., 2013) found out that an active explorative interaction comes along with a acuity in the nanometer range. In the case of a passive or static interaction (no motion relative to the environment) the spatial acuity is in the range of 0.2mm and not gender specific (Gellis and Pool, 1977).

When physically contacting a object or surface with the fingertips, the top layer of the epidermis, the *stratum corneum* with its ridges is forming the contact. This skin region is important in contact mechanics and thus described in more detail in section 1.3, where surface properties of skin are outlined.

1.2.2 Somatosensory System

The tactile sense is based on receptors which are capable of detecting specific stimuli and on conversion of the signals into sensory information. Peripheral nerves are not restricted to one stimulus type, meaning that a stimulation excites several receptors-types and thus leads to a high amount of information, simultaneously present. This information redundancy, however, is handled by the underlying sense in a way similar to a filter where a certain appropriate amount of important information is selectively chosen.

Besides temperature, pain and proprioception (information about position and movement of the body), mechanoreceptors form one modality of the somatosensory system (SS) - the area of the brain involved in tactile perception. Figure 1.6 (a) shows the SS and the distinct pathways for the somatic sensation, namely the spinothalamic pathway, responsible for the perception of pain and temperature and the dorsal column-medial lemniscal pathway, responsible for the tactile sense.

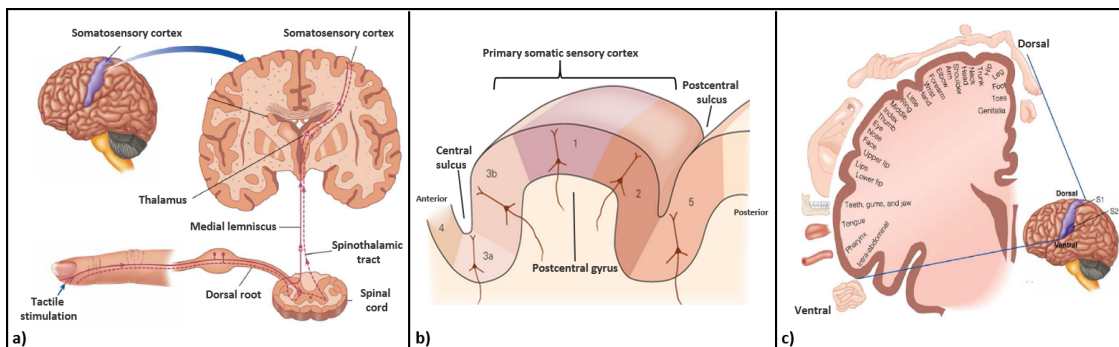


Figure 1.6: The somatosensory cortex (SS). a) Two pathways of SS:

The dorsal column - medial lemniscal pathway (information on touch, red solid line); The spinothalamic pathway (information on pain and temperature, red dashed line). b) The postcentral gyrus of the parietal lobe. c) Somatotopic organization: The sensory homunculus representing the body parts at distinct location in the SSs. The size of each body part represents the sensitivity. After Purves et al. (2008).

The SS is located in the postcentral gyrus of the parietal lobe of the brain and includes the Brodmann's (BA) area 3a, 3b, 1 and 2 (see Figure 1.6, b), where mainly area BA 3b and BA 1 respond to cutaneous stimuli (Purves et al., 2008, Chap. 9). Sensory information is transmitted to the somatosensory cortex by ascending pathways. Here the dorsal column - medial lemniscal pathway, the pathway pro-

1.2 Tactual System - Somatosensory System

viding tactile information to the thalamus and cerebral cortex is of interest. As depicted in Figure 1.6 (a), tactile information is received by the mechanoreceptors in the fingertip and transmitted via afferent fibers (see red solid line) to first order neurons in dorsal root ganglion cells, while ipsilateral ascending tracts in the spinal cord passes on the information to second order neurons of the cuneate nucleus in the dorsal part of the medulla. In the brainstem a decussation (midline crossing) takes place, where a new tract (medial lemniscus) is formed on the contralateral side and ascends in the third order neurons of the thalamus, finally terminating in the parietal lobe of the cortex (for a more detailed description see Roudaut et al. (2012); Lumpkin et al. (2010)). Figure 1.6 (c) shows the sensory homunculus - the somatosensory sensitivity-map with respect to the distinct human bodyparts. The size of each bodypart indicates the amount of cortex-area involved in sensation and processing, emphasizing that face- (especially the lips) and hand parts are the largest and thus the most sensitive ones. To address the sense of touch, the EEG-protocol used for the the work in this thesis included electrode-positions located over the hand- and finger areas of the somatosensory cortex (see section 2.4 for the EEG-protocol).

1.3 Mechanical Properties of the Skin

The human skin can be classified into hairy or glabrous skin. Glabrous skin, which is located only on the plantar and palmar surfaces is in relation to the hairy skin just a small ratio of the whole skin. This skin type is very sensitive in detecting fine details due to the increased innervation density of mechanoreceptors (Boada et al., 2010). In the following, mechanical properties that contribute to the overall tactile sensation are clarified.

The body is capable to deform. The skin is stretched (or compressed) in all directions from small stresses, e.g., the skin of the joints of the finger when typing on a keyboard, to high stresses for instance when skin is indented by a sharp object. As long as there is no skin tearing due to high tensional forces, skin returns back to its initial state. The duration of the recovery process, i.e., the time it takes for the skin to return back to the initial flat position is dependent on two main parameter. First, the duration the skin is impinged, which is linearly correlated with skin recovery and second, the "skin-age", where younger skin recovers faster than older skin. This arises from the fact that skin mostly consists of elastic solids (collagen and elastin fibres) and viscous fluids or ground substance (water and highly hydrated glycosaminoglycans mass outside the fibres), and thus represents a highly viscoelastic system (Weinstein and Boucek, 1960; Shevchenko et al., 2009).

Figure 1.7 (a) shows the stress-strain relation of the skin, where three distinct phases can be distinguished. Initially the compound of fibers is in a relaxed state (beginning of phase I), where collagen and elastin fibers are present in a compact and densed matrix, resulting in a low dynamic stiffness. If a force or tensile stress is applied (end of phase I, phase II), stress increases with strain. The fibers are initially in a helical/curled state and thus forces are small until an uncurled state is reached (Jor et al., 2011). In phase III, the fibers are aligned straight along the load axis and the stress- strain relation shows a linear behaviour (Everett and Sommers, 2013). After releasing the force, the skin subsequently turns back to its original relaxed state. In this case, the system is called perfectly elastic (Pawlaczyk et al., 2013). Further stretching of the fibers beyond phase III causes the development of traumas and ruptures or tearing of the skin (Jor et al., 2011). Especially for elderly people the probability of tearing and ruptures is very high. The viscoelasticity of skin is dependent on skin ageing. As years go by, viscoelasticity is reduced due to degenerative changes of the skin, disorganization and loss of collagen fibers and

1.3 Mechanical Properties of the Skin

reduced vascular tissue (Farage et al., 2009) (Moronkeji and Akhtar, 2015, Ch.10).

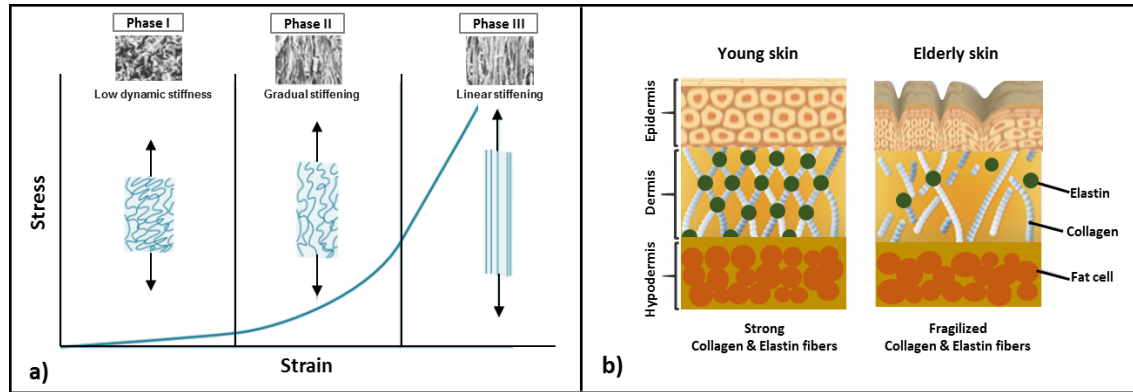


Figure 1.7: Stress-strain behaviour of the skin. a) Typical responses of the skin to mechanical stress. After (Kalra et al., 2016; Jor et al., 2011). b) Schematic representation of skin-ageing. Aging of the skin lead to a disorganization and loss of collagen fibers.

Figure 1.7 (b) shows a schematic comparison of younger and older skin demonstrating the effect of ageing. Thereby younger skin has strong collagen and elastin fibers, whereas older skin incorporates fragilized fibers resulting in a soft and wrinkled skin. The stiffness is characterized by the slope of the linear region of the stress-strain curve and is defined by the elastic *Young's modulus* (E), which is the ratio of the tensile stress σ and extensional strain ϵ and is defined by Hooke's Law, $\epsilon = E/\sigma$ (Boyer et al., 2009). The E-modulus of the human skin is mainly determined by torsion tests, indentation tests and suction tests, with moduli of 0.42-0.85 MPa, 6-20 MPa and 0.05-0.15 MPa, respectively and doubling with age (Pawlaczyk et al., 2013; Agache et al., 1980). Thus, the structure of the skin gives rise to complex mechanical properties of the skin, ranging from viscoelastic, through anisotropic, to nonlinear and heterogenous mechanical properties (see Jor et al. (2011) and references therein).

Surface Properties of the Skin

The glabrous human skin at fingertips (see Figure 1.8) consists mainly of skin surface lipids, sweat glands, and epidermal ridges (fingerprints). The latter define the roughness of the skin and are arranged in pattern types of arches, loops and whirls with inter ridge distances of about 500-680 μm (Urribarrí et al., 2016). The

surface roughness R_z of the skin, i.e., the average of the vertical distance between highest peak and lowest valley varies from region to region over the body and is in the order of 62-99 microns at fingertips (Derler et al., 2009). In contrast, R_z for smooth glass is $0.01 \mu\text{m}$. Each individual fingerprint is unique and the basic shape and pattern usually does not change throughout the lifecycle. This is part of the explanation why biometric security is a growing branch. Given that the usual way of using passwords or codes may be easily decrypted, the measurement of unique physical characteristics for identification and authentication purposes, such as the fingerprint reader in smartphones allows for more security.

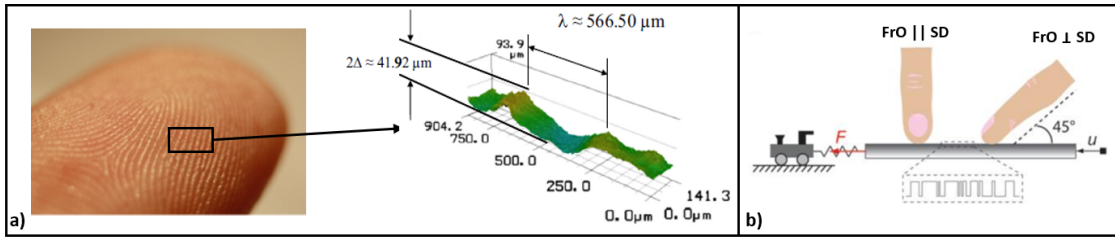


Figure 1.8: a) Topography of the fingertip by a replica made of a synthetic rubber compound (ProvilNovoLightCD2, VEM Metallurgie, NL) (Urribarrí et al., 2016). b) Evaluation of fingerridge-orientation (FrO) to sliding direction (SD) (Prevost et al., 2009).

However, the role of fingerprints in the overall perception chain is still discussed, but said to serve either mechanical or tactile functions. In 1954, Cauna postulated that like in vision the lens is connected to the retina, fingerprints are an essential part of the tactile sense and that they enhance spatial discrimination (see Manfredi et al. (2014)). Scheibert et al. (2009), described two potential functions underlying fingerprints. The first function is the reinforcement of adhesion and friction, i.e., the enhancement of the skid resistance, the second function is the magnification of tactile perception. The authors probed the impact of fingerridges on the skin vibration spectrum and a possible spectral amplification by using an artificial fingersensor equipped with ridges (Prevost et al., 2009). They recorded the friction force between the sensor-ridges and the surface under two conditions, ridges oriented perpendicular or parallel to the sliding direction (see Figure 1.8, b). They observed that just for the perpendicular case spectral amplification took place. Fagiani et al. (2011), studied the frequency spectra of induced vibrations propagating in the finger induced by friction between the skin and the explored surface. In doing so, they placed an accelerometer on the fingernail and performed measurements by

1.3 Mechanical Properties of the Skin

changing the scanning speed and the sample surface roughness in terms of changing the wavelength in periodicity. They showed that for increasing velocities prominent frequency peaks shifted to higher values and are dependent on the ratio between the surface roughness wavelength and the fingerridge wavelength. They concluded that especially the body with the smaller wavelength is the main contributor to the frequency spectra peaking. The same observations have been made by Manfredi et al. (2014), where the authors measured skin-vibrations using a laser-Doppler vibrometer. They could show that the induced vibrations indicated distinct frequency components which could be assigned with high accuracy to the specific textures. Moreover, they concluded that ridges are capable in enhancing textural features that are too small to be resolved spatially.

As an additional interesting information Barnes et al. (2004) concluded in their work that the emotional attraction of a material is dependent on the ratio of the roughnesses between the fingertip and the surface. If the ratio $Roughness_{fingertip}/Roughness_{surface}$, was ≤ 1 subjects felt unpleasant, whereas for ratios ≥ 1 surfaces were felt more pleasant.

1.4 Contact Mechanics and Friction

This section serves as an introduction to the fundamentals in contact mechanics at the skin-material interface. Tactile perception is based on skin deformation induced by mechanical loads during object manipulation or tactile exploration of surfaces and thus is connected to skin tribology (Darden and Schwartz, 2015). The viscoelastic properties of skin in sliding contact is described to be similar to that of a soft elastomer (Johnson et al., 1993). Skin is a very complex matter and constantly changing its properties due to constantly changing stress rates during contact (Jones and Lederman, 2006). This gives rise to the importance of finger-friction which is a key mechanism of tactile sensing.

Figure 1.9 shows a schematic representation of the physical touch and sliding-contact between fingertip and Braille-display as implemented in this work. The contact zone (blue line), which is the decisive factor in tactile perception is formed by:

- i) The skin topography and ridges.
- ii) The mechanical properties (MPs) of the skin including mechanoreceptors (MR), elastic fibres (eF) and viscous fluids (vF).
- iii) The MPs of the counter surface.

Thus, the interplay of all these factors and additional parameters, such as normal load, velocity, contact area, skin hydration and lubrication gives rise to the assumption that fingertip-friction is very complex but a key-parameter in tactile sensing.

The following description of the factors and parameters involved in friction is mainly based on the work of van Kuilenburg et al. (2015), Darden and Schwartz (2015), and Adams et al. (2007).

The skin incorporates mechanoreceptors which respond to distinct external changes arising from stress, strain and vibrations (see section 1.2), allowing for the perception and judgment of materials properties. Figure 1.10 shows a schematic representation of physical stimuli and the sensorial percepts considering a static (indentation, i.e., normal deformation) and a sliding (vibrations) contact. When indenting a surface one can judge on the softness of a material, i.e., the compliance, by relating the applied force with the deformation depth of the material (see Figure 1.10, a).

1.4 Contact Mechanics and Friction

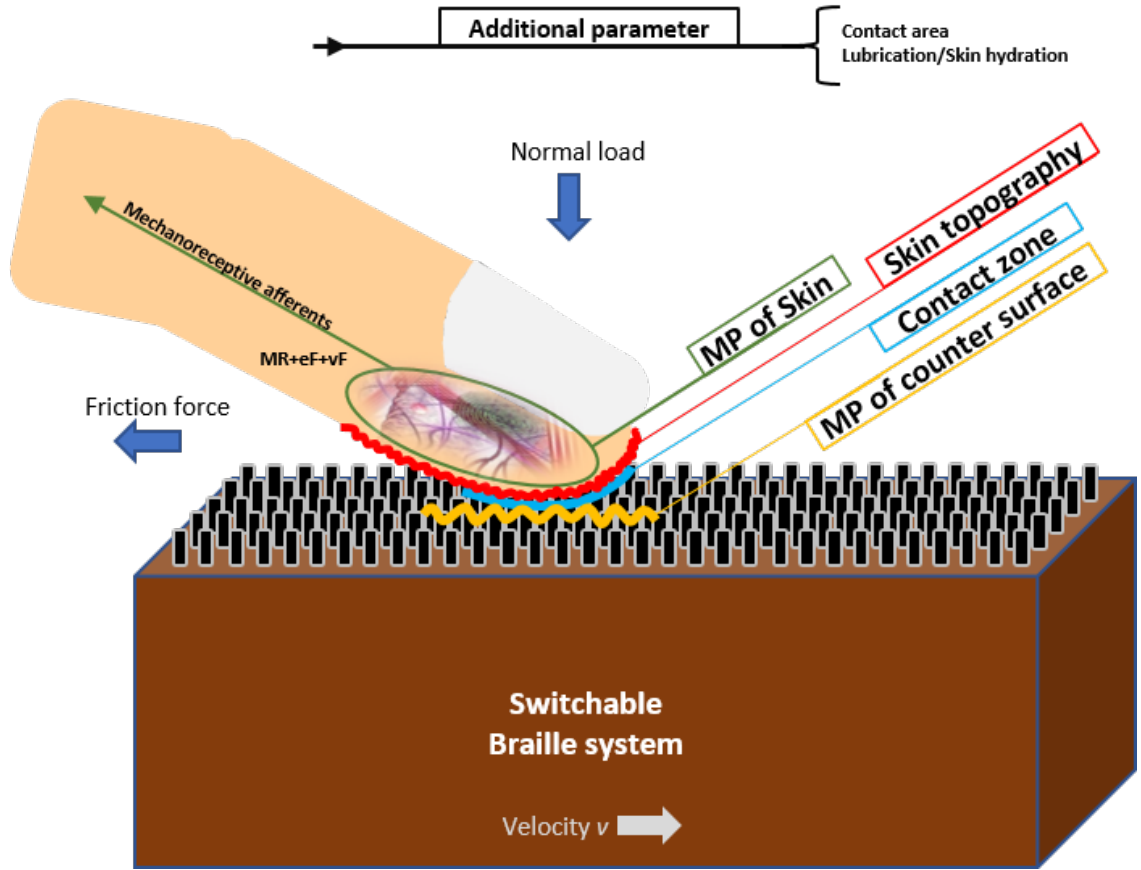


Figure 1.9: Schematic representation of the contact of the fingertip with a switchable Braille display as implemented in this work. Important factors contributing to the decisive contact zone (blue line) and hence the tactile sensing: Mechanical properties (MP) of the skin (green circle) including elastic fibres (eF) and viscous fluids (vF); Skin topography/ridges (red line); Mechanical properties (MP) of the counter surface (yellow line). The interplay of all factors gives rise to the fingertip-friction as key parameter, which is influenced by additional parameters, such as normal load, velocity, contact area, skin hydration and lubrication.

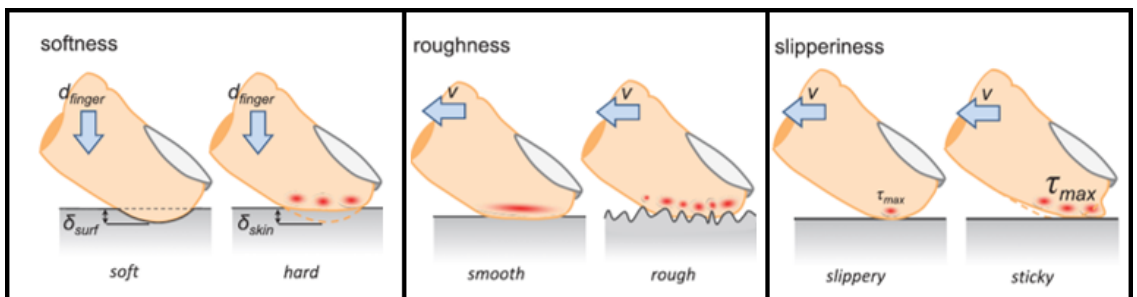


Figure 1.10: Schematic representation of the sensorial properties softness, roughness and slipperiness (adapted from van Kuilenburg et al. (2015)).

This basically describes the elastic modulus E of a material, where applied stresses are related to resulted strains. The sliding of the fingertip over a surface, in contrast to a static touch, induces frictional vibrations which propagate in the hand and thus give information on the roughness and slipperiness (see Figure 1.10, b) and c)). The friction force itself is a sum of two terms following the classical two-term model given by Bowden and Tabor: $F_{fric} = F_{adh} + F_{def}$, where F_{adh} is the adhesive friction, F_{def} the deformation or hysteresis force and F_{fric} the total friction force (van Kuilenburg et al., 2013). For dry and smooth surfaces, it is assumed that friction is only dependent on adhesive mechanisms while deformation can be neglected (Adams et al., 2007). Due to this fact friction can then be described by the linear relation $F_{fric} = F_{adh} = \tau A_{real}$, where F_{adh} can be calculated from the shear strength of the interface τ and the real contact area A_{real} (Johnson et al., 1993). When sliding the fingertip over rough surfaces friction appeared to be dependant on both, adhesive friction and deformation friction (Derler et al., 2009).

In 1699, Amonton postulated a direct proportionality between the friction force and the normal force known as the friction coefficient: $\mu = F_{Fric} / F_{Nor}$, where F_{Fric} is the friction or lateral force and F_{Nor} the normal force. It was assumed that μ is constant and does not depend on the contact area or the sliding velocity. However, related to the viscoelastic properties of skin, it is believed that the skin follows Amontons law just over a limited range of loads and that contact area and velocity play a crucial role in extended ranges (Savescu et al., 2008).

Other prominent factors: Friction force is an essential parameter in the sliding contact between the fingertip and a surface. However, since friction depends strongly on adhesion, the contact area plays also a crucial role. Reported in van Kuilenburg et al. (2015), the contact area increase proportional to the normal load following a power law: $A \propto F^n$ with exponents ranging from 0.15 – 1.33. It should be mentioned that with contact area the real contact area is meant. It is known that the apparent contact area is significantly larger than the real contact area (Van Der Heide et al., 2013). As depicted in Figure 1.11 the apparent contact area is reduced due to inter-asperity contact explaining the real contact area. In the case when the contacted surface has low roughness, however, the area of real contact may approach the area of apparent contact (Van Der Heide et al., 2013).

Skin incorporates sweat glands with pores at the surface for secretion purposes. When skin moisture increases, the skin softens which leads to a higher friction due to increase in contact area and shear stress.

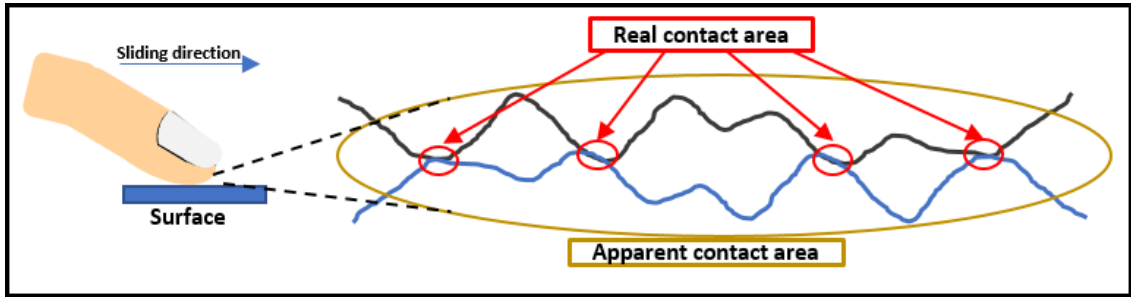


Figure 1.11: Schematic representation of the real contact area.

Dinc et al. (1991), evaluated the effect of varying sliding velocities on the friction between the fingertip and flat or rather rough polymers. They found that an increase in sliding speed results in a decrease of friction. In the case of dry friction the sliding work at all is based on the rupture of junctions where intermolecular van der Waals interactions at each contact are formed. When hydration comes into play, the bridging between fingerprints and surface-asperities increases. This results in higher shear forces and thus in an increase of the friction. However, the friction of skin is still not fully understood with respect to mechanoreception, making it crucial to extend scientific research on this topic.

1.5 State of the Art

The skin is the outer most barrier of the human body, responsible for many factors including protection, regulation and sensation (see section 1.2) and is the first bodypart in physically interacting with the environment. Tribological experiments involving human skin have recently attracted increased attention, attributing the outstanding importance in daily life situations. Of particular importance are studies which investigate the influence of skin hydration (Adams et al., 2007) and the effect of surface lipids and sweat (Sivamani et al., 2003), often with an emphasis on interactions with textiles (Gerhardt et al., 2008; Derler et al., 2007) investigating frictional aspects. The experimental procedure of those studies mainly consists of a rubbing of the fingertip against a surface sample. On the other hand studies with a focus on innovational material and surface structure design investigate for instance the modulation of friction using well defined biomimetic elastomer fingertip with ridges rubbed against a glass probe (Wandersman et al., 2011; Scheibert et al., 2009). However, those tribological experiments are limited to the friction and wear of the human skin. The perception, i.e. the neural response to sensory exogenous stimuli is rarely investigated. The relation between materials properties and surface pattern on the one hand, and feel upon touch on the other hand has recently been investigated by a number of psychophysical studies, which correlate the perception of individuals with frictional forces acting on their fingertips. Insights from these studies, carefully extracted from the subjective data with its biases, include the minimal structure size of features which are still detected by frictional touch and a relation between friction force fluctuations and the pleasantness of touch (Skedung et al., 2013; Klöcker et al., 2012). Other studies including measurements of peripheral neural signals - microneurography, i.e. signals directly originating from the nerve cells as measured at the extremity, have confirmed the importance of frictional shear strain in the fingertip skin for perception (Olausson et al., 2010). Although those studies give rise to the understanding of receptors behaviour and nerve firing rates, the sensory pathway underlying perception is not involved (Abraira and Ginty, 2013). The development of noninvasive recording and imaging techniques, like the electroencephalogram (EEG) are of great importance in neuroscience and meanwhile subject of a wide field of research. The EEG enables for the measurement of brain electrical activity representing changes in potential differences over different brain regions at the scalp. EEG activity evoked by an

exogenous stimulus represents the brain's response to this stimulus and thus is called event related potential (ERP). Related to the work in this thesis are studies of characteristic waves in the EEG which are evoked by a mechanical stimulation of the fingertip, mainly focusing on attentional paradigms (Pfurtscheller et al., 2001; Avilés et al., 2010; Forster and Eimer, 2004). However, considerations on relations between stimulus intensity and EEG amplitude or latency, as for example in the research field of auditory ERPs showing an antiproportional behaviour between intensity and latency (Corona-Strauss et al., 2009), little information is available for the tactile sense (Hashimoto, 1987; Hashimoto et al., 1992).

Somatosensory Evoked Potentials (SEPs)

Somatosensory event related potentials (SERPs) or somatosensory evoked potentials (SEPs) are electrophysiological responses which can be evoked by either a electrical stimulation of peripheral nerves (median or tibial nerve) or a mechanical stimulation of the mechanoreceptors in the skin. The electrical stimulation of peripheral nerves is quite good investigated and mainly conducted for clinical diagnosis, such as the intraoperative monitoring of neural pathways to prevent nerve injuries (see International Federation of Clinical Neurophysiology (IFCN) (Cruccu et al., 2008)). For example the electrical stimulation of the median nerve activates large and mixed nerve bundles governing and innervating several hand parts due to the activation of a large amount of sensor and motor-receptors (Gaetz et al., 2017). In contrast, a mechanical stimulation of skin-receptors, as for example in sliding the fingertip over a surface, innervates nerve fibers with similar functional characteristics in a more localized way (Caruso, 1995). To this end, the mechanical stimulation of one fingertip independently may then reduce the amount of the different kind of involved afferences compared to the median nerve stimulation. The analysis of event related neural responses is in general based on the signals morphology. Peaks and valleys at different time points (relative to the stimulus onset) can be assigned to distinct neural processes occurring along the sensory pathway. The nomenclature of ERP-components is defined and described by different parameters: The polarity (i.e., positive or negative deflection), the latency (i.e., the time interval between stimulation and response in *milliseconds*) and the amplitude (which usually vary in value due to stimulus intensity and the electrode-site signals are observed from, i.e., ipsi- or contralaterally).

In contrast to auditory- or visual ERPs with its many identified and investigated components, information on the signals-morphology and components of tactile

evoked ERPs are not as extensive. Few studies focusing on discrimination and attention, where subjects task was to detect a target stimulus out of repeated standard stimuli revealed information. Figure 1.12 a) and b) depicts representative examples of somatosensory ERPs and their components accordingly labelled to their deflection and temporal latency.

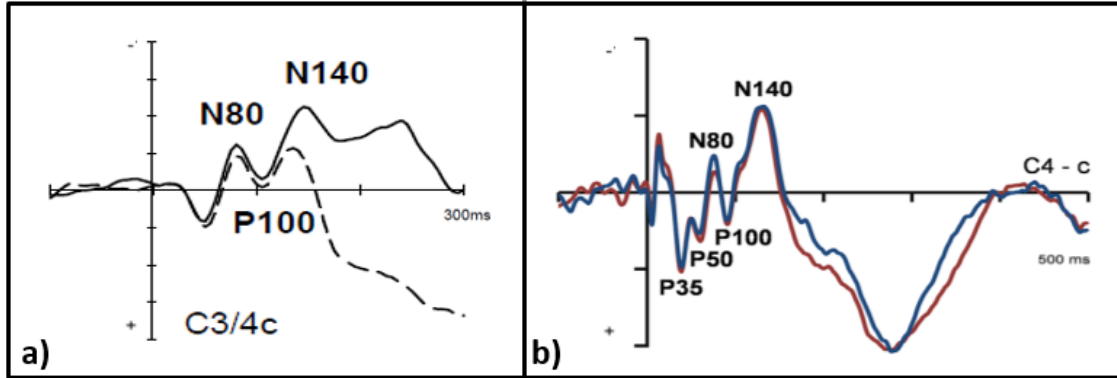


Figure 1.12: Examples of somatosensory evoked potentials (SEPs) and their prominent components labelled with a letter (positive (P) or negative (N) polarity) and number (temporal latency relative to the stimulus onset). a) Adapted from (Forster and Eimer, 2004) and b) from (Soto-Faraco and Azañón, 2013).

The signals were recorded from contralateral C3/C4 electrode (with respect to the international 10-20 EEG system), with following prominent components: P35 (20-40ms), P50 (40-60ms), N80 (70-90ms), P100 (90-120ms), N140 (120-160ms), first part of the late positive deflection (LPDa, 200-300ms) and second part of the late positive deflection (LPDb, 300-500ms) (Soto-Faraco and Azañón, 2013; Forster and Eimer, 2004). ERPs are a widely used tool in research on visual and auditory perception (Picton, 2010). Somatosensory ERPs can be classified into early and middle (latency less than 50 ms to 100 ms), and late (latency of 50 ms to 100 ms and higher) responses. Early and middle latency responses are thought not to involve cognitive processing whilst representing neural coding of the exogenous physical stimulus while late components do involve mental processing being ruled by the subjective judgement (Hashimoto et al., 1988).

Experimental studies

Compared to the auditory or visual modality, the scientific quantification on psychological studies investigating the tactile perception due to fingertip tribology is poorly investigated but have recently attracted increased attention. This section serves as literature review of relevant studies conducted by other groups which are described in detail below.

In the work of Eimer and Forster (Forster and Eimer, 2004) the authors conducted experiments in studying the relationship between spatial and non-spatial attentional selectivity in tactile perception. The experimental design and procedure consisted in a tactile stimulation of the index finger of either the right or left hand using a thin metal pin vertically moved towards the fingertip. First, experiments were conducted by varying on the one hand the stimulus frequency (high or low) of the pin due to the change in interpulse intervals and on the other hand the stimulation site, i.e., left or right finger. Subjects were asked to direct attention to one of the possible combinations of stimulus frequency and location, while keeping gaze direction to a cross on a screen. Figure 1.13 (a) shows the time course of the elicited ERPs including prominent N80, P100 and N140 components. When attention was paid to location, ERPs elicited to tactile stimuli at attended locations (solid lines) exhibit an enhanced N140 components compared to unattended locations (dashed lines).

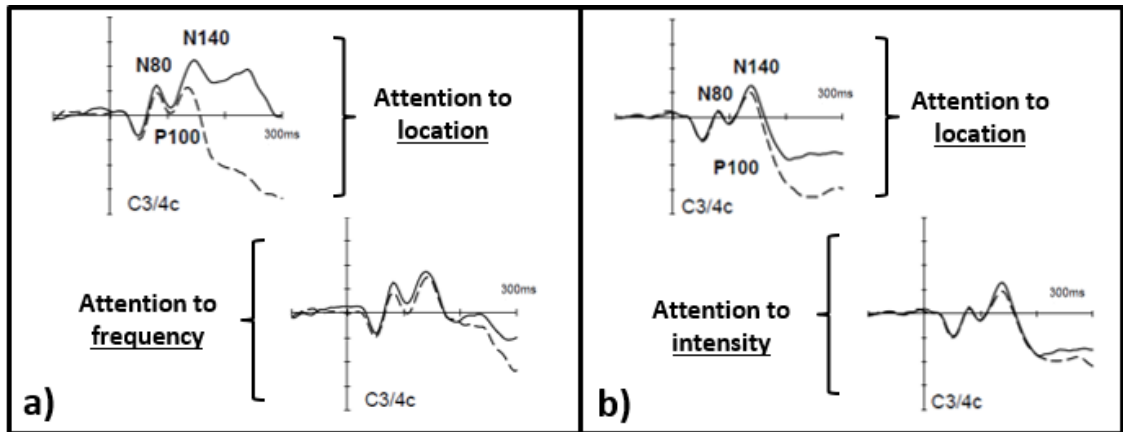


Figure 1.13: Attentional selection of spatial (stimulation location) and non-spatial (frequency, intensity) attributes of tactile stimuli a) Experiment 1: Attention effects on stimulation location and stimulation frequency. b) Experiment 2: Attentional effects on stimulation location and stimulation intensity. Solid lines: attended ERP. Dashed line: unattended ERP (Forster and Eimer, 2004)).

When attention was paid to stimulus frequency, ERP were already affected in the P100 range, with enhanced negativity for stimuli in the attended frequency.

In order to validate the independence of spatial and non-spatial selectivity in tactile perception, the authors introduced a second experiment. Here, stimulus frequency was kept constant while subjects were asked to focus on the combination of location (left or right finger) and stimulation intensity (soft or strong). Similar to the first experiment, spatial attention affected the N140 component followed by a negativity for stimuli at attended locations (see Figure 1.13, b). When attention was focused on the intensity, N140 was enhanced for stimuli in the attended intensities, compared to the unattended intensities. However, the study showed that ERP assessments upon effects of attention to frequency and intensity, compared to attention on location, were observed earlier. Thus, the authors concluded that selective attention towards spatial (location) and non-spatial (frequency, intensity) attributes in touch occur simultaneously. In another work, Forster and Eimer studied the influence of spatial attention on tactile perception (Forster and Eimer, 2005). In this study they observed the same prominent ERP components (N80, P110, N140), and reported that if vision and gaze is directed to the stimulated finger, even when occluded, ERPs were affected such in amplitude and latency.

Compared to Eimer and Forster, the work conducted by Avilés et al. (2010) investigated neurophysiological responses of tactual perception due to the sliding of stimuli along the fingertip. For this they constructed a tactile spinning wheel (TSW) to provide a series of different textured surfaces to the resting index finger of the subjects, while simultaneously measuring induced neural correlates. The setup, depicted in Figure 1.14 (a) consisted of a circular board with sockets for integrating the distinct stimulation blocks and a trigger system to link the onset of stimuli to the recorded EEG signals. Thereby the stimuli differed in spatial frequency, i.e., different interridge-distances (λ) and groove depths (d). Stimulation was performed by sliding the various stimulation blocks at a constant rotational speed underneath the static fingertip, with fingerridges oriented perpendicular to the direction of rotation. Figure 1.14 (b) shows the temporal profile of forces, which were recorded using a force sensor. The profiles exhibit three main phases which indicate the onset of stimulus (the very first contact with the stimulus), a phase where force steadily increases until reaching a plateau (sliding contact), and the offset of stimulus (the release of fingertip-block contact). During experiments neural correlates were recorded in a tactile discrimination task. Three different stimuli (target) and

a non-target stimuli (smooth stimulation block) were included in the study. During each run of the TWS the amount of target and non-target stimuli were varied, i.e., 8 block positions in all were randomly occupied by targets and non-targets. Subjects task was to report on the amount of perceived target stimuli after each run and to give a total number on targets at the end of the experiment.

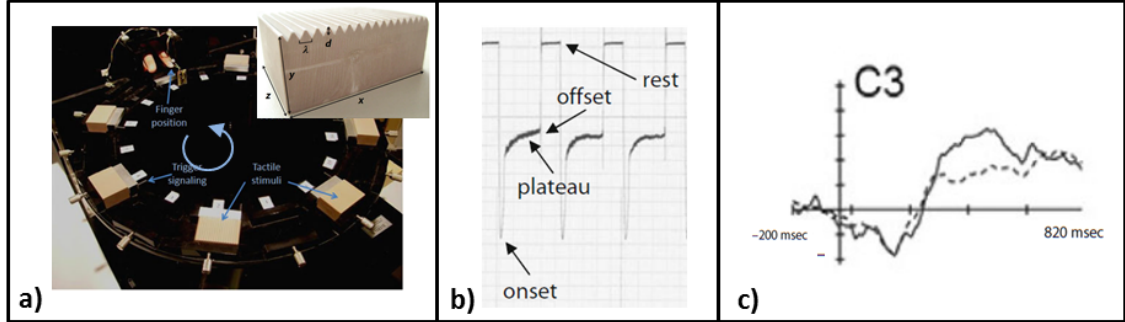


Figure 1.14: Device to present textured stimuli to touch. a) The tactile spinning wheel (TSW) with finger position and stimulation block (upper right). b) Forces recorded during stimulation show three phases: stimulus onset - a steadily increase in force until reaching a plateau - stimulus offset. c) ERP waveforms for electrode C3 (dashed line: unattended ERP; solid line: attended ERP) (Avilés et al., 2010)).

Figure 1.14 (c) shows the ERPs obtained for the attended (target stimuli) and unattended (smooth block) stimulations. The results clearly demonstrate that the attended case (solid line) revealed a P300 component, while for non attended stimuli the P300 component was absent. Furthermore, subjects reached a detection rate of almost 100% for the correct counting of target stimuli. However, the authors presented a device that allows for the investigation of surface textures and showed attentional based results (P300 component) but did not report on the induced vibrations due to the different tactile stimuli.

However, investigations with respect to the distinct EEG frequency bands showed synchronization effects of oscillatory activity in especially the β band, which is believed to be a marker for movement effects. Hence, this indicates that apart from sensory also motor cortex is activated in tactile experiments when actively exploring a material's surface. In this context, Pfurtscheller et al. (2001) performed experiments by mechanically stimulating the static fingertip in order to assess information on whether poststimulus β oscillations occur in the absence of the active movement of the finger. Figure 1.15 (a) shows the stretched finger and the stimula-

tion device, which consisted of four pins (0.7mm in height and 0.3mm in diameter) for stimulating the fingertip in a vertical manner. EEG electrodes were attached over the sensorimotor cortex and the obtained data was bandpass filtered in the β band classified into three bins (12-16Hz, 16-20Hz and 20-24Hz). To check for band power changes over time event related desynchronization (ERD) and event related synchronization (ERS) were calculated.

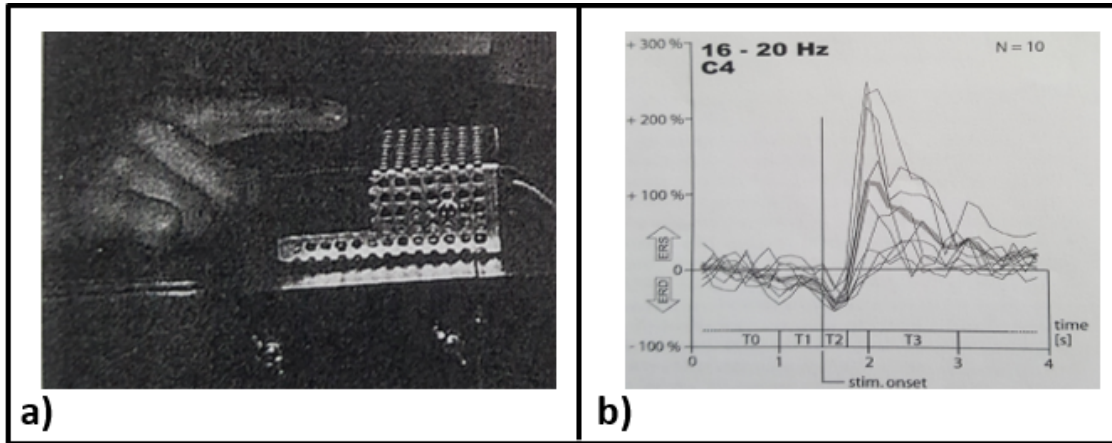


Figure 1.15: Tactile skin stimulation of the fingertip and induced bursts of β oscillations a) Dot matrix printer head for stimulating purpose. b) Grand average ERD and ERS for the 16–20Hz frequency band over four distinct time windows (T0: reference; T1: anticipation; T2: ERD range; T3: ERS range). The y-axis represents the percentage values of band power deviation from the baseline (horizontal solid line) Pfurtscheller et al. (2001)).

Figure 1.15 (b) shows the grand average ERD/ERS curves for the selected 16-20Hz frequency band (this sub β band showed the largest differences) plotted over distinct time windows (T0, T1, T2, and T3). As depicted, relative to the baseline (T0, no effects here), an initial blocking of β oscillations (500msec previous to stimuli onset, T1) followed by a decrease in synchronization (ERD, from onset until 250msec) establish. Subsequently, synchronization of β oscillations at approximately 250msec with a maximum centered within 1 sec after stimulus onset became apparent, indicating modulations of motor cortex specific β oscillations. Those results, however, underpin the fact that the stimulation of a static fingertip with its mechanoreceptive afferences can also modulate β oscillations originated from the motor cortex. The authors furthermore concluded that the anatomical connections of ventral posterior lateral axons of the mechanoreceptors via cortico- cortical projections to the motor

cortex may be responsible for this.

In the study conducted by Hashimoto (1987), the authors investigated SEPs elicited by short air-puff stimuli with varying intensities and stimulation frequencies delivered to the right hand. To do so, they developed a high-speed air control system (see Figure 1.16, a) with the air nozzle oriented perpendicular to the stimulation site. The air puffs had a diameter of 1.8mm and a cross sectional area of 2.5mm^2 . Stimulus intensity was controlled by the pressure applied to the air control system and varied between $0.5\text{--}6\text{ kg/cm}^2$, resulting in air puffs with respective peak forces of $0.1\text{--}1.5\text{N}$.

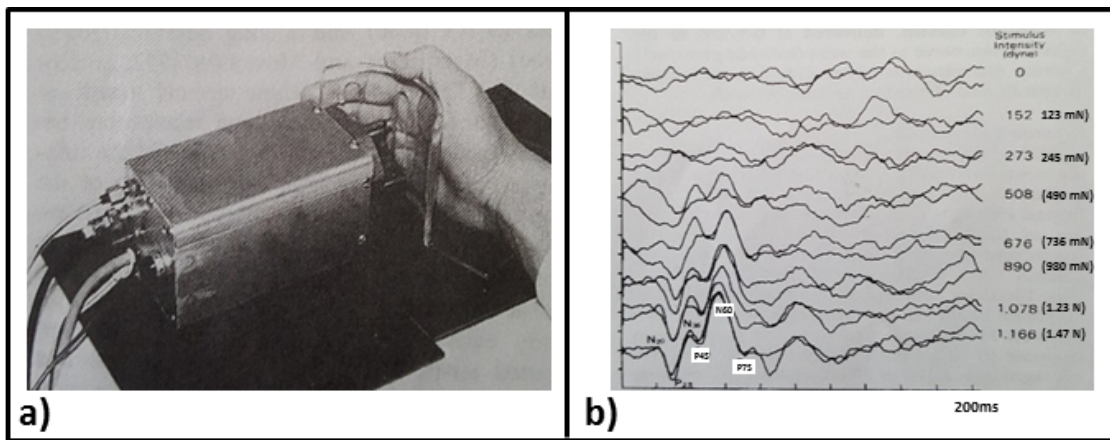


Figure 1.16: Stimulation of the hand due to air-puffs. a) Experimental setup developed in Hashimoto (1987). b) Early SEPs recorded at varying stimulus intensities (low to high from top to bottom) (Hashimoto et al., 1992).

Figure 1.16 (b) shows the elicited SEPs recorded from the contralateral sensory area. The variation in stimulus intensity shows clear components with higher amplitudes and decreased latencies, following a W-shaped constellation (N20, P27, N35, P45, N60 and a P75) for intensities > 400 dynes (appr. 360mN). A stepwise variation of the stimulation frequencies from 0.5 to 3Hz resulted in a lowering of amplitudes and increasing of latencies. However, the most interest result drawn from the study was the investigation of a negative correlation between the stimulus intensity and the SEP latencies (see Figure 1.16, b) most visible for the prominent N60 peak. Similar results have been observed for the tactile stimulation of the sole of feet, where the authors analyzed early SEPs as function of the stimulus intensity (Hashimoto et al., 1992). They found that the ERP amplitudes increased with stimulus intensity, and

that the latency of the peaks decreased.

It is noteworthy that in the above presented studies the main focus was on neurological aspects. However, to also present some insights focusing on tribological aspects describing the physical processes at the fingertip/object interface one last study is presented. Closely related to the work presented in this thesis, Darden and Schwartz (Darden and Schwartz, 2015) give insights on the physical contact and forces acting between fingertip and Braille-dots embossed into paper. Friction is believed to play a important role in Braille-reading. Thus, the study was to investigate the frictional mechanism, i.e. adhesion, deformation and coefficient of friction μ (CoF) during Braille-reading. Two points of investigations were pursued - on the one hand the sliding behaviour between the fingertip and one single dot and on the other hand the sliding contact across multiple dots. For the single dot experiment (SDE) stripes of thick paper with dots embossed and stabilized from the underside to maintain the shape during sliding were prepared. For the multiple dot experiment (MDE) dots were embossed on paper sheets taking into consideration a directional spacing, either vertically or horizontally (see Figure 1.17 c and d). In all measurements normal and friction forces were measured upon a left to right sliding of the fingertip over the dots. Figure 1.17 (b), (c), and (d) illustrate the results for the CoF for the SDE, the MDE- vertical arranged, and the MDE-horizontal arranged, respectively. For the SDE experiment the sliding contact resulted in two distinct CoF portions, indicating the contact with the background of the paper (appr. 0.25, white circled) and the traverse of the dots relief (appr. 0.3, green circled). Since fingertip is slid from left to right and thus the traversing of both dots took place simultaneously, friction force obtained in the case for multi dots arranged vertically (see figure 1.17, c) was found to behave similar as in the single dot experiments. If dots are horizontally oriented (see figure 1.17, d), the temporal evolution of the CoF differed from the other two cases. The sliding of fingertip count for two more plateaus, indicating the contact with the background (1), the contact with one dot (2), the contact with two dots (3) and vice versa. As the distance between the dots is varied, no changes could be observed for the CoF with respect to MDE vertically arranged. In the horizontal case, however, reducing the distances resulted in CoFs similar to the SDE-case. With respect to the contribution of deformation and adhesion aspects on the CoF in a sliding contact as proposed, the authors concluded that deformation of the fingertip is the driving force while adhesional effects could be neglected.

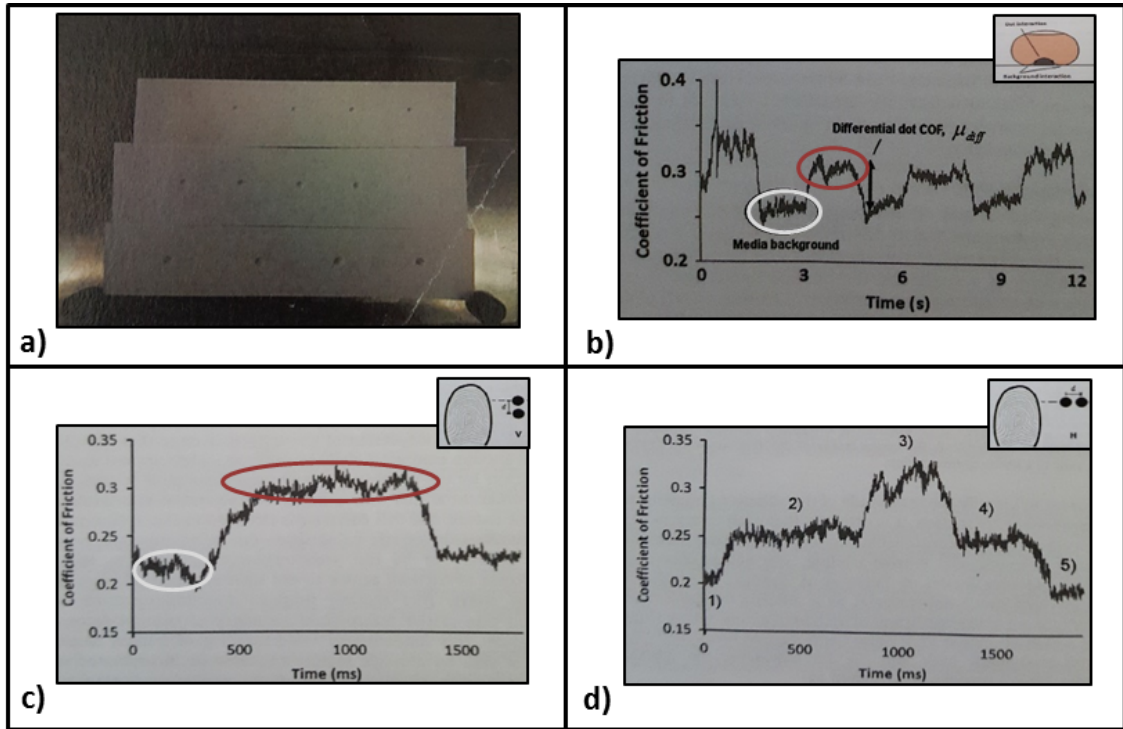


Figure 1.17: Skin behaviour on coefficient of friction (CoF) in Braille reading. a) Three paper samples of embossed dots with varying heights (from top to bottom: 0.48, 0.75 and 1mm) prepared for SDE b) SDE results showing the CoF for left to right swipe of a fingertip across dots indicating two stages of friction. c) CoF for the MDE in a vertical arrangement of dots ($d = 6mm$). For this constellation of dots, a variation of the interdistance parameter d did not influenced the frictional behaviour. d) CoF for the MDE in a horizontally arrangement of dots ($d = 6mm$) showing distinct phases of the CoF: 1&5) -background, 2&4) -single dot, 3) -multi dot. For this constellation of dots, a variation of the interdistance parameter d influenced the frictional behaviour, where a reduced d (2.5mm) resulted in a single frictional plateau (Darden and Schwartz, 2015).

1.6 Contribution of this Work - Motivation

The overall goal of the emerging scientific discipline of haptics is the understanding of the causal chain from the contact of the skin with materials to the brain dynamics representing recognition of and emotional reaction to those materials. Therefore, it is of great importance to consider and integrate perspectives from two usually not connected and associated disciplines, namely the neural engineering and the materials research field, especially the tribology field. To discover relations between surface texture, tactile friction, and the resulting brain dynamics the main contribution of this work was the development of a framework, including tools and methods, for extracting reliable and prospective measures. Towards this goal the initial step was the implementation of an appropriate setup for the integration of two existing experiments. The first was a dedicated tribometer for the measurement of sliding friction between materials and the fingertip of a test person. The second was a setup for electroencephalographic (EEG) measurements with high bandwidth over extended periods of time.

To test the setup a preliminary study was conducted. A rigid aluminum block with machined ridges on the surface was used for stimulation purposes by sliding it along the fingertip. The stimulus event was the very first contact between the block and fingertip, i.e., the first contact after a non-stimulation period. Results initially seemed to indicate an antiproportional relation between the friction intensity and the latency of the prominent P100 wave, described in Öezgün et al. (2015), but did not show consistency across subjects.

Brain dynamics are complex and the statistical methods for the extraction of signals related to frictional stimuli require repeated trials with defined trigger, indicating the start of a particular stimulus induced event related potential (ERP). The key ingredient of the main study was therefore a surface with switchable roughness, namely a Braille-display, i.e., a dense array of programmable extending pins which allows for the design of studies with varying stimulus pattern and arbitrary inter-stimulus intervals. This Braille-display is usually used for blind and visual impaired people in providing access to information by palpation. Each time when pins are switched a trigger-signal is recorded along with the EEG indicating the exact start of an ERP sequence in time. In contrast, for the preliminary study the extraction of ERP trials was based on a "*virtual*" triggering. Thereby "*virtual*" means that for each single-trial the change in physical force, when fingertip and block contacted

each other for the very first time, was computationally detected and defined as the trigger-point indicating the start of the respective ERP sequences. For further analysis on the experimentally obtained and pre-processed data, the next key step was the development of a data processing pipeline. The first method relies on the analysis of tactile evoked responses based on phase synchronization effects to reveal the degree of phase locking of the ERPs. Therefore instantaneous phase information was extracted which enable for the investigation of inter-trial wavelet phase synchronisation stability (WPSS). Additionally, using the WPSS method we were able to compare between different stimulation paradigms for time intervals of the the N50 and P100 waves where corresponding results an findings will be formulated in Özgün et al. (2018a).

In the research field of auditory ERPs it was shown that the relation between stimulus-intensity and the latency of neural response exhibit a antiproportional behaviour (Corona-Strauss et al., 2009). For tactile perception there is little information regarding this relation. In order to verify this relation another method was introduced, which instead of averaged trials focuses on the analysis of single-trial sequences of tactile evoked ERPs. Amplitudes and latencies of ERPs vary from trial-to-trial. The linear averaging of a certain amount of trials might average out important information, lead to changes in shape, diminishes amplitudes and thus might be insufficient to reveal changes in cognition (Ouyang et al., 2011). In contrast, ERP-images as the result of repeated stimulation include subsequent trials arranged line by line where any event related phenomenon might be better detectable and not distorted. However, since tactile induced ERP sequences are small in amplitude (lower μV range) important information could be masked by background EEG which leads to a poor signal-to-noise ratio (SNR). To enhance the signal-to-noise ratio (SNR) of single-trial ERPs, a denoising/restoration technique was introduced. The method basically consists of a combination of two approaches where a 2-D filtering of the ERP-image is followed by the denoising of the instantaneous phase information of the respective ERP-trials. For the image filtering procedure the nonlocal means method (NL-means), which takes advantage of the self-similarity of image-patches (few pixels of the image) across the image is used. For each patch a weighting factor indicating the self-similarity with respect to the other remaining patches is calculated and enhanced in contrast accordingly. The second approach focuses on the instantaneous phases of single trials by applying the cyclic variational denoising of second order as in Bergmann et al. (2014) to the indi-

vidual frequency bands up to 30Hz. In this way, neural correlates of the exogenous (friction profiles) and endogenous (e.g., dynamic brain states) processing become noticeable as more clear traces in the time-domain ERP-images. Preliminary results were published in Öezgün et al. (2015) indicating an antiproportional relation between the trace-latency and the stimulus intensity of tactile induced ERPs.

The stimulus intensity was defined to be the frictional change, i.e., the absolute difference in friction-force calculated between the portion of the signal where the fingertip is not stimulated and the portion of the signal where stimulation is performed. Tribological results obtained between the fingertip and Braille-display for different stimulation paradigms have been described in the recently published work Özgün et al. (2018b). It was concluded that the direct evaluation of ERP time-domain information (amplitudes and latencies) seems not to be sufficient enough in distinguishing between different frictional stimuli exposed to the human fingertip indicating the complexity of the tactile sense.

This work addresses the challenges listed above by providing pioneering steps in understanding basic neural, as well as tribological aspects in a strongly interdisciplinary environment.

Structure of the work

The structure of the work is as follows: In Chapter 2, a detailed explanation of the materials and methods is provided. The materials part is a detailed description of the measurement setup with respect to the tribological as well as the neural measurement unit. This section also comprises an explanation of the stimulation paradigms as well as the EEG protocol and the pool of included subjects. The method part includes on the one hand the procedure how data was acquired and pre-processed, and on the other hand a description on the methods used for the analysis. This is provided both for the neural correlates of haptic perception as well as the obtained tribology based data sets. In Chapter 3, the experimental results are presented. Interrelations between EEG and friction data are depicted and described in a final step. The fourth chapter gives a discussion on the outcome of this work followed by an outlook about possible future work. Conclusions on the basis of data and findings are drawn at the end of this work.

2 Materials and Methods

This chapter provides a detailed account of the underlying framework of this thesis. Within this framework two approaches have been implemented, in order to evaluate the simultaneous measurement of fingertip friction and EEG recordings, as a method to investigate contributions of friction to the process of haptic perception. Core difference between the two approaches was the used stimulus material. In a preliminary study (further on denoted as *Part (A)*) a passive rigid block with a machine-structured surface was used, while for the main study (*Part (B)*) the stimulation was conducted using a programmable Braille-display with a matrix of actively switchable pins.

The organization of this chapter is as follows. First, information is provided about the participants, the experimental design and the distinct stimulus materials used in the studies. Subsequently, a detailed description on the measurement setup, settings and adjustments that have been applied to measure frictional properties as well as neural activity during tactile stimulation of the fingertip is given. The later part of this chapter describes the data processing pipeline which includes the process by which data was collected and the methods applied for analyzing and interpreting the data obtained within this work.

2.1 Participants and Inclusion Criteria

In total, thirty right handed volunteers (24 males and 6 females with a mean age of 30.5 ± 6.6) all employees from the Leibniz Institute for new Materials (INM, Saarbrücken, Germany), participated in the two studies. The first study included ten, while the second twenty subjects. All measurements were performed in accordance to the declaration of Helsinki and approved by the responsible Ethics Committee at the medical council (Ärztchamber) of the state of Saarland, Germany (identification number: 112/17).

Before entering the experimental phase, volunteers were asked for known neurological diseases, whereby excluded when affected. After experiments were done, acquired data was visually inspected for artifacts (e.g. huge oscillations due to eye blinking or movements) and if trigger signals have been recorded properly. An-

other quantification was introduced to evaluate the quality of the obtained ERP sequences, i.e. signals were objectively evaluated with respect to the reproducibility. To check the consistency and stability of the measured EEG signals, a correlation waveform index (CWI) was defined as suggested in Strauss et al. (2013) and Bernarding et al. (2013). The CWI was used to support objectively the visual detection of a clearly identifiable waveform of the N50-P100-N140 complex of the measured EEG signals. For this, each single EEG response to each stimulus was separated into sub-matrices, containing either all *odd* or all *even* sweeps. Then, the matrices were separately averaged and the resulting vectors x (average of the even sweeps) and y (average of the odd sweeps) were saved. After this, the correlation coefficient $\rho \in [-1, 1]$ between the resulting waveforms x and y was calculated.

$$\rho := \frac{\sum_{i=1}^N (x_i - \bar{x})(y_i - \bar{y})}{\sqrt{\sum_{i=1}^N (x_i - \bar{x})^2} \sqrt{\sum_{i=1}^N (y_i - \bar{y})^2}}, \quad (2.1.1)$$

where $\bar{x} := N^{-1} \sum_{i=1}^N x_i$ and $\bar{y} := N^{-1} \sum_{i=1}^N y_i$. After comparing different tactile evoked somatosensory responses with the corresponding correlation coefficients ρ , a CWI of 0.4 was defined. Correlation coefficients ≥ 0.4 , calculated for the interest range of the EEG data (stimulus onset until 300ms), corresponds to a clearly identifiable tactile induced somatosensory waveform according to a visual analysis by an expert.

Somatosensory evoked potentials are small in amplitude (smaller 10 μV) and prone to noise. To extract the tactile evoked neural correlates, the segmented EEG data was checked for artifacts. For this, artifacts were rejected if the maximum amplitude threshold of each EEG-trial exceeded $\pm 20 \mu\text{V}$.

The subjects inclusion criteria for the studies were: (i) no neurological diseases, (ii) CWI higher than 0.4, (iii) at least 80 % artifact free EEG data.

Finally, for the study in Part A (stimulation block), a total of 9 subjects (8 males and 1 female) with a mean age of 28.6 ± 4.6 were included in the analysis. For the study in Part B (Braille-display), a total of fifteen subjects (11 males and 4 females) with a mean age of 25.9 ± 3.1 were included in the analysis.

2.2 Experimental Design and Stimulus Material

Experiments were carried out in a quiet, darkened room and lasted approximately 2 h including preparation of the subject and electrodes placement. Participants sat in a comfortable chair with armrests, whereby for the right arm an extra armrest especially adapted to the experimental procedure was used. This armrest served for the support and to prevent tiredness and uncomfortableness due to a stretched arm during the whole experiment. To prevent any auditory influences on the ERPs (e.g. the sound of the stages) foam ear plugs and a headphone were worn. The volunteers were asked to relax, not to fall asleep, to close their eyes and to avoid any motion during measurements. They were also asked not to direct their attention to anything specific but to rather attempt a fully relaxed state of mind. That state should be maintained until the experimenter gave a tap on their shoulder. The palpation of a surface's texture comprises a bundle of contributions which elicit manifold impressions and goes beyond just mechanoreception. It is without doubt that in the course of sliding and moving of fingertips also the kinesthetic sense (sensation of movement in muscles, tendons and joints) contributes to the perception. This combination enables to detect smallest irregularities in surface topography (down to micro meters) but also enlarge the complexity because of continuously changing parameters. To reduce the complexity and the amount of parameters that contribute to the overall tactility, subjects need to take a passive role. For this, in contrast to the stimulus which is slid, the index finger of the participants was kept stationary using a holding plate with an oval window at the bottom. In this way the fingertip was exposed to the stimulus which was presented in a reciprocal-manner (forward and backward), each direction had 180 runs, lasting in a total of 30 min. The sliding velocity of the stimuli was kept constant (7 mm/s) which is relevant to a tactile exploration of a surface or texture. The experimental procedure, schematically shown in Figure 2.1 proceeded as follows. First, participants were asked to place their right index-finger on the holding plate, a guiding frame with circular opening at the bottom. The stimulus apparatus was then slid back and forth along the exposed fingertip area. Within each slide the stimulation was presented in a subsequent manner. The course of one single trial consisted of a stimulation period (yellow part) where prior to and after to no stimulation was conducted (blue part). In this way forces acting between the fingertip and the stimulus material as well as neural correlates were collected simultaneously. In order to become accustomed

to the experimental environment, at the beginning of each measurement session the setup and the procedure were introduced to the participants followed by some test-slides.

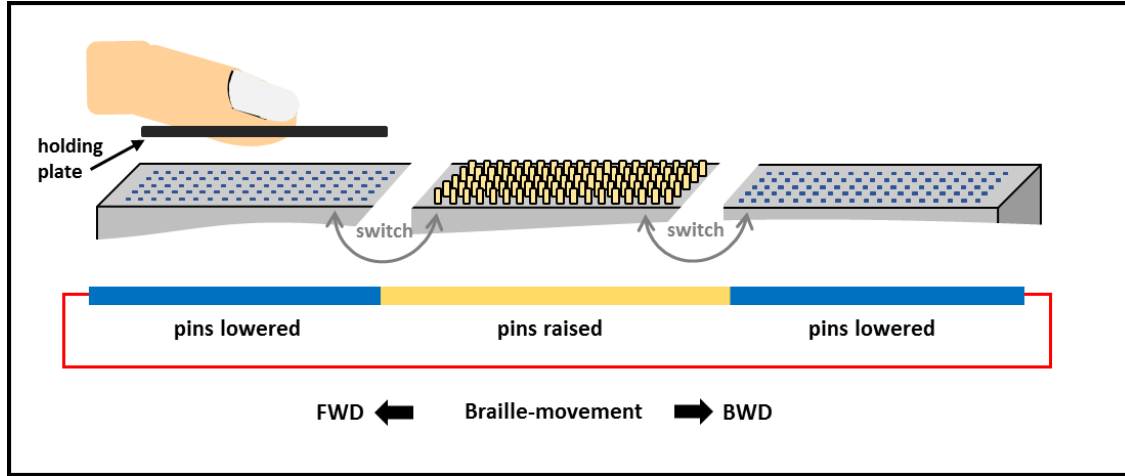


Figure 2.1: a) Schematic illustration of the stimulation procedure using the example of the Braille-device. During each course the fingertip is exposed to the stimulation (i.e., the raising of pins) in a subsequent manner (from blue over yellow to blue).

The experimental design was basically the same for both studies, but they differed in the stimulus material. Figure 2.2 (a) depicts the typical measurement environment for the investigated studies. The participants sat in a comfortable chair with a guiding armrest and the right index finger placed on the the holding platform as requested during measurements.

Part A: Structured Surface Figure 2.2 (b) shows the aluminium block as integrated for the tactile stimulation of the fingertip in the preliminary study. The block consisted of ten triangular shaped ridges with centre-to-centre distances of 1mm and base-to-cone heights of 0.5mm, arranged perpendicular to the sliding direction.

Part B: Braille-display For this study, a programmable Braille-display was integrated for stimulation purpose. Figure 2.2 (c) depicts the Braille-display. The display consisted of a matrix of 32x5 equidistantly arranged pins, with each pin individually controllable. The dot spacing in each direction, i. e. centre-to-centre distances between the pins are 2.5mm with a maximal stroking height of 0.6mm.

2.2 Experimental Design and Stimulus Material

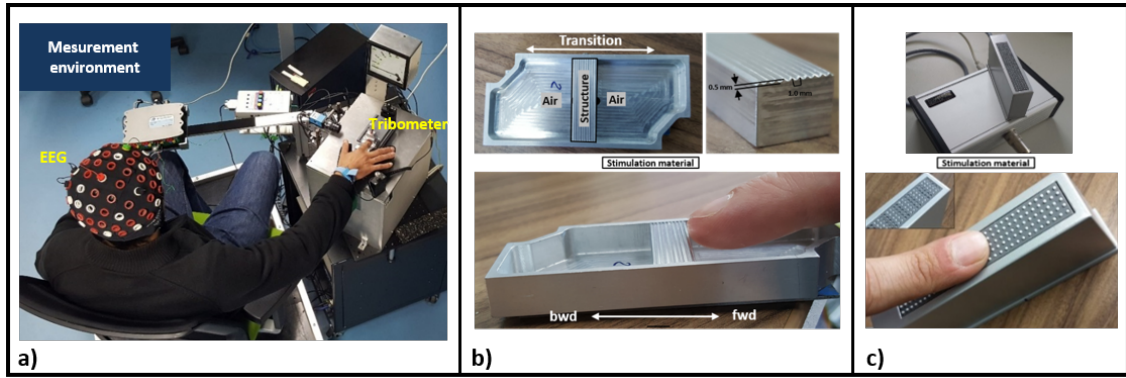


Figure 2.2: a) Measurement environment. The setup consisted of a tribometer and the EEG system. b) Part A: Tactile stimulation of the index finger performed by a sliding of a static surface along the fingertip. c) Part B: Tactile stimulation of the index finger performed by sliding of a Braille-display of actively switchable pins along the fingertip.

At the beginning of each measurement the Braille-display was adjusted in height such that there was a light contact with the fingertip when the pins were lowered, whereas the raising of pins did contact the fingertip. This was performed to mimic a realistic Braille-reading scenario. During each course in sliding the Braille-display along the fingertip, the stimulation consisted in the raising of either one, three or five lines of pins. Thereby, the pins were randomly raised to the subject's fingertip for a certain time span and lowered again, hence leading to a mechanical stimulation of the fingertip.

The diagram illustrates the experimental setup for the Braille-based EEG interface. It consists of the following components and connections:

- PC1 (LabView):** Controls the stage and acquires tribological data, generating StS and BtS signals. It is connected to a **Sound card** and a **USB** port.
- PC2 (Matlab/Simulink):** Acquires EEG data and trigger signals. It is connected to a **USB** port.
- BNC-2110:** An interface box with **AO** (Analog Output) and **Trigger out** ports, connected to PC1.
- Amplifier:** Receives signals from the BNC-2110 and outputs **x-axis**, **y-axis**, and **z-axis** signals.
- g.TRIGbox:** Receives **Braille-trigger signal (BtS)** and **Stage-trigger signal (StS)** from PC1. It outputs **BtS** and **StS** signals to the **g.USBamp**.
- g.USBamp:** Receives **BtS** and **StS** signals from the g.TRIGbox and outputs **EEG** signals to the **Headphones**.
- Braille-system:** Receives **Operate** signals from PC1 and the **Stage-controller**. It is connected to the **Braille-display**.
- Stage-controller:** Receives **Operate** signals from PC1 and the **Braille-system**. It outputs a **Stage** signal to the **Braille-display**.
- Finger holding system:** Holds the **Braille-display**.
- Braille-display:** Outputs **fwd** and **bwd** signals to the **Force-sensor**.
- Force-sensor:** Outputs **fwd** and **bwd** signals to the **PLS-85**.
- PLS-85:** The base unit for the **Braille-display** and **Force-sensor**.

The tribological signals obtained during the sliding contact between the fingertip and the Braille-display were captured by a three dimensional compact-sized

2.3 Measurement Setup

force sensor (K3D40, ME- Meßsysteme, Germany) mounted onto a translation stage (PLS-85, PI-Micos, Germany). For each axis of the force sensor, an one-channel straingauge amplifier (GSV-2FSD-DI, ME-Meßsysteme, Germany) was used and connected to a shielded analog input adapter (BNC2110, National Instruments). To collect the data, the BNC2110 was linked to an analog to digital converter (PCI 6229, National Instruments), a built-in component, that provided the personal computer (PC1) with the data. Each time when the translation stage was moved (forward and backward), a trigger signal (StS) was send out of from the PCI 6229 and transmitted via the BNC2110 to the trigger conditioner box (g.TRIGbox, Guger Technologies GmbH, Austria). The onset of the stimulus was defined as the raising of the Braille pins. To indicate this event and to be able to extract the respective portions of the EEG-signal, a second trigger signal was send out each time when the pins were raised (Braille-trigger signal - BtS). This trigger-signal was generated by the software of the Braille-system on PC1 and transmitted via the sound-card to the g.TRIGbox. The Braille-display underneath the fingertip was moved with a stage-motion controller (SMC corvus-eco, PI-Micos, Germany) controlled by the laboratory virtual instrument engineering workbench *LabView* (Version 7.10, National Instruments) installed on PC1. Both, the Braille-system and the stage-controller were operated via the USB computer interface of PC1. Physical forces (normal and friction) acting between the fingertip and the respective stimuli were digitized at 512Hz. EEG signals are quite small in amplitude and prone to noise. Thus, the EEG was recorded using a commercially available biosignal amplifier g.USBamp (Guger Technologies , Austria) which was connected to a second personal computer (PC2). The PC2-system thus acquired the brain activity and the trigger signals (StS and BtS) provided by the g.TRIGBox and g.USBamp. EEG-electrodes were attached to the scalp over the somatosensory cortex, using an electrode cap with distinct electrode-sites following the international 10-20 system. Electrodes were placed contralateral (C3, Cp3), ipsilateral (C4) and mid-line (Fz) to the stimulation site, with a common reference at vertex (Cz) and the ground electrode placed at the upper forehead (nasion). Electrode impedances were kept below 5k Ω . EEG-data was digitized at 512Hz and offline filtered, using a zero-phase band-pass FIR filter with cutoff frequency of 2 and 32Hz, respectively. For the purposes of the PC2-system the licensed mathematical computing software *Matlab&Simulink* (Version R2015b, Mathworks) was used.

2.4 Data Processing Pipeline

2.4.1 Preparation and Segmentation of the Data

Preparation of the Data

An important step was the synchronization of EEG and force signals. EEG and force data were recorded with different systems (g.USBamp controlled by MatLab for the EEG data and PCI-6229 controlled by LabView for the force data) at the same sample rate of 512 Hz. A relative difference in the actual sample rate in the order of 2×10^{-5} made it necessary to re-sample the force data in order to match the trigger signals in EEG and force data within 1 ms over the duration of 30 min. Let $N = t \cdot f_s$ denotes the new length for the corrected force-data, where $t = l \cdot t_{trial}$ is the acquisition-time of the Matlab-system, with l the length of the EEG-vector, t_{trial} the acquisition time of a trial, and f_s the sampling frequency. For the LabView-system the corrected acquisition-time is obtained by $t - \Delta t$. Each n -th sample in the Matlab-system is assigned to a new sample $\alpha = n \frac{t}{t - \Delta t}$ for the LabView-system, which lies between $\lfloor \alpha \rfloor$ and $\lfloor \alpha \rfloor + 1$, whereby $\lfloor \alpha \rfloor$ indicates the integral portion of α .

A corrected vector a_n is calculated, which resamples the force data to the sample-length of the Matlab-system

$$a_n = f_{\lfloor \alpha \rfloor} \cdot [1 - (\alpha - \lfloor \alpha \rfloor)] + f_{\lfloor \alpha \rfloor + 1} \cdot [\alpha - \lfloor \alpha \rfloor].$$

Figure 2.4 shows the effect of the resampling-process. When force data is segmented (for the segmentation procedure see next subsection) without resampling the onset of the force, indicated by the red dashed line, exhibit a time-shift of approximately 30ms towards the end of the measurement. However, when resampling is performed the time-delay is corrected. The onset of the force, which is the first contact between the fingertip and the Braille-pins, is now aligned for each single trial to fit the respective EEG-data.

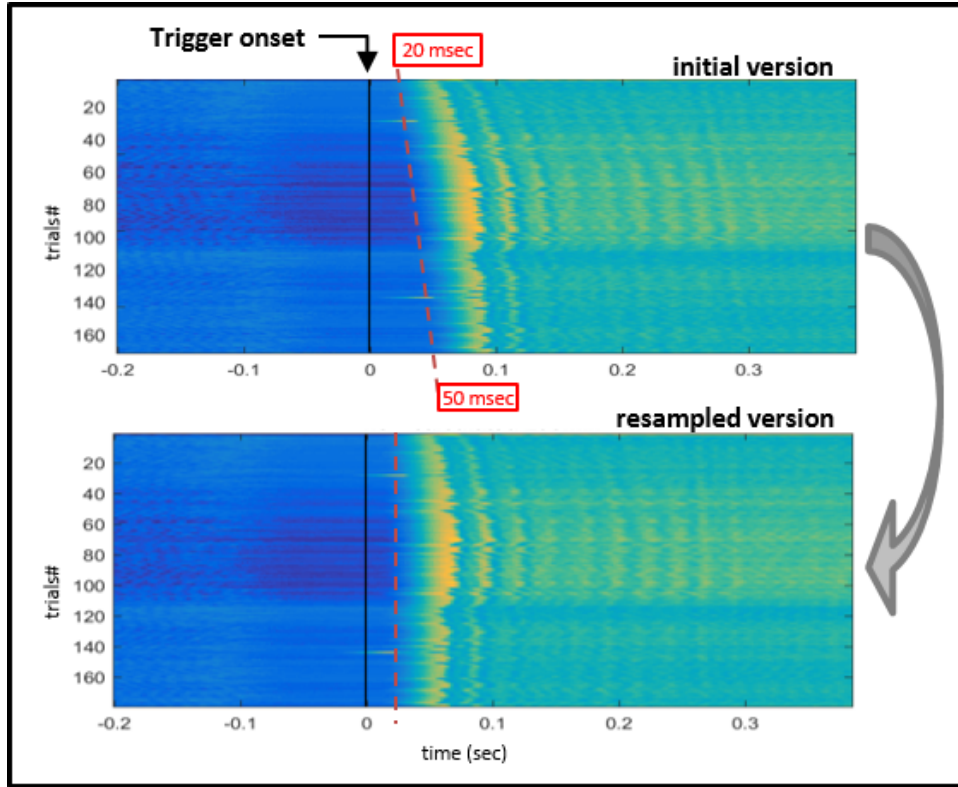


Figure 2.4: Resampling of the force data. Top figure shows the initial version while the bottom figure the resampled version.

Data Segmentation

Brain dynamics are complex and the statistical methods for the extraction of signals related to a external stimuli require repeated trials. Of huge importance are respective trigger signals, indicating the start of ERPs. The resulting matrices include single trials, i.e. single signals of subsequent trials arranged line by line resulting in so called single trials in matrix representations (see Figure 3.12, a). Any event related phenomenon will be revealed as a trace in the ERP-image. Thereby traces refer to potential maxima or minima which occur with a certain latency with respect to the event in most or all trials. Figure 2.5 depicts the schematic overview for the overall stimulation sequence including the pre/post - stimulation interval (pStI), the stimulation interval (StI) and the trigger signals. Each single trial, either forward (FWD) or backward (BWD), lasted 5 sec. The stimulation itself (StI - interval) was randomly chosen to be 1, 1.5 or 2 seconds within the respective run.

In this context FWD and BWD are defined as the direction the stage is slid relative to the subjects. FWD means towards proximal phalanx of the fingertip whereas BWD describes the stimulation of the fingertip towards distal phalanx.

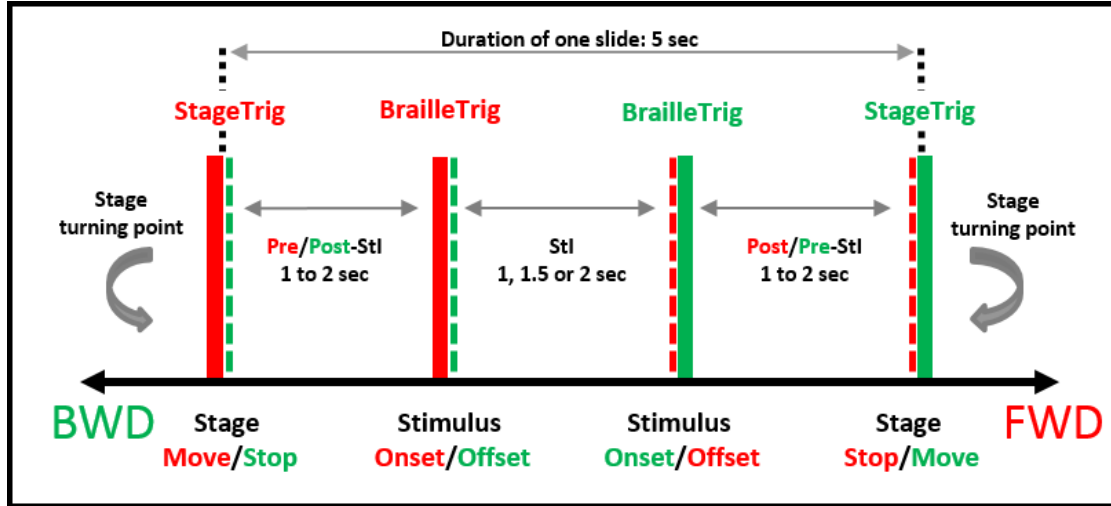


Figure 2.5: Schematic representation of trigger signals used for the segmentation of the data when Braille-display is used. The pre/post stimulus interval (StI) was chosen randomly between 1 and 2 sec, while the StI was defined as either 1, 1.5 or 2 sec. The inter-stimulus interval (ISI) varied between 2 and 5 sec. Red marked bars indicate the FWD-directed slide, whereas green the BWD-directed ones.

The pStI interval was kept between 1 and 2 sec, resulting in a overall random variation of the inter-stimulus interval (ISI) from 2 sec to 5 sec. For the stimulation of the fingertip using the Braille-display, as shown in Figure 2.5, trigger-signals are transferred when, a) the stage is moved (*StageTrig*), and b) whenever pins are raised (*BrailleTrig*). For analysis purposes, EEG and tribological data was segmented 200ms prior and 800ms after stimulus onset.

For the preliminary study in Part (A), when the machined block was used for stimulation-purposes (see Figure 2.2, b), only the *StageTrig* was used. Despite several options for integrating a trigger-mechanism indicating the finger-structure contact, including an electric trigger released when the fingertip was approaching the structure, EEG signals were always distorted, i.e. an electric cross-talk occurred. To overcome this problem and still manage to detect the ERP-trials, first data was segmented with respect to the stage-trigger and further on re-segmented to the stimulus onset in a computational manner described below.

Virtual triggering: Due to the stimulation procedure (see section 2.2, Part A) the very first fingertip-structure contact resulted in a noticeable change in force (see section 3.1, Figure 3.1) most pronounced in the morphological course of the normal force signals. On this basis, for each single trial and subject the portion of the normal force signal, including this transitional change in force, was scanned for a value lower than a calculated threshold. The threshold was calculated by taken into consideration the mean of the pre-stimulus interval plus two times the standard deviation of the mean of the pre-stimulus interval. The associated sample-number was then defined as a virtual trigger-point, i.e., defined as the stimulus-onset and saved for each trial. The lateral force and ERP trials were then re-arranged in a shifted manner using the computationally detected single trial onsets.

2.4.2 Step Intensity Calculation

After the segmentation of the force data, single trials are arranged line by line in matrices (see Figure 2.6, top). For further evaluation the step intensity (sI) was introduced. The sI indicates the change in force, i. e., the absolute difference between the baseline and the portion of the signal where forces reach the highest values. The sI is estimated by taken into consideration the time range $[-20, -60]$ ms of the pre-stimulus interval and the time range $[30, 70]$ ms of the post-stimulus interval as indicated by the grey boxes in Figure 2.6, top. Then the five (as a good compromise) lowest values for the pre-stimulus range and the five highest values for the post-stimulus range were identified, separately averaged and subtracted from each other. Figure 2.6 (bottom) schematically shows the estimation of the sI. The grey bullet points indicate the level of averaged pre- and post stimulus force intensities, while ΔF the difference. This procedure is performed for each single trial using a self-written and automated Matlab-script.

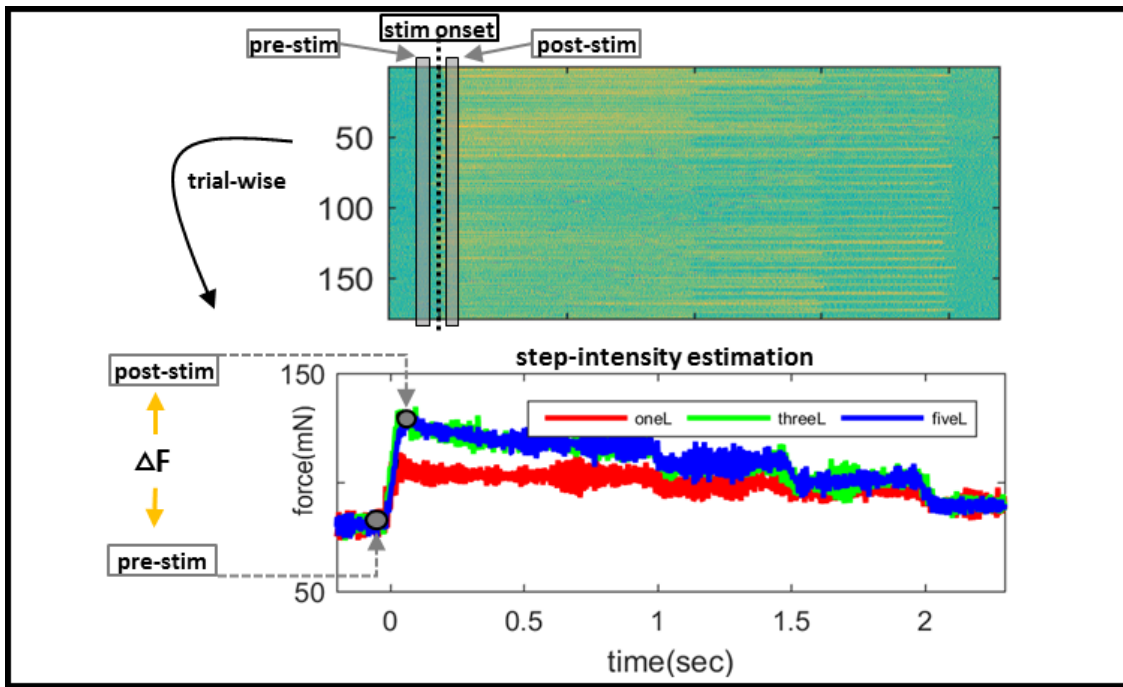


Figure 2.6: Estimation of the step-intensity (sI). Top figure indicates the range values are identified from. The bottom figure depicts the illustration of the sI-estimation. ΔF indicates the sI estimated between the grey bullet points.

2.4.3 Wavelet Phase Synchronisation Stability (WPSS)

In order to determine the quality and stability of the tactile induced responses over the stimulus sequence in terms of time-resolved phase information, the wavelet phase synchronization (WPSS) which is based on the phase information of single trials is introduced. Since the wavelet transformation is an key element of the WPSS, this section provides first a short description of the wavelet transform (see Daubechies (1992); Aguiar and Soares (2011) for more information) and thereafter the description of the WPSS calculation.

Continuous Wavelet Transform

The wavelet transform is an important tool to analyze time-frequency connections of a signal. Especially when signals show a non-stationary behaviour, this method is well suitable for investigating local characteristics of the signals (Klein et al., 2006).

The analysis procedure is to adopt a wavelet function (called analyzing or mother wavelet) $\psi(\cdot) \in L^2(\mathbb{R})$. The function chosen to be used as the mother wavelet has to satisfy the *admissibility condition* given by

$$0 < \int_{\mathbb{R}} |\Psi(\omega)|^2 |\omega|^{-1} d\omega < \infty. \quad (2.4.2)$$

Here $\Psi(\omega)$ is the Fourier transform of the wavelet. Note, that here one conclusion can be drawn to satisfy the above equation. The admissibility condition implies $\Psi(0) = \int_{\mathbb{R}} \psi(t) dt = 0$. This means that the transform of the wavelet function has zero mean, i.e., the wavelet oscillates around the time-axis. Let $\psi_{a,b}(\cdot) = |a|^{-1/2} \psi(\frac{\cdot - b}{a})$, where $a, b \in \mathbb{R}$, $a \neq 0$. By translation and dilation of the mother wavelet, a family of wavelet-functions can be obtained. Thereby the scale a regulates the width of the wavelet (stretching or compression), whereas the translation factor b shifts the wavelet in time. The continuous wavelet transform \mathcal{W}_ψ of a signal $x \in L^2(\mathbb{R})$, which maps the in the time-scale or time-frequency domain, respectively, is given by the inner L^2 -product

$$(\mathcal{W}_\psi x)(a, b) = \langle x, \psi_{a,b} \rangle_{L^2} = \int_{\mathbb{R}} x(t) \psi_{a,b}^*(t) dt, \quad (2.4.3)$$

where $*$ denotes a complex conjugation.

(Wavelet) Phase Synchronisation Stability (WPSS)

The WPSS has been applied to objectively quantify attention correlates of single-trial auditory late responses (ALR) (Strauss et al., 2005, 2008). Information on the stability of the instantaneous phase was also used in the auditory framework for the observation of attention (Low et al., 2007). In the tactile framework, however, assessments on the stability of the instantaneous phase can also be used to get information on the synchronisation of EEG data belonging to different stimulus paradigms. The synchronisation stability $\Gamma_{a,b}$ of a sequence $\mathcal{X} = \{x_m \in L^2(\mathbb{R}) : m = 1, \dots, M\}$ of M SEP-trials can be defined by

$$\Gamma_{a,b}(\mathcal{X}) := \frac{1}{M} \left| \sum_{m=1}^M e^{i \arg((\mathcal{W}_\psi x_m)(a,b))} \right|. \quad (2.4.4)$$

The wavelet phase stability in Equation 2.4.4 implies, that the synchronization stability yields a value in $(0, 1)$. Thus a perfect synchronization stability is given for $\Gamma_{a,b} = 1$ (phases are perfectly coherent), whereas for values close to zero a decreasing stability.

In this thesis, the chosen wavelet ψ was the 6th derivative of the complex Gaussian wavelet. The selection of this wavelet is based on its specific symmetry. It is known that this wavelet acts as a linear phase filter and avoids phase distortions Bradley and Wilson (2004). It should be noted that each scale a can be associated with a "pseudo" frequency f_a in Hz by $f_a = f_\psi / aT$, where T is the sampling period (inverse of the sampling frequency), and f_ψ the center frequency of the wavelet ψ .

Consecutive-Trial Resolving Analysis (CTRA)

On the basis of the previous section, instantaneous phases are checked for synchronization stability with respect to different frequency-bands (i.e., scales a) and time ranges. It is of great interest to evaluate where exactly in time and for which frequency-band the instantaneous phases show most stable synchronization effects. For this, WPSS trials for the extracted frequency-band and time range are averaged in a consecutive manner, i.e., trials are averaged iteratively in time and across participants. Mathematically this can be described as follows.

Let $U^I \subset Z$ denotes the set of samples that corresponds to this intervals obtained at stimulation intensity I . For a fixed scale a and time range U^I the M -consecutive

2.4 Data Processing Pipeline

representation (over trials) of the synchronisation stability in Equation (2.4.4) is defined by the sequence

$$\Lambda_{a,b}^I[M] = (\Gamma_{a,b}^1(\mathcal{X}^I), \Gamma_{a,b}^2(\mathcal{X}^I), \dots, \Gamma_{a,b}^M(\mathcal{X}^I)). \quad (2.4.5)$$

Then Equation (2.4.5) averaged for U^I is given by

$$\bar{\Lambda}_a^I[M] = |U^I|^{-1} \sum_{b \in U^I} \Lambda_{a,b}^I[M]. \quad (2.4.6)$$

In other words, Equation (2.4.6) represents the CTRA of the grand mean WPSS $\Gamma_{a,b}$ in Equation (2.4.4) estimated for the different stimuli, which indicates a trend in synchronization stability over time.

2.4.4 Denoising of ERP-images

In the signal processing step a key challenge is the separation of stimuli related neural activity from the EEG background. ERPs elicited by distinct external stimuli are quite weak in amplitude whereas the background EEG activity is large (Bronzino, 1999). Thus, in general data is linearly filtered within specific frequency bands and segmented with respect to the stimulus onset to facilitate the EEG analysis. Typically, when those stimulus-locked responses are arranged in ERP-matrices, traces become apparent. However, it still appears that background activity masks the appropriately processed ERPs and thus lead to a poor signal-to-noise ratio (SNR) (Glaser, 2012) where traces unfortunately become less visible. To enhance the SNR of single trial ERPs following denoising/restoration schemes are introduced and applied to somatosensory evoked sequences arranged in ERP-images.

Nonlocal Means (NL-means)

The nonlocal means (NL-means) method is a 2D image denoising/restoration scheme which exploits the self similarity of ERP-images by image patch methods and have attracted significant attention in recent years (Strauss et al., 2013; Buades et al., 2005). In contrast to 1D techniques, in general 2D methods allow to take into consideration regularities which might occur as the result of repeated stimulation. 2D methods like the nonlinear and anisotropic proposed in Mustafa et al. (2010) are powerful but need prior knowledge to successfully restore images. In particular they need directional and edge-based information on the trace for preservation purposes. The 2D nonlocal means (NL-means) method, however, exploits similarities between single trials and thus is not dependent on a prior knowledge. The procedure that is in general followed in the NL-means denoising consists of comparing each pixel with its closest neighborhood to other pixels either in the same patch or in other image patches. The result of the procedure is a weighted averaged similarity version of the input image of comparisons between similar pixels (see Buades et al. (2005); Awate and Whitaker (2006) for more information). The NL-means can be mathematically described as follows.

Let $\mathcal{A} = \{s_n \in \mathbb{R}^M : n = 1, 2, \dots, N\}$ be a set of N sampled somatosensory ERP sequences within the time-interval $[0, M/f_s]$, where f_s is the sampling frequency and M the sample number of a particular experiment. The ERP-images $S \in \mathbb{R}^{N \times M}$ can be constructed from \mathcal{A} such that $S = (s_1, s_2, \dots, s_N)^T$. For fixed physical stim-

2.4 Data Processing Pipeline

ulus settings, evoked individual sweeps s_n of S are time-locked to the stimulation and thus result in morphologically stable transient potential fluctuations that form the typical ERP-components. The direct result of such reproducible fluctuations yield regular changes and thus correlated intervals in the rows of S and induces self-similarity in the ERP-images. In contrast to conventional 1-D ERP denoising procedures $\mathcal{D}_1 : s_n \mapsto \tilde{s}_n$, where $\tilde{s}_n \in \mathbb{R}^M$ is a denoised version of s_n , we are interested in a denoising operator $\mathcal{D}_2 : S \mapsto Q$, where $Q \in \mathbb{R}^{N \times M}$ is the denoised version of the 2-D ERP image S . From $Q = (q_1, q_2, \dots, q_n)^T$ the individual denoised trials $q_n \in \mathbb{R}^M$ ($n = 1, 2, \dots, N$) can be extracted after the 2-D denoising process. Physiologically meaningful amplitude and latency changes can be extracted from q_n . Thus the D2-denoising approach allows for an integration of regularities over multiple stimulations into the denoising process. To apply the NL-means algorithm for the aforementioned \mathcal{D}_2 denoising of ERP-images, each sample (entry or pixel in S) s_i , $i = 1, \dots, J$, with $J = NM$, is replaced by a denoised version q_i in the following way: Each pixel s_i is compared together with its neighborhood to other ERP-patches (the very same neighborhoods of other pixels s_j). For each comparison a weight coefficient $\xi_{i,j} \in \mathbb{R}$ ($i, j = 1, \dots, J$) is assigned to the center pixel s_i , depending on the similarity of the image patches. In other words, the similarity of the neighborhood of s_i to the neighborhood of s_j . The restored/denoised entry q_i is now the weighted average of all the surrounding entries in S such that

$$q_i = \frac{1}{\gamma_i} \sum_{j=1}^J \xi_{i,j} s_j, \quad (2.4.7)$$

with $\gamma_i = \sum_{j=1}^J \xi_{i,j}$. Let I be an appropriate index set such that the 2-D patches of the ERP-image with the center s_i and s_j are given by s_{i+I} and s_{j+I} . We further introduce the vector $\varphi_\sigma = (\varphi_{\sigma,k})_{k \in I}$ which denotes a sampled version of a 2-D Gaussian kernel with standard deviation σ . The weights which quantifies the similarity of s_{i+I} to s_{j+I} are given by

$$\xi_{i,j} = e \left(-\frac{1}{\lambda} \sum_{k \in I} \varphi_{\sigma,k} |s_{i+I} - s_{j+I}|^2 \right). \quad (2.4.8)$$

The parameter σ is steering the influence of neighboring pixels on the weight and $\lambda > 0$ is controlling the amount of denoising. The application of Equation 2.4.7 to all

pixels in the ERP-image finally yields its denoised version Q . Each row in Q is now the denoised single trial q_n of $s_n (n = 1, \dots, N)$, but in contrast to 1-D procedures, stemming from a \mathcal{D}_2 -denoising process. For the somatosensory ERPs in this work following settings were applied. We used a 10x10 patch-size, $\sigma = (2.5, 5.0)^T$, and $\lambda = 4000$.

2D Phase Valued Denoising

Apart from denoising of data based on similarities observed in ERP-images, it was also demonstrated in Corona-Strauss et al. (2009), that time-domain information is highly linked to regularities of the phase information across trials. Thus, denoising can also be applied to the instantaneous phase information of single sequences.

Let $\mathcal{A} = \{s_n \in \mathbb{R}^M : n = 1, 2, \dots, N\}$ be a set of N sampled somatosensory ERP sequences within the time-interval $[0, M/f_s]$. Here M denotes the sample number and f_s the sampling frequency. From \mathcal{A} the single trial matrix $S \in \mathbb{R}^{N \times M}$ can be constructed, such that $S = (s_1, s_2, \dots, s_n)^T$, where in the case when physical stimulus settings are kept constant, individual sweeps s_n are time-locked to the stimulation. The Hardy space projected version $G \in \mathbb{R}^{N \times M}$ with $G = (g_1, g_2, \dots, g_n)^T$ is computed by the Hilbert transform of S for a narrow frequency band (Gaussian filter centered at f_c) with a full width at the half maximum (FWHM) of τ (width of the Gaussian distribution).

The single trial matrix of the instantaneous phase $\Theta \in [-\pi, \pi)^{N \times M}$ is now simply given by $\Theta = (\vartheta_1, \vartheta_2, \dots, \vartheta_n)^T$ with $\vartheta_n = (\vartheta_{n,1}, \vartheta_{n,2}, \dots, \vartheta_{n,m})$ and $\vartheta_{n,m} = \arg(g_{n,m}) (n = 1, 2, \dots, N, m = 1, 2, \dots, M)$.

The remaining challenge is the removal of noise in the phase valued data. Therefore the recently developed variational approach in Bergmann et al. (2014) and Schubert (2016), which introduces a denoising of phase valued data by minimizing first and second order differences is used. For our 2-dimensional data Θ the functional to be minimized consists of horizontal and vertical cyclic first and second order differences d_1 and d_2 , and mixed order or diagonal (mixed) differences $d_{1,1}$. While the first order differences are just the (arc length) distance on the circle, the second order differences are determined by looking at all possible unwrappings of the circle onto the real line and the corresponding second order discrete difference there. For more details see Bergmann et al. (2014) and Schubert (2016).

For non-negative regularization parameters $\alpha := (\alpha_1, \alpha_2)$, $\beta := (\beta_1, \beta_2)$, and γ not all equal to zero we are looking for the minimizer $\Phi \in [-\pi, \pi)^{N \times M}$ of

$$J(\Phi) = J(\Phi, \Theta) := F(\Phi; \Theta) + \alpha TV_1(\Phi) + \beta TV_2^{hv}(\Phi) + \gamma TV_2^d(\Phi), \quad (2.4.9)$$

where

$$\begin{aligned} F(\Phi; \Theta) &:= \frac{1}{2} \sum_{i,j=1}^{n,m} d(\vartheta_{i,j} \varphi_{i,j})^2, \\ \alpha TV_1(\Phi) &:= \alpha_1 \sum_{i,j=1}^{N-1,M} d(\varphi_{i,j}, \varphi_{i+1,j}) + \alpha_2 \sum_{i,j=1}^{N,M-1} d(\varphi_{i,j}, \varphi_{i,j+1}), \\ \beta TV_2^{hv}(\Phi) &:= \beta_1 \sum_{i=1,j=2}^{N-1,M} d_2(\varphi_{i-1,j}, \varphi_{i,j}, \varphi_{i+1,j}) + \beta_2 \sum_{i=2,j=1}^{N,M-1} d_2(\varphi_{i,j-1}, \varphi_{i,j}, \varphi_{i,j+1}), \\ \gamma TV_2^d(\Phi) &:= \gamma \sum_{i,j=1}^{N-1,M-1} d_{1,1}(\varphi_{i,j}, \varphi_{i+1,j}, \varphi_{i,j+1}, \varphi_{i+1,j+1}). \end{aligned}$$

While the data term $F(\Phi; \Theta)$ ensure similarity of Φ and Θ , the remaining summands, also called the fidelity term, force φ to have a small first and second order cyclic total variation. The values α, β and γ introduce the possibility to weight the terms and hence introduce a preference for the minimizer. For instance choosing β_1 and α_2 large compared to the other parameters, results in a linear smoothing of the first dimension, whereas the reduction of the total variation along the second dimension. Figure 2.7 depicts an example for the denoising procedure of a artificial signal demonstrating the effect of applying first order differences, second order difference or both combined. Figure 2.7 (b) depicts the results using only the TV_1 regularization, which is more appropriate to constant areas of the signal, while else (i.e., linear, quadratic and exponential parts) staircasing effects appear. In the framework of TV-regularizer staircasing is a artifact which introduces artificial boundaries in regions of smooth-varying intensities. When TV_2 regularization is only applied (see Figure 2.7, c) restoration shows better results for linear parts while worsen for flat areas. Figure 2.7 (d) represents the combination of both regularization terms. This case shows best results for both, the constant and linear parts. The minimization is computed using the cyclic proximal point algorithm (CPPA), which is based on proximal mappings (see Parikh and Boyd (2014) for a more recent overview). However, for the study proposed in this thesis, we choose $\alpha = (2, 4), \beta = (2, 1.25)$ and $\gamma = 0$.

To reconstruct the waveform in the time domain, we construct $\tilde{G} \in \mathcal{C}^{N \times M}$ by combining the absolute values of G with the regularized phase values in Φ such that $\tilde{g}_{n,m} = |g_{n,m}| e^{j\varphi_{n,m}}$ ($n = 1, 2, \dots, N, m = 1, 2, \dots, M$).

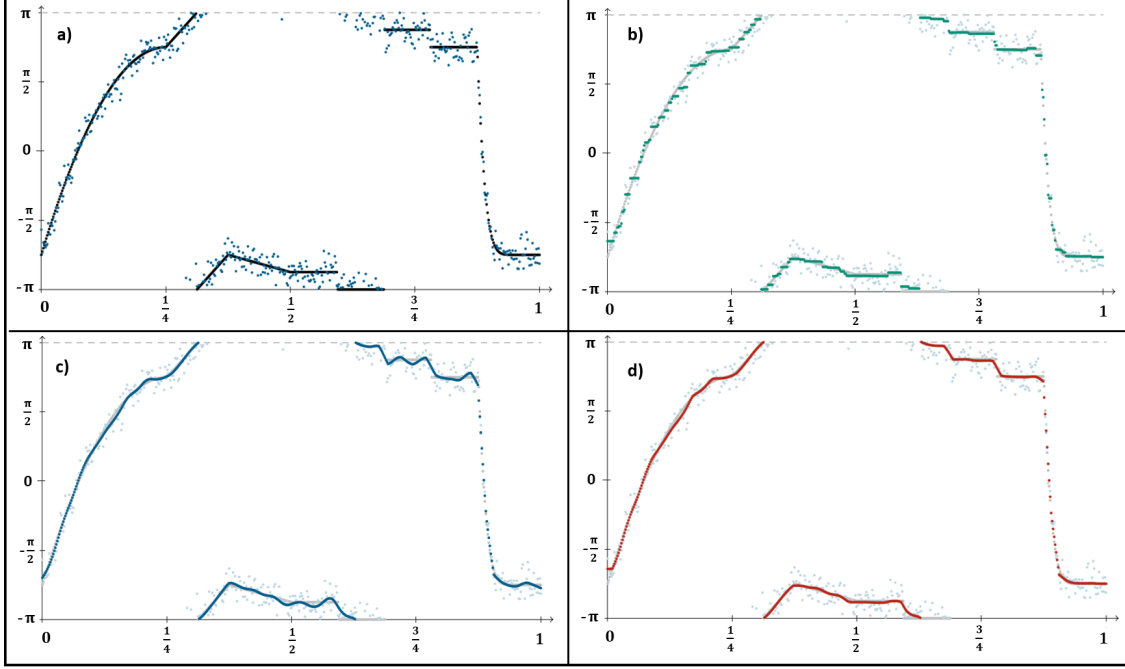


Figure 2.7: Denoising of a phase valued signal with CPPA. (a) Original signal (solid black) added with wrapped Gaussian noise ($\sigma = 0.2$) (blue dots). (b) Reconstructed signal (green) using TV_1 regularizer results in staircasing. (c) Reconstructed signal (solid blue) using TV_2 shows weak results at constant areas. (d) Reconstructed signal (solid red) using $TV_1 \& TV_2$ shows best results (Bergmann et al., 2014).

To preserve the original mid and high frequency morphology of the waveform, the spectral information of \tilde{G} was added to the not filtered, spectral information of S . Finally, the denoised version is then given by the real part of the time-domain representation of the complex signals resulting from these combined spectra.

For visualization-purposes of the denoising scheme, Figure 2.8 depicts an example for somatosensory ERP-trials. The top right figure shows the original ERP-image after tactile stimulation of a subject's fingertip using the Braille-display. Despite the apparent trace visible across the trials, extracted unprocessed single trials does not show any noticeable peaking but rather a homogenous oscillation (see Figure 2.8, top left). When the denoising is applied (lower right) a clearly recognizable trace can be seen. Moreover, the extraction of the very same single trials (as chosen

2.4 Data Processing Pipeline

for the unprocessed matrix) clearly show the prominent P100 wave, not visible in the unprocessed versions.

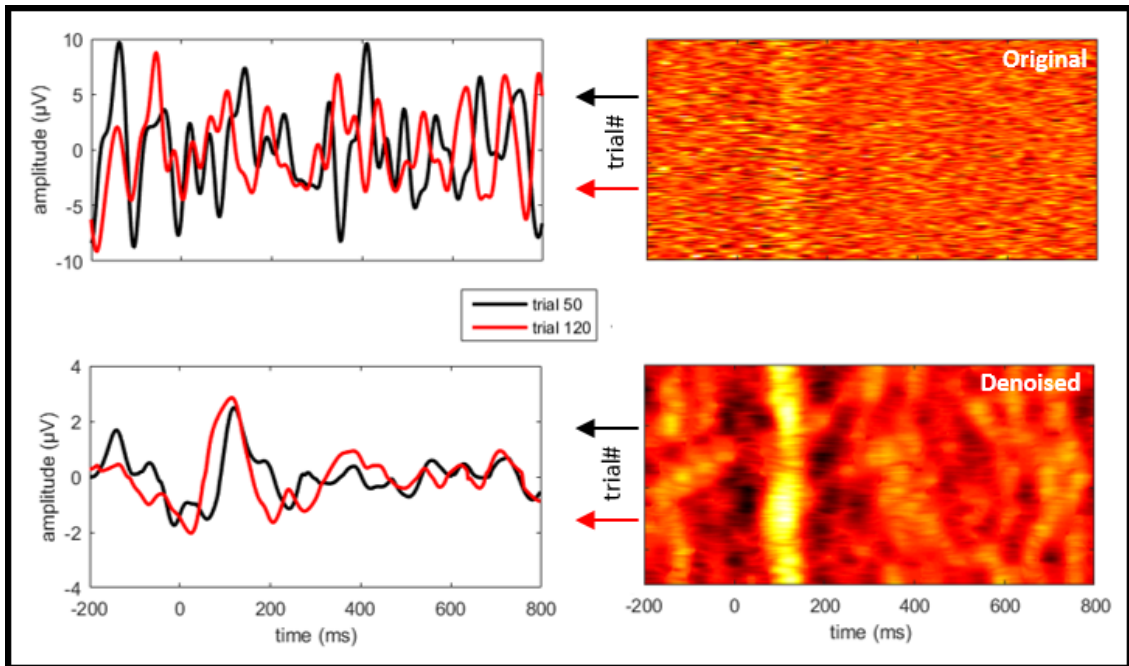


Figure 2.8: Single-trial enhancement. Right top: Original ERP image. Right bottom: Processed ERP image. Left bottom: The processed trials clearly shows the prominent P100 wave peak whereas the unprocessed (left top) trials does not.

3 Results

3.1 Part A: Experiments - Structured Surface

In this section we will shortly present some results for the preliminary study in Part A. Here, the tactile stimulation was performed by sliding a manufactured aluminum block with ridges on top (see section 2.2) along the fingertip of the participants.

3.1.1 Tribology of the Structured Surface

Figure 3.1 (a) shows the single trial in matrix representations of the friction force for one participant. Signals of subsequent trials are plotted as function of time one line after the other with the force intensities color-coded from 0mN (dark blue) to 400mN (light yellow). The data is segmented with respect to the transversal motion of the stimulation stage, which means that the actual event, i.e, the very first contact between the fingertip and structure is not directly known.

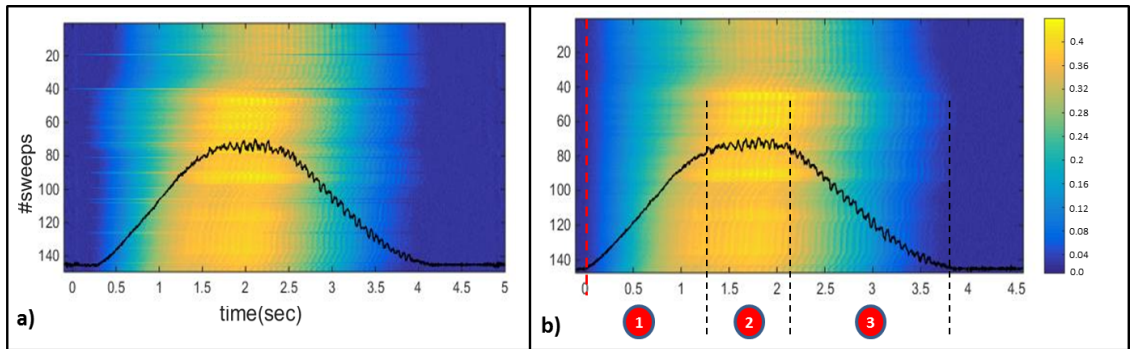


Figure 3.1: Friction measurements from one subject. a) Single trials in matrix representation ($n=160$). The stimulus onset at time zero indicates the movement of the translation stage. The black curve plotted over the matrix representation represents the averaged time domain waveform over 160 trials. Amplitude is color-coded from dark blue (small) to light yellow (high) b) Aligned version of (a) (see text) Red dashed line indicates the very first contact with the structure. Three distinct phases are apparent in the signals morphology.

The black curve plotted over the respective matrix representation indicates the

averaged time domain waveform over all 160 trials. When the stage starts sliding (at time zero), a change in friction force is obtained at around 300ms. This change indicates the first contact of the fingertip with the stimulation block and hence can further be regarded as the stimulation onset. Considering the single trial-matrix in the background a variability in force onset is apparent. Frictional profiles are changing over time and trials (see variance in force onset). Figure 3.1 (b) represents the virtually triggered (see section 2.4.1) version of (a) with respect to the onset of the friction force. Indicated by the red dashed line, all trials are shifted in time such that the onsets fall together for all trials. After stimulus onset three distinct phases were observed for the signals morphology of the friction force. First, an linear increase in friction until approximately 1.3 seconds. Second, a plateau which is persistent for approximately 1 sec with a mean magnitude of approximately $\Delta = 400$ mN, and finally, a linear decrease in friction force when the finger gets out of contact. This morphological observation was the same for all participants and forces (lateral as well as normal forces). The slope of the friction can be considered as a marker for the fingertip geometry. However, the slope in phase 1 and phase 3 of the averaged waveform shows relatively small differences, where the increase in force is a little faster in terms of reaching a steady state.

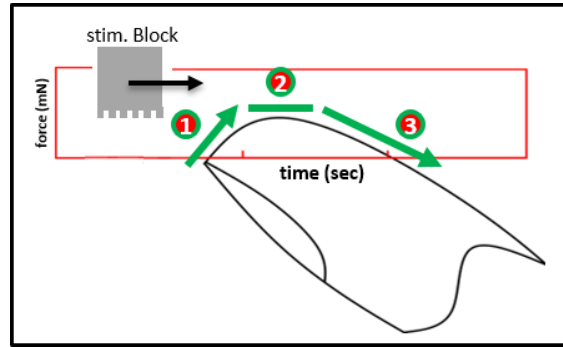


Figure 3.2: Schematic representation of the temporal evolution of the friction force describing the link to the fingertip-geometry. Three distinct phases are observed. 1) Onset of friction as a result of the contact between fingertip and the moving structure, continuously increasing with stronger surface contact. 2) Largest surface contact. 3) Decrease in contact until contact is lost.

It took approximately 1.2 sec for the friction force to reach a steady-state, while the off contact process lasts for approximately 1.5 sec. Those signal characteristics can be attributed to the fingertip geometry. Figure 3.2 shows the fingertip

3.1 Part A: Experiments - Structured Surface

geometry and the distinct phases which establish during the sliding contact with the stimulation block. This schematic view illustrates the observed time-evolution of the friction profile. The oscillation of the friction force is changing over time, most pronounced around the plateau. This observation, since the fingertip-block contact around the plateau is most profound, shows that friction is modulated by the convoluted contributions of the surface ripples and the fingertip ridges. The left panel of Figure 3.3 shows the fingerprint and the respective ridge to ridge distances for one individual person. For this person ridges appear to be in average 0.7mm away from each other. The middle panel depicts the surface characteristics of the stimulation block captured by a digital microscope. The ripple to ripple distance is approximately 1mm in average.

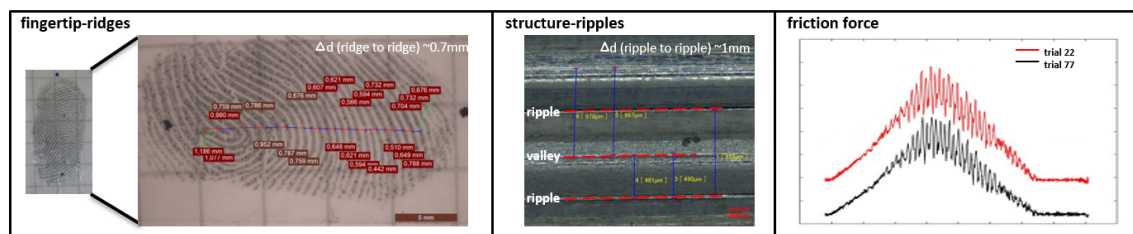


Figure 3.3: Friction force (right figure) as the result of convoluted contributions from the fingertip ridges (left figure) and the surface ripples (mid figure).

To the right, the friction force as the result of convoluted contributions from the fingertip ridges and the surface ripples is shown. It can be seen that friction has a slight oscillation at the beginning which increases with the degree of roughness, i.e. the degree of profound contact between the two bodies increases.

3.1.2 Electrophysiological (EEG) Activity

Figure 3.4 illustrates the process in producing ERP-images. Thereby, single trials are arranged line by line and plotted as a function of time with the amplitude of each trial encoded in colors (transition from negative (black) to positive (white) values). In Figure 3.4, to the right, the top figure shows the original ERP-image for one participant. The signals are recorded at electrode C3 and filtered offline from 2-32Hz. In general the idea of ERP-images is to indicate prominent characteristics and commonalities in terms of neural processing which might occur due to repeated stimulation usually visible as traces across trials. However, traces are not found in

the original ERP-image. This observation was quite the same for all participants in this study. After applying the denoising method (see section 2.4.4) to the ERP images, the matrix exhibits now pronounced traces where the most prominent one ranges from about 250 ms to 100 ms in a shifted manner, as shown in the lower panel of Figure 3.4.

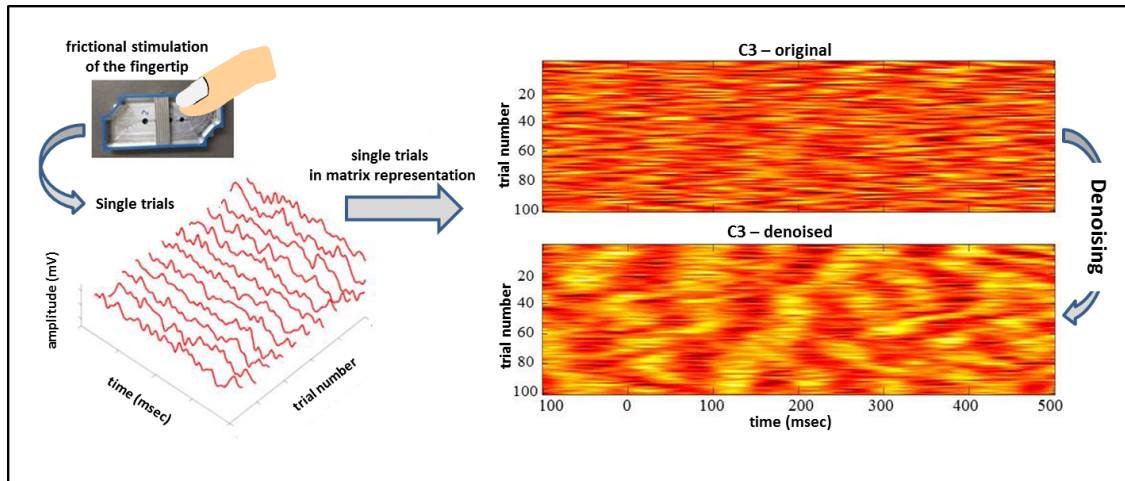


Figure 3.4: Frictional stimulation of the fingertip and the single trials arranged in ERP-images. Top figure to the right shows the original ERP-image, while the lower the denoised version of the original ERP-image.

However, apart from the indubitable advantage of the denoising method, the image clearly indicates a great variability in latency from trial-to-trial. Thus, the widely accepted approach of across-trial averaging in the time domain, for identification and characterization of ERPs is not an appropriate choice, since important information would be lost in this case.

3.2 Part B: Experiments - Braille-display

In this study, tactile stimulation was performed using a programmable Braille-matrix (see section 2.2) which was slid along the fingertip of the subjects. The stimulus was delivered in a reciprocal, repeated sliding of the Braille-display and consisted of a raising and lowering of different numbers of lines of pins along the sliding direction of the Braille-display. Two main cases were investigated:

- case (i): variation in stimulation lines (one line versus three lines) but same stimulation manner, i.e., lines of pins are raised.
- case (ii): same stimulation pattern (either one line or three lines) but different stimulation manner, i.e., raising versus lowering of pins.

3.2.1 Tribology of the Braille-display

Figure 3.5 (a) shows the single-trial matrices of the friction forces for one subject, plotted as a function of time (from a pre-stimulus interval of 200ms to a post-stimulus interval of 800ms). Data is segmented with respect to the stimulus onset (dashed vertical line at 0 ms), which indicates the raising of pins and hence the fingertip-pins contact. The top image depicts the 180 trials including all stimulation pattern presented randomly to the participants fingertip. In the lower three matrices, extracted from the top matrix, the friction data for each Braille-pattern is presented separately. The blue lines indicate the time domain signals averaged over the respective trials showing a clear change in force, when pins are raised.

In Figure 3.5 (b) the averaged time domain signals for the distinct stimulation pattern are summarized. All three paradigms, either for the friction (top) or normal force (bottom) show similar morphological characteristics composed of an initial offset, a sudden change in force at stimulation onset and a subsequent plateau when sliding of the Braille-display proceeds. The initial offset prior to the stimulus onset ($t=0\text{ms}$) indicates that the participants fingertip was in slight contact with the Braille-display before stimulation was presented. This offset amounts to 20mN for the friction force and 60mN for the normal force. When pins are raised (at 0ms) a change in force occurs. When comparing the step intensities, no significant differences are obtained for the three- and five-line stimulation neither for the fric-

tion (15mN) nor normal forces (40mN). In contrast, the one line stimulation shows approximately half the step intensities for friction and normal forces.

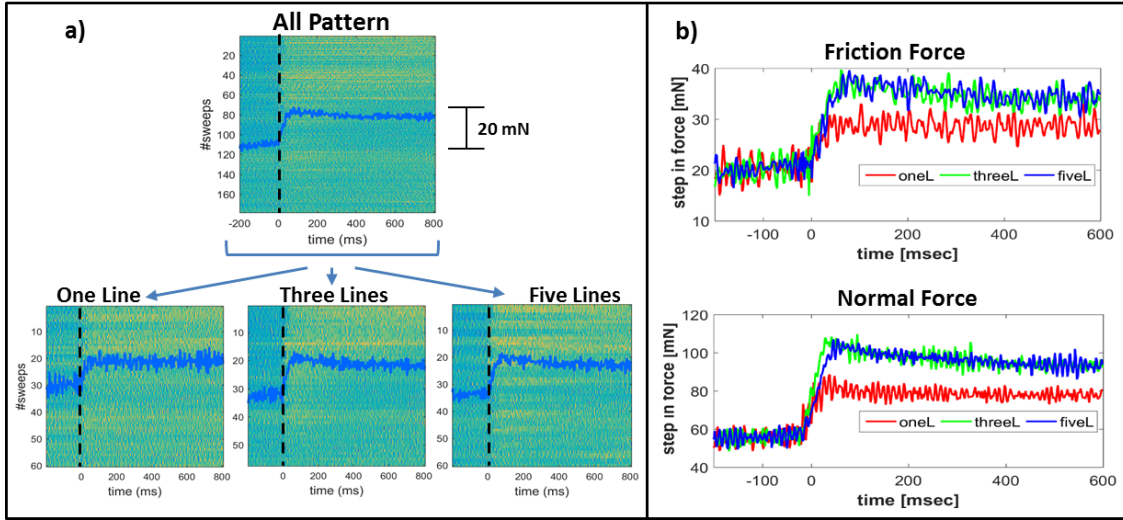


Figure 3.5: Physical measurements from one subject. a) Single trial matrices ($n=180$) representing the friction forces including all stimulation pattern (top) and each pattern separately (lower three). The dashed vertical black lines indicate the stimulus onset while the blue lines plotted over the matrix representations the respective averaged time domain signals (over trials) b) Averaged friction (top) and normal (lower) forces for the one, three and five line stimulation paradigms.

It should be noted, that some of the following results presented in this subsection have already been published in Özgün et al. (2018b).

Figure 3.6 shows the step intensities for the normal forces acting between the fingertip and the sliding Braille display with one, three or five lines of Braille-pins raised. Step intensities are plotted for the individual participants, indicating an increase of normal forces when pins are raised. In the case, of one line of pins raised (black filled squares) the values scatter in the range from 20mN to 100mN for the individual participants. The explanation of this scatter can be attributed to distinct parameters such as differences of fingertip curvature, skin compliance, and actual height distance between finger and Braille display. In the case, of three lines of Braille-pins raised, the step in normal force is larger by a factor of about two compared to only one line raised. This is also visible in the grand averages depicted in Figure 3.14. For all five lines raised, the step increase in the normal force was almost the same as it was for the three lines of pins. This suggests that the interaction of the outermost lines of pins on the Braille-display with the curved fingertip is too small

3.2 Part B: Experiments - Braille-display

to be detected when the finger is aligned parallel to the lines of pins, as shown in Figure 3.6 (b).

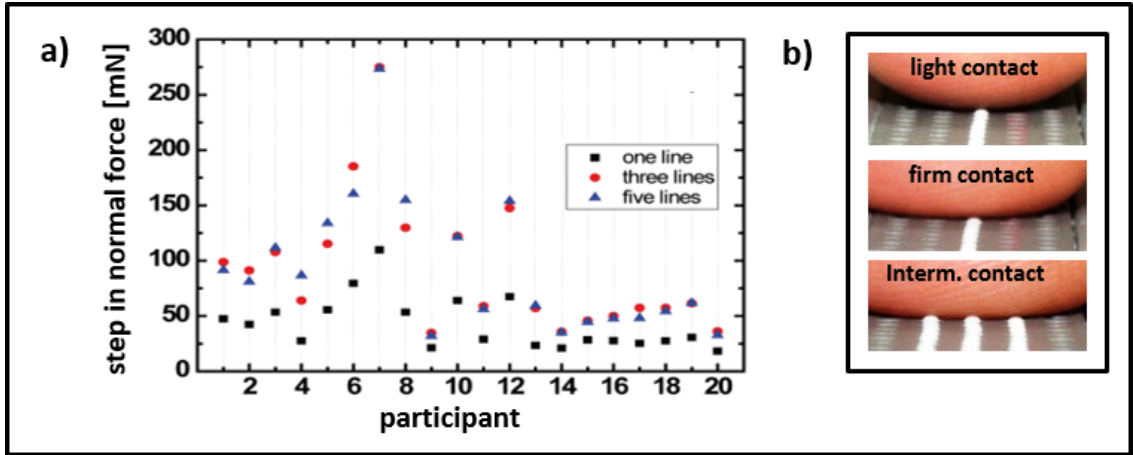


Figure 3.6: Forces acting on the moving Braille-display upon raising one, three, or five lines of Braille pins. (a) Step in normal force when the pins are raised for all participants. Each data point in represents the average of 60 trials. (b) Distinct contact modalities: Light contact, one line of pins raised. Firm contact, one line of pins raised. Intermediate contact, three lines of pins raised.

Figure 3.7 represents the step changes in lateral force obtained when pins were raised. It can be seen that for some participants the lateral force increased while it decreased for others. This situation can be understood considering a variation in height of the fingertips with respect to the Braille display between the participants. We refer to the schematic representation in Figure 3.8, for explanation. Across participants two distinct types of signals-characteristic have been observed. If the fingertip was touching the surface of the Braille-display only lightly (see *Type I*), the average lateral force for lowered pins was very low (blue highlighted portion of the signal). Raising the pins into contact with the fingertip resulted in an increase of the lateral force (yellow highlighted part) until due to the viscoelastic conformation of the skin steady state friction is reached (green highlighted part). In contrast, a firm contact revealed an inverted course of the friction force (see *Type II*). If the fingertip was already in firm contact with the surface of the Braille display, there was significant friction even if the pins were lowered (blue highlighted portion of the signal). When pins are raised, lateral force lowers due to a reduction in the strength of the contact between surface of the Braille display and fingertip, i.e., pins in contact are defining the contact strength (yellow highlighted part).

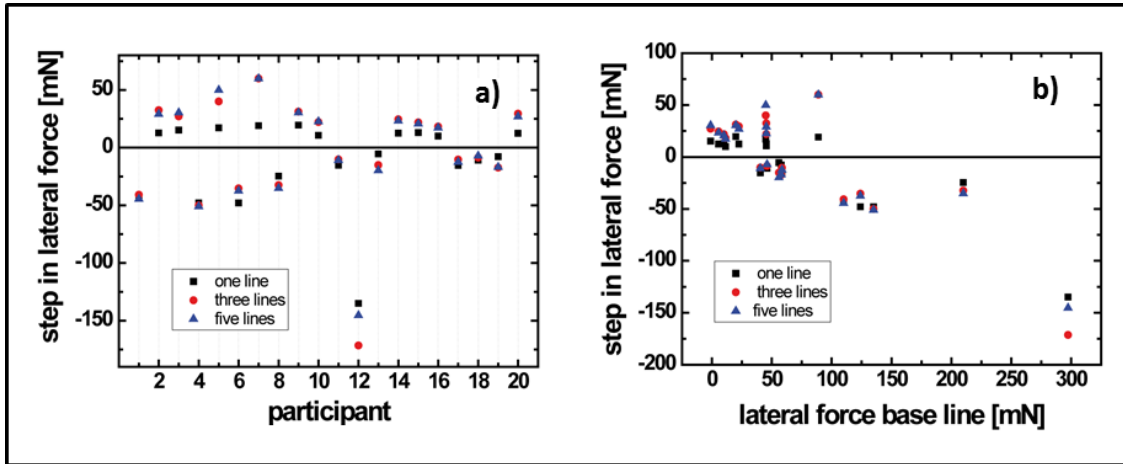


Figure 3.7: Lateral forces acting on the moving Braille display upon raising one, three, or five lines of Braille-pins. (a) Step in lateral force when the pins are raised. Note that the step in lateral force is positive for some and negative for other subjects. (b) Step in lateral force when the pins are raised as function of the average lateral force when the pins are still lowered. The average lateral force indicates the strength of the contact between fingertip and surface of the Braille-display. Each data point in (a) and (b) represents the average of 60 trials.

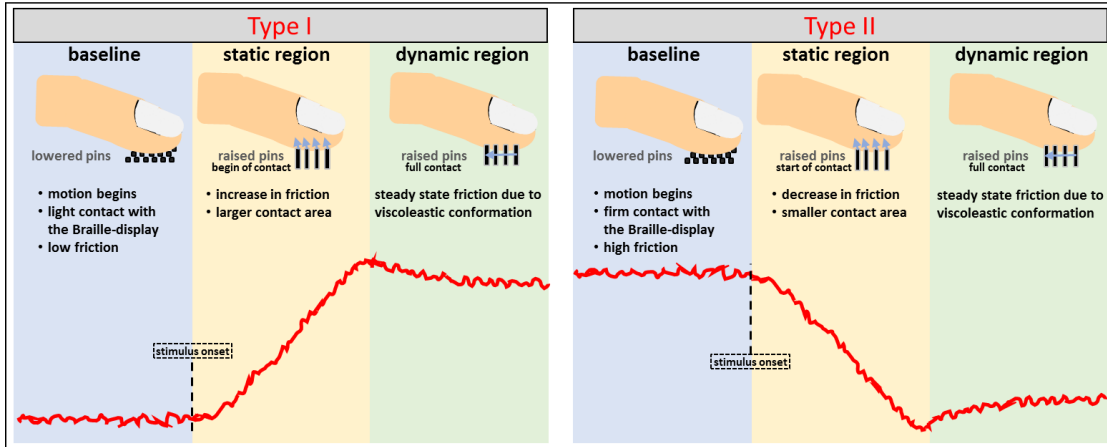


Figure 3.8: Schematic representation of characteristic signal-morphologies between the passive fingertip and Braille-display in sliding contact. Two main types are pronounced. Type I: Course of the friction force when fingertip is in a light contact with Braille-display. Type II: Course of the friction force when fingertip is in a firm contact with the Braille-display.

After a certain minimum in lateral force, when sliding proceeds, friction increases again which can be attributed to the larger contact strength, since more pins are involved (green highlighted part). The averaged lateral force for the pre-stimulus interval (when pins are lowered) is a measure for the contact strength between fingertip and Braille display. When taken this measure into account by plotting the step-intensities in dependence of the contact strength (see Figure 3.7, b), a clear trend is revealed. It can be seen that steps in lateral force caused by the raising Braille pins changed from positive to negative for stronger average base line forces. This means that for contact forces higher than approximately 30mN in the pre-stimulus interval, lateral force more likely show Type II, whereas lower contact forces exhibit rather Type I signal-characteristics. Apart from the two possible types of signals characteristic, two main components contribute to the lateral force. First, the friction between the fingertip and the surface of the Braille-display, and second, the friction between raised pins and fingertip.

Figure 3.9 shows the normal and friction forces for two participants, highlighting the comparison of a light contact (a) with a firm contact (b) of the fingertip with the Braille-display. Therein, the two images on the left reflect averaged curves for the condition when pins are raised, and for the condition Braille-pins are lowered on the right. In the case of a light contact and Braille-pins raised (at $t = 0$), normal force increased within 40ms to a maximum, while the lateral force increased step-like by about 20mN with a delay to the normal force step. For the condition when Braille-pins are lowered, normal and lateral force return to the initial values in the same step-like fashion. In the case of a firm contact and Braille-pins raised (see Figure 3.9, b), the lateral force first decreased by about 40mN (within 40 ms) and subsequently increased by about 20mN within the next 60ms due to interaction with the raised pins. When pins are lowered again, both, normal and lateral force, show a steep decline within the first 40ms, especially, the lateral force increased again segueing to a steady state value after 300ms. Those observed temporal developments of the obtained forces are very similar to the viscoelastic force relaxation reported by Nakazawa et al. for a step in shear strain of a fingertip Nakazawa et al. (2000).

Figure 3.10 shows the characteristic development of the friction coefficient μ for the distinct contact strengths that establish between the participant's fingertip and the surface of the Braille-display. When considering Figure 3.9 (a) and (b) it can be seen that force curves look quite different. However, despite this fact the friction coefficient μ shows a similar temporal development (see Figure 3.10).

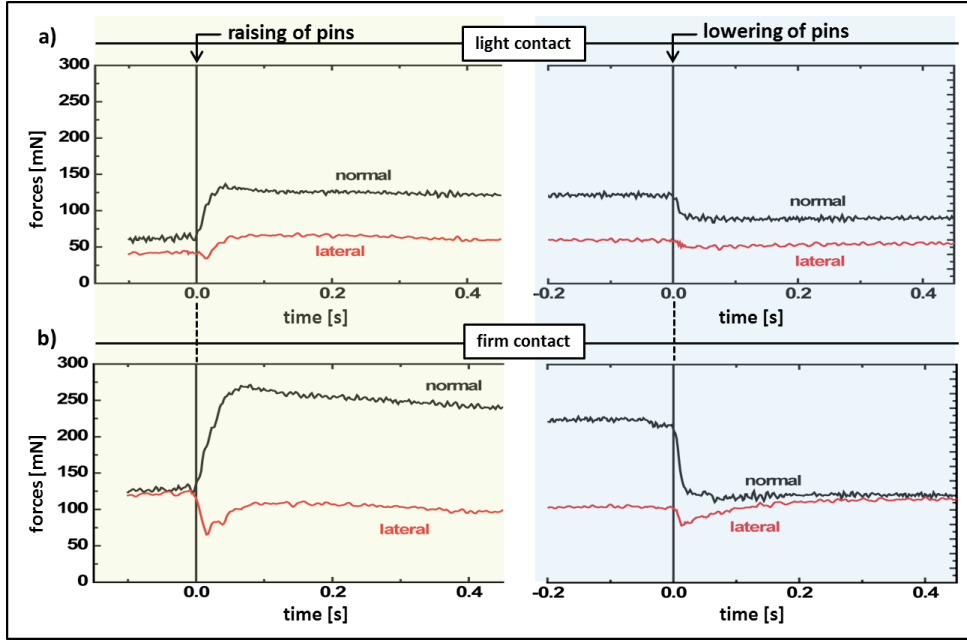


Figure 3.9: Characteristic force vs time curves for the comparison of the distinct contact strengths between participants fingertip and surface of the Braille-display. Light (a) and firm (b) contact strength for the raising (left panel) and lowering (right panel) of Braille-pins, respectively.

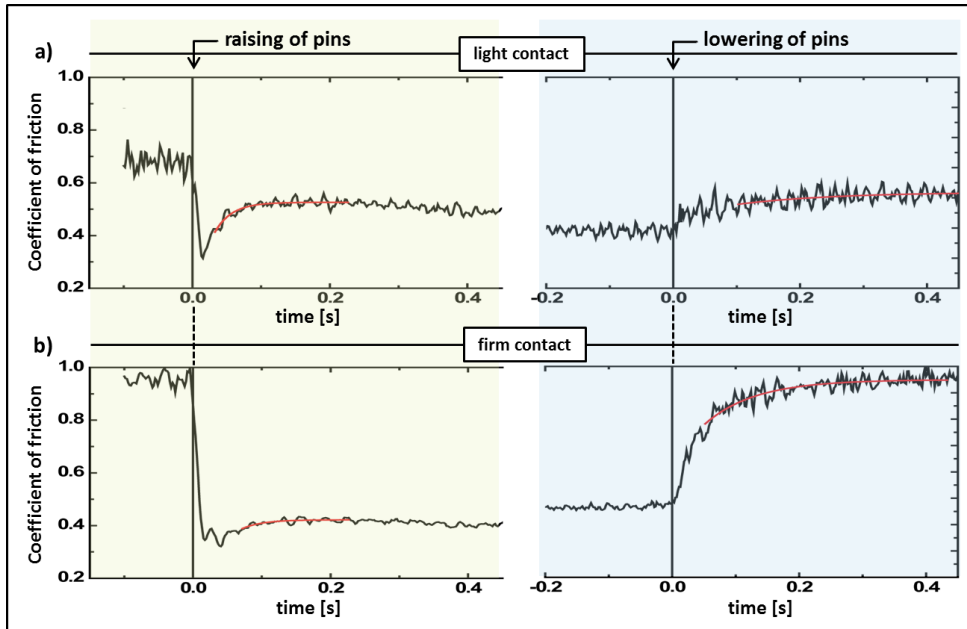


Figure 3.10: Characteristic development of the friction coefficients μ for the distinct contact strengths. Light (a) and firm (b) contact strength for the raising (left panel) and lowering (right panel) of Braille-pins, respectively.

For both investigated contact strengths, the coefficient of friction dropped within 40ms after raising the pins, due to a reduction of contact between fingertip and surface of the Braille-display. The friction coefficient then increased again and reached a steady-state value after about 100ms. We assume that these 100ms are the characteristic time to establish steady-state friction between the raised pins and the deformable skin of the fingertip. The interaction with the lines of raised Braille pins left lines of depressions at the fingertips. This deformation of the skin at the fingertip could be observed for fractions of a second when the finger was taken off the Braille display during an experiment. This situation is depicted in Figure 3.11, where a photograph of the fingertip was immediately taken after one line of Braille-pins are rubbed 200 times against the fingertip. However, for the condition when Braille-pins are lowered (see Figure 3.10, right), μ increases step-like within 40ms, with a further increase towards a steady-state value which was reached after 300ms. Concerning the time-frame until steady state, we assume that this time is required to re-establish the full contact between fingertip and surface of the Braille display, when the previous deformation of the skin by the pins is relaxed.

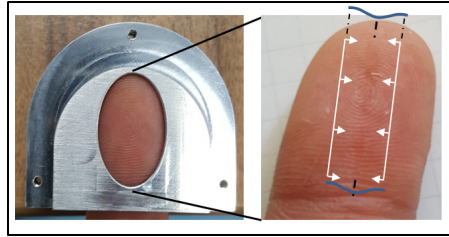


Figure 3.11: Skin depression after rubbing one line of Braille-pins 200 times against the fingertip of a participant. Blue plotted lines indicate the skin depression of the fingertip within the white frame with arrows pointing towards the skin deformation

When we model the increase of friction coefficient as an exponential approach (shown here for the two subjects as red lines in Figure 3.9) to the new value for all participants, we obtain characteristic time constant of 35 ± 10 ms after raising the pins and 156 ± 70 ms after lowering the pins. The standard deviation of the characteristic times for our participants is similar to that reported by Wiertlewski and Hayward for the cut-off frequency of elastic response in fingertips among seven participants (Wiertlewski and Hayward, 2012).

3.2.2 Electrophysiological (EEG) Activity

Figure 3.12 shows exemplary the electrophysiological results for an individual subject. The top Figure in 3.12 (a), represents the ERP-image associated to 180 trials of presenting one of three distinct Braille-pattern randomly to the subjects fingertip. The averaged time domain waveforms are plotted as blue lines on top of the ERP-images while the vertical dashed line (at time zero) indicates the stimulus onset. Amplitudes are encoded in colors, from black (small) to white (large) values. In the lower three ERP-images, responses to each particular stimulation pattern are shown separately.

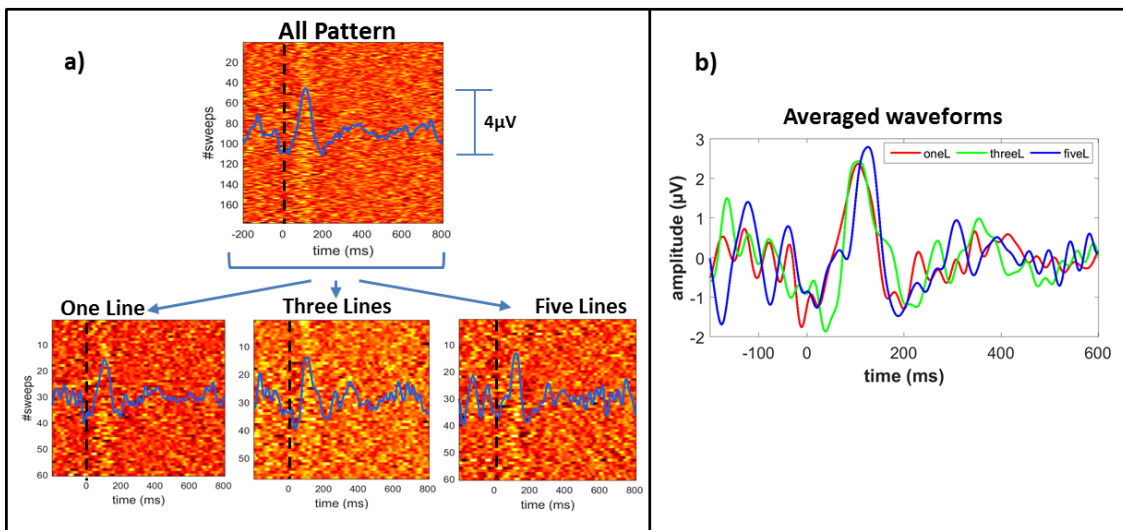


Figure 3.12: Somatosensory event related potentials (ERPs) from one subject. a) Top figure: ERP-image including all single trials sequences ($n = 180$), with Braille-patterns randomly presented to the subjects fingertip. Lower figures: ERP-images for each Braille-pattern stimulation, provided separately. Dashed vertical black lines indicate the stimulus onset. The blue lines reflect the averaged time domain signal (over trials). A clear positive trace is apparent around 100ms (P100), also noticeable in the averaged waveforms in (b).

The images exhibit a clear positive trace, noticeable approximately 100ms after stimulus onset, which corresponds to the prominent P100-wave in the averaged waveforms shown in Figure 3.12 (b). Earlier to this positive wave, a negative wave (N50-peak) is noticeable in the averaged waveforms. For the above shown representative example, the latency of the prominent P100-wave for the one and three line stimulation were similar (around 100ms). In contrast, the latency of the five lines

3.2 Part B: Experiments - Braille-display

stimulation was delayed by approximately 20ms. The calculation of the peak-to-peak amplitudes (between N50 and P100 waves) for the averaged responses revealed quite similar values for the different stimuli (approximately $4\mu\text{V}$). Despite the noticeable ERP-components observed for the different stimuli, there is no significant difference between the ERPs.

However, the tactile stimulation of the fingertip due to a variation in Braille-pins (one, three and five lines) and the raising of pins into contact showed pronounced ERP-waves. For all subjects included in this study similar prominent waves were apparent in the ERP-sequences, whereas the results shown above were from one subject with clearly visible ERP-traces.

Figure 3.13 shows simultaneously recorded forces and EEG signals from another subject.

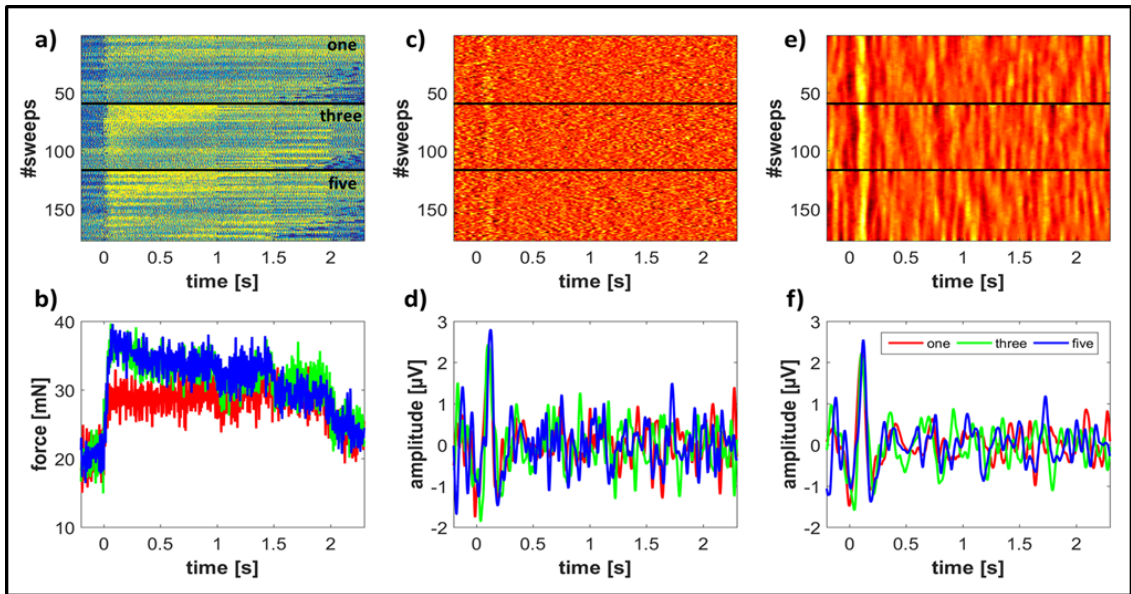


Figure 3.13: (a) Single-trial-image representing the lateral forces as function of time for 180 trials. Braille-pins are raised at $t=0$ for a duration of 1s, 1.5s, and 2s in a randomly fashion. The color scale ranges from 10mN (blue) to 45mN (yellow). Each block, separated by a horizontal black line, shows the single-trials of the lateral force the different Braille-pin stimulations. (b) Across-trial averages of the lateral force as function of time for one, three, and five lines of raising pins. (c) ERP-images for C3, simultaneously recorded with the force data in (a). (d) Averaged EEG signal at C3 as function of time. (e) Denoised version (see section 2.4.4) of the ERP-images in (c). (f) Averaged version of the denoised EEG signal at C3 as function of time.

In order to identify differences between the signals for the different stimulation-pattern, Figure 3.13 (a) and (c) shows force and ERP-sequences arranged in respective blocks, separated by black horizontal lines. Indicated by the difference in color-contrast around the stimulus-onset, Figure 3.13 (a) shows that steps for the three and five lines stimulation are larger as compared to the one line stimulation. This observation is also noticeable in the averaged waveforms in Figure 3.13 (b), as shown for another subject in Figure 3.5. The neural responses to the different stimuli, shown in the sorted ERP-image in Figure 3.13 (c), exhibit traces for all three patterns approximately 100ms after stimulus onset (see light yellow color coded path across trials). The averaged ERP-waves, taken over a block of 60 trials each, (see Figure 3.13, d), reveal similar signal characteristics as presented for the subject in Figure 3.13 (b). After stimulus onset, a negative N50-wave followed by a positive, well pronounced P100 wave and a subsequent N150 are most apparent. The resting state EEG signals, show fluctuations at all times with main frequencies-components attributed to the alpha-band.

To enhance the signal-to-noise-ratio (SNR) and to improve the analysis of the event related portion of the EEG-signals, a combination of two denoising methods (see section 2.4.4) was applied to the ERP-images. First, instantaneous phases of individual trials were extracted and denoised with respect to the alpha-band, by utilizing Hardy-space projected versions of the ERP-images (via tight Gabor frames). Second, the nonlocal means denoising, which takes advantage of the image representation of the data in ERP-matrices. The denoised image is constructed by image patches of a few pixels from the original image, where patches with similarities at different positions in the original image receive a higher weight. However, the time domain representation of these "phase-regularized" and "self similarity-enhanced" trials show a crucial improvement in the SNR of cortical processing correlates, as shown in Figure 3.13 (e) and (f).

Grand Average Representation:

In the following grand average representations of forces and EEG signals are presented.

Figure 3.14 shows a compilation of the grand averages over $n = 15$ participants where from top to bottom the normal forces, friction forces, the coefficients of friction, and respective neural correlates are represented as a function of time. The friction coefficient $\mu = F_{Fric}/F_{Nor}$ is defined as the ratio between the friction force F_{Fric} and the normal force F_{Nor} that specifies the amount of friction between the fin-

3.2 Part B: Experiments - Braille-display

gertip and the Braille-display. Each column in Figure 3.14 represents the respective results for the distinct cases described above.

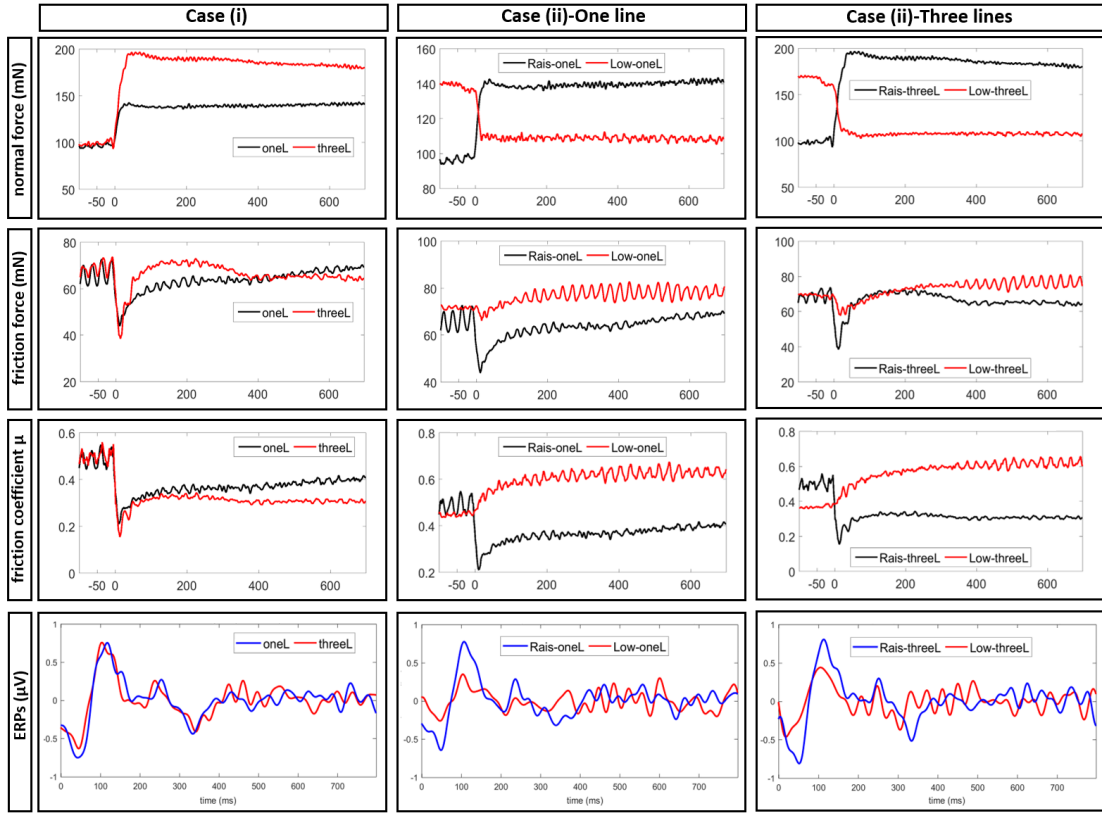


Figure 3.14: Compilation of the grand averages over $n = 15$ participants. From top to bottom: normal forces, later forces, friction coefficients and evoked ERPs for the distinct cases.

case (i): Raising pins - One Line vs. Three Lines: The normal force signals show a clear difference in magnitude between the one and three line stimulus. Both grand averages show prior to the stimulus onset (at time zero) a baseline of about 100mN which means that in average subjects contacted the Braille display when pins are still lowered. When lines of pins are raised the force increases within 50ms to 140mN (one line) and 190mN (three lines). The step intensity (sI) (see section 2.4.2) approximately doubles from 40mN to 90mN when comparing one and three lines of raised pins. After a step increase, the normal forces remain at the elevated value. For the friction forces a baseline of about 65mN prior to the stimulus onset is followed by a steep decline in friction within approximately 20ms after stimulus onset before increasing again to a plateau after 300ms. The coefficients of friction

for both stimulation pattern indicate a similar $\Delta\mu$ of about 0.25. The ERPs show a quite similar signal morphology which has also been observed for the individual subject in section 3.2.2, Figure 3.13. After stimulus onset the main components of, N50-, P100-, N140-, P250- and N330- wave are subsequently apparent before turning to a quasi-flat positive plateau with minor oscillations until 800ms.

case (ii): Raising vs Lowering Pins - Same Braille -pattern: In Figure 3.14 the grand averages for the same stimulation patterns (one line and three lines) but different stimulation manner (raising and lowering of pins) are shown separately in the second and third column. For both stimuli, the normal and the friction forces show a larger step intensity when pins are raised. Step intensities for the raising stimuli are higher by approximately 50 % compared to the lowering stimuli. The step intensities of the friction forces between the raising and lowering of pins differ roughly by a factor of four for the one line stimulation (20mN/5mN), and a factor of three for the three lines stimulation (30mN/10mN). The step change in $\Delta\mu$ shows for both cases and the raising of pins almost same values (approximately 0.3). In contrast, $\Delta\mu$ shows the half in step change when pins are lowered, but similar values in respect to both cases (approximately 0.15). The averaged ERP sequences for the lowering condition (red curves) show quite same prominent waves within the first 200ms. Note that the blue lines are the very same signals shown in case (i). For both stimulations ERP-amplitudes are larger when pins are raised which can be attributed to larger stimulus intensities.

However, ERPs are changes in amplitude and latency. Somatosensory ERP-components are small in amplitudes and embedded in the background EEG, which is in the order of several magnitudes higher. It is widely accepted that the components generally refer to the underlying cognitive processes and brain activity indexed by the potential (Woodman, 2010). However, across-trial averaging, which does not consider the across-trial variability of ERP amplitude and latency, might thus average out physiologically relevant information. This might be a reason why no significant differences can be observed in the averaged waveforms in Figure 3.13 (d) and the grand average waveforms in Figure 3.14 (case(i)).

In table 3.1 we have shown mean and standard deviation of the grand averages for the P100-amplitude, latency, and the step intensities for the normal and friction forces. For the sake of completeness the table also relates, besides the one and three lines of Braille-stimulation, information for the five lines of Braille-pattern. In general, there is a tendency for elevated P100-amplitudes when comparing multiple-

3.2 Part B: Experiments - Braille-display

lines of stimulations pattern with single-line stimulation pattern. In particular the three lines show highest amplitudes (approximately one fifth higher than the one line stimulation) and smallest latencies (3ms earlier than the one line stimulation).

Table 3.1: Mean and standard deviation values for the P100-amplitudes/latencies and intensities of the force-steps for each stimulation-condition

	One Line	Three Lines	Five Lines
P100-Amplitude (μV)	1.66 \pm 0.81	1.94 \pm 0.74	1.67 \pm 0.78
P100-Latency (ms)	105 \pm 16	102 \pm 17	108 \pm 19
Friction Force Step-Intensity (mN)	24.79 \pm 30.79	34.35 \pm 36.91	33.40 \pm 30.67
Normal Force Step-Intensity (mN)	43.58 \pm 24.61	94.60 \pm 62.78	94.48 \pm 62.39

In respect to the calculated force-steps, grand averages show noticeable smaller values for the one-line stimulation, whereas the three and five lines of stimulations show quite similar step-heights. In contrast to the one line stimulation, the observed normal and friction steps for the three and five lines of stimulation are higher by a factor of 2 and 1.5, respectively. Considering especially the friction forces for the different stimulation patterns, table 3.1 indicates greater magnitudes in standard deviations than the means. From Figure 3.7 it can be seen, that the temporal evolution of friction forces across subjects exhibited either a positive or a negative step-deflection, which was dependant on the contact strength between the subjects fingertip and the Braille-display with respect to the pre-stimulus interval. Moreover, friction forces obtained for cases of a negative deflection showed larger step heights. However, the standard deviations and means were determined by calculating the absolute of step-heights (see section 2.4.2) for all subjects in the study, thus explaining the greater magnitudes in standard deviations.

3.2.3 Wavelet Phase Synchronization Stability (WPSS)

Wavelet phase synchronization was analyzed as an alternative powerful tool to detect characteristics in the EEG signal which are typically for the different stimuli. In this respect results are shown for the different cases that have been observed in this thesis.

case (i): Raising pins - One Line vs. Three Lines: Figure 3.15 (a) shows the phase stability $\Gamma_{a,b}$ for the one line (left) and three lines stimulation (right). Here, the representation schematically illustrates two cubes including all $\Gamma_{a,b}$ over subjects. Figure 3.15 (b) shows the averaged difference between the two cubes in (a), which is

$$D_{u,v}(a, b) = \frac{1}{N_u} \sum_{n=1}^{N_u} \Gamma_{a,b}(\mathcal{X}_u^n) - \frac{1}{N_v} \sum_{n=1}^{N_v} \Gamma_{a,b}(\mathcal{X}_v^n).$$

Here, $\mathcal{X}_{u \ n=1}^{nN_u}$ and $\mathcal{X}_{v \ n=1}^{nN_v}$ denote the EEG responses belonging to the one and three line stimulation. N_u and N_v represent the number of trials in the respective groups. The wavelet scales form the y-axis, from 10 (30.7Hz) to 90 (3.4Hz), with a scale discretization by 1 plotted over the first 800ms after stimulus onset. The magnitude is encoded in colors varying from black (smallest) to white (largest) values. Figure 3.15 (c) shows the results for the one way ANOVA significance test (significance level $p < 0.05$) which was calculated as follows. Each pixel in the significance map represents the ANOVA-test between a certain scale and time-point of the one- and three-line stimulation over all subjects, which is schematically indicated by the grey bullet point and dashed grey line in Figure 3.15 (a).

Thereby p -values smaller than the significance level are assigned to 1 (white areas) while otherwise to zero (black areas). The white spots in the resulting significance map thus indicate significant differences between the one and three line stimulations. Major positive differences appear in the time range 100-400ms after stimulus onset for specific scales. For scales in $[10, 20]$ (correspond to beta band) differences are more pronounced in the 100-200ms range. Scales in $[20, 60]$ (correspond to alpha band) show significant differences in the 200-400ms range while for scales >60 major differences in the synchronization stability are noticeable for the 400-600ms. As an example, Figure 3.15 (d) shows the averaged synchronization stability for EEG responses which belong to the one and three lines stimulations for the specific scale $a = 28$ (frequency of 10.9Hz, i.e., in the alpha band). It can be seen that

3.2 Part B: Experiments - Braille-display

significant differences in the synchronization stability are associated with the time range between 100-200ms and 200-400ms after stimulus onset.

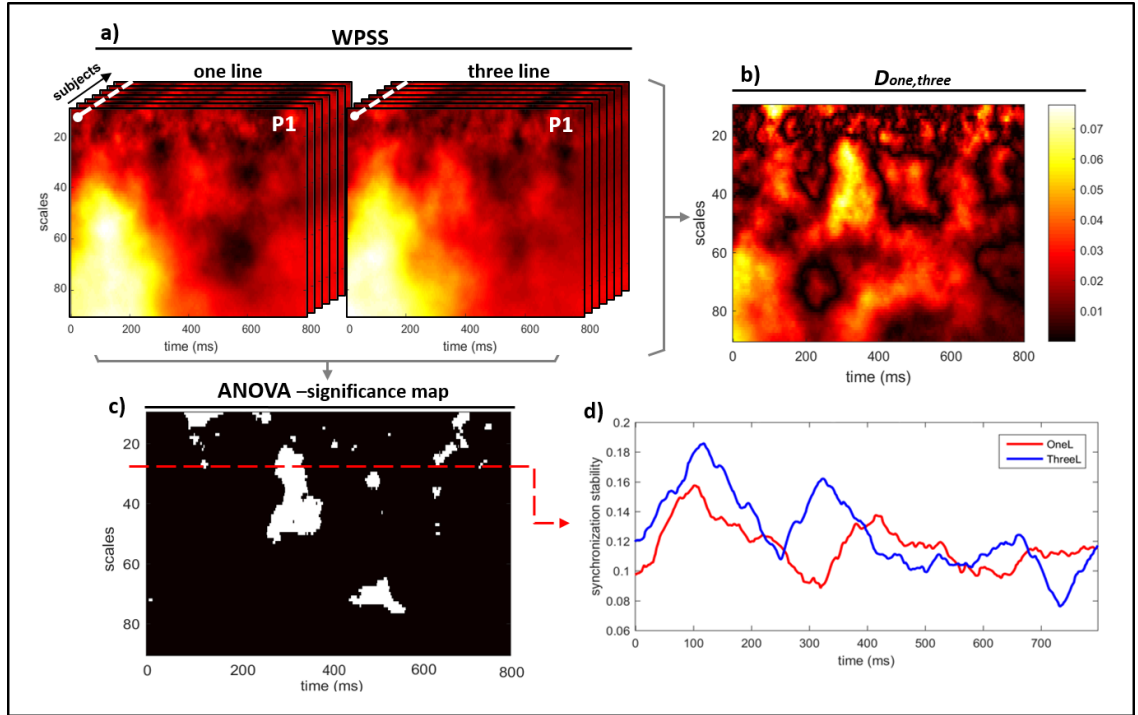


Figure 3.15: *Case (i): Raising pins* One line vs. Three lines. a) WPSS for discrete scales a and time b . b) Averaged difference $D_{one,three}(a, b)$ of the synchronization stability of the two stimuli in (a). c) Calculated significance map between WPSS for both stimuli in (a) using ANOVA-test ($p < 0.05$). White areas indicate significant differences associated with (b). d) Averaged difference of the synchronization stability for scale $a = 28$ (dashed red line) as example.

The differences for the 100-200ms interval presumably arises from brain activity associated with the somatosensory cortex including the P100 (80-130ms) and the N140 (140 -200ms) waves (Forster and Eimer, 2004; Soto-Faraco and Azañón, 2013), with a stronger synchronization for the three line paradigm.

case (ii): Raising vs Lowering pins - Same Braille-pattern: For this case we just show in Figure 3.16 (a) the averaged difference of the wavelet phase stability between ERPs obtained for the one line stimulation but with respect to the raising (i.e., stimulus onset) and lowering (i.e., stimulus offset) of pins and in Figure 3.16 (b) the respective significance map ($p < 0.05$) calculated between the WPSS of the two conditions in case(i). For this case, major positive differences appear in the

time range 50-250ms after stimulus. Within this time range statistically significant differences are found for scales in $[20, 60]$.

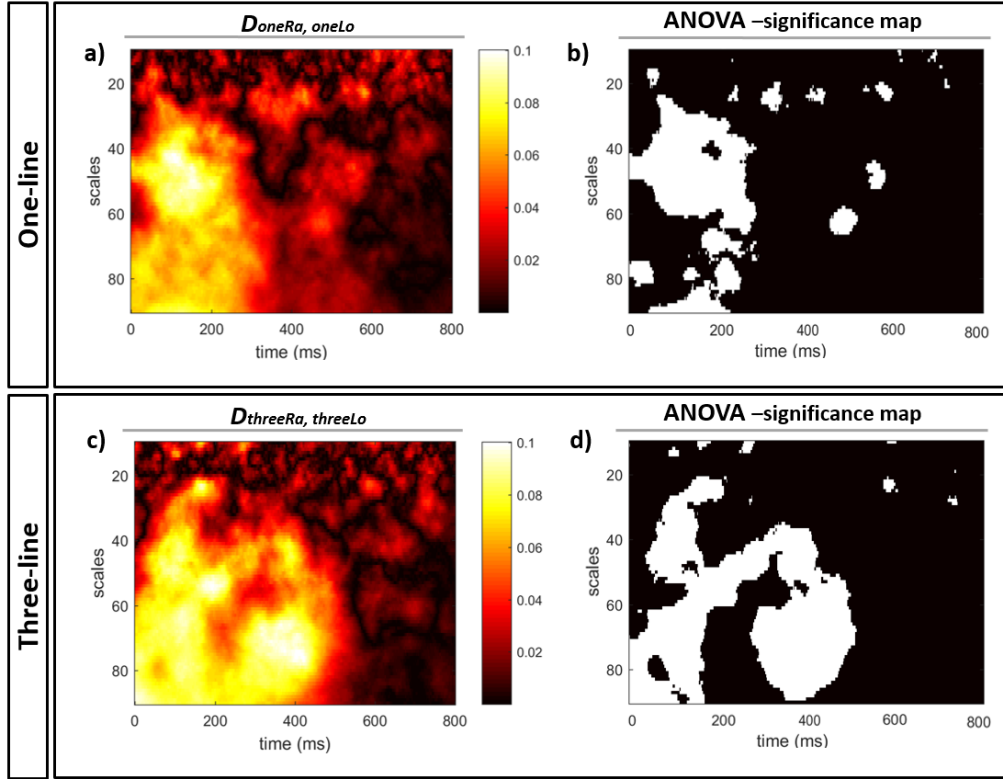


Figure 3.16: Case (ii): Raising pins vs lowering pins. Averaged difference of the synchronization stability for discrete scales and time for the one line stimulation $D_{oneRa, oneLo}(a, b)$ (a) and three lines stimulation $D_{threeRa, threeLo}(a, b)$ (c). Calculated significance map using ANOVA-test ($p < 0.05$) for the one line stimulation (b) and three lines stimulation (d). White areas indicate significant differences associated with (a) and (c).

Figure 3.16 (c) shows the averaged difference of the calculated wavelet phase stability for the case when three lines of pins are raised and lowered. The ANOVA significance map (significance level $p < 0.05$) between the two data sets for the three-line stimulation is shown in Figure 3.16 (d). Major differences between those two groups are found in the time range 50-200ms (scales in $[30, 50]$, lower alpha-band (6.1-10.2Hz)) and 250-450ms (scales in $[50, 90]$, theta-band (3.4-6.1Hz)).

Figure 3.17 depicts the averaged synchronization stability for the one line paradigm (a) and three line paradigm (b) for $a = 46$ (frequency of 6.68Hz, i.e., upper theta band) as example. This scale was chosen as the compromise between the temporal

resolution and differences in the frequency band.

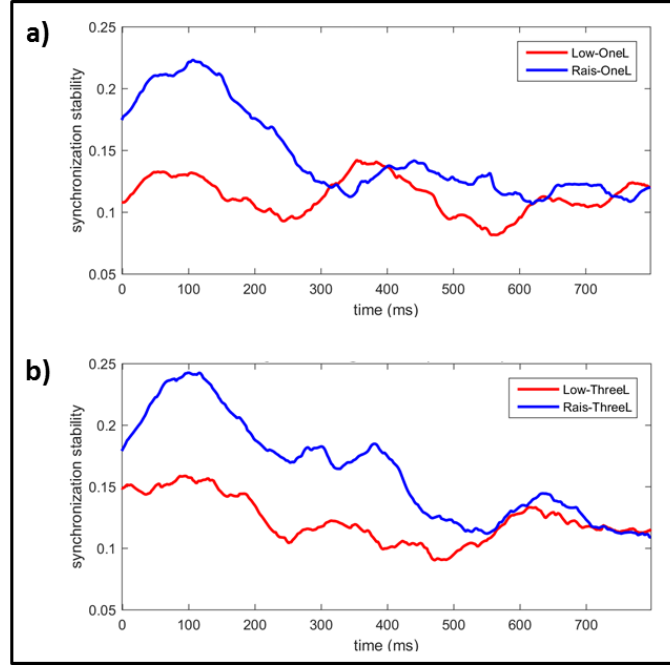


Figure 3.17: *Case (ii)*: Raising pins vs lowering pins. Averaged difference of the synchronization stability for scale $a = 46$ associated to the one line stimulation (a) and three lines stimulation (b).

For larger scales the differences are still positive but less localized because of a decreasing temporal resolution which traces back to the wavelet transform. For the one line stimulation, differences of the synchronization stability are larger in the time interval between 0-250ms, while the three line stimulation shows significant differences associated to the time interval between 0-400ms. In both cases the raising of pins (blue curve) induces a larger synchronization stability than the lowering of pins (red curves). When comparing the results of the averaged WPSS in $[0, 400]$ ms for the one line and three lines stimulation, the three lines stimulation shows much larger synchronization stability for both, the raising and lowering of pins.

Consecutive-Trial Resolving Analysis (CTRA)

The consecutive-trial resolving analysis (CTRA) was performed to assess information on the temporal evolution of the synchronization stability. In the following, we restrict our interest to the quantity $\bar{\Lambda}_a^I[M]$ in Eq. (2.4.6). This quantity indicates the synchronization stability over M -consecutive averaged WPSS trials for a fixed

scale and given time range. Figure 3.18 shows the results for the observed cases.

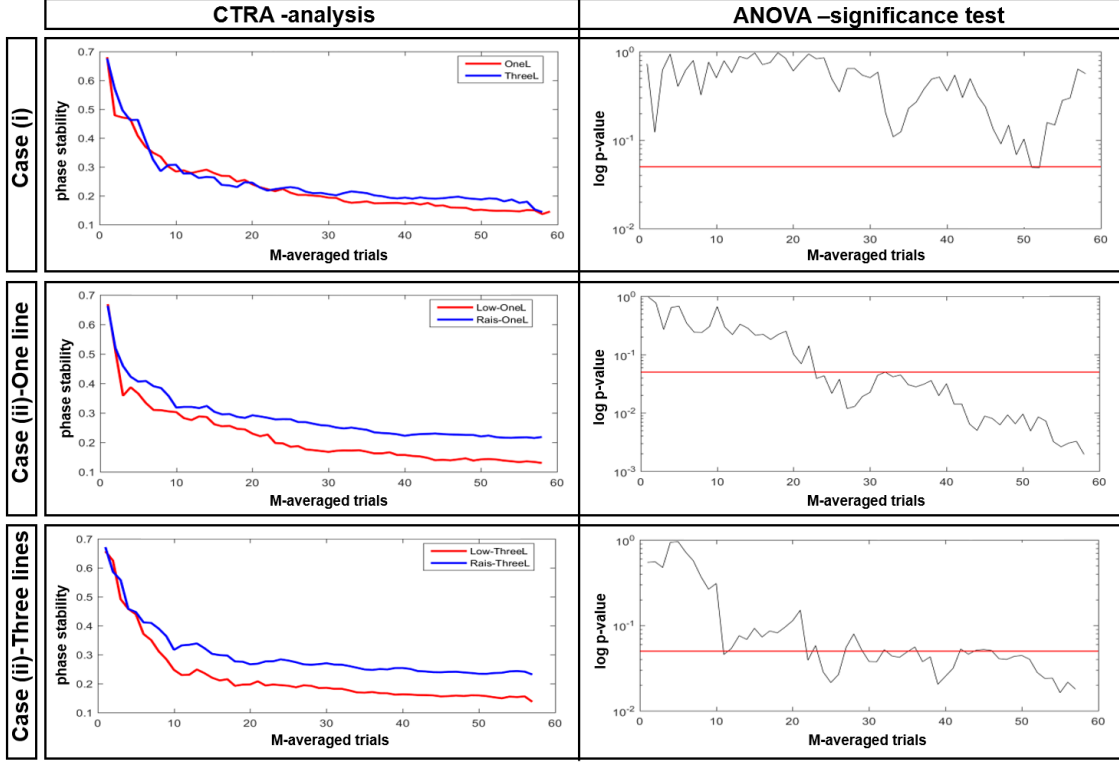


Figure 3.18: Left panel: Consecutive-trial resolving analysis (CTRA) of the mean of $\bar{\Lambda}_1^I [60]$ and the time interval between 80ms and 150ms. Right panel: Analysis of variance - ANOVA-test ($p < 0.05$) in a semi logarithmic graph. Significance level is highlighted as a red solid horizontal line. Note: Extracted scale for $case(i) = 28$ and for $case(ii) = 46$.

In particular, the left panels show the CTRA $\bar{\Lambda}_1^I [60]$ over 60 trials for the distinct cases, i.e., the consecutive average (over 60 trials) of the mean of the synchronization stability measure. The right panels represent the ANOVA-significance test ($p < 0.05$) obtained between the respective CTRA-analysis of the mean of $\bar{\Lambda}_1^I [60]$ shown in the left panels. EEG signals show a prominent positive P100 wave consistently present over all subjects. Thus, the time interval was chosen between 80ms and 150ms. Comparing the CTRA-analysis for the raising of the distinct stimulations-pattern in case(i), a similar trend is apparent over the course of the experiment. This trend is also observed in the ANOVA-test ($p < 0.05$) on the right panel, i.e., no significant differences are visible between both stimulations. In Figure 3.18 we show the same analysis with corresponding ANOVA-tests for the case(ii). Here, in contrast to case(i), two conditions are regarded, namely the raising and the lowering

3.2 Part B: Experiments - Braille-display

of either one (second row) or three lines (third row) of pins. For both stimulations it we observed that the raising of pins (blue curves) shows a larger CTRA, i.e., a larger synchronization stability in the course of the experiment. When comparing the corresponding ANOVA tests, the one line stimulation (second row) converges for a smaller amount of trials ($n=20$) to stable significant ($p < 0.05$) values. The three lines stimulation converges for $n=30$ trials to significant values.

4 Discussion

The work presented in this thesis focuses on neural correlates evoked by a tactile stimulation of the human fingertip. The stimulation was performed by a programmable Braille-display which was moved along the resting fingertip. Stimulation paradigms consisted of distinct setup of pin lines (one and three lines) randomly presented to the fingertip by raising and lowering pins into and out of contact.

4.1 Tribology of Fingertip

Signal-Characteristics of the Friction Force

The friction forces showed two distinct types of signal-characteristics, which we attributed to the differences in physical contact-strength between the fingertip and the Braille-display. Before each measurement, the Braille-display was adjusted in height in a way that there was light contact with the fingertip when pins were lowered, whereas the raising of pins brought them into stronger contact with the fingertip.

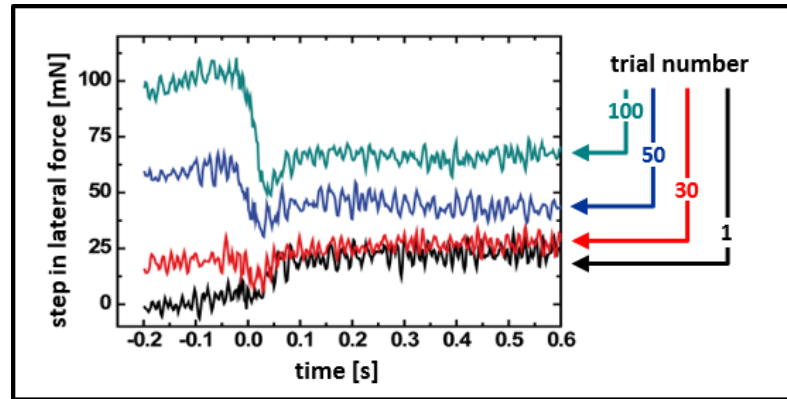


Figure 4.1: Temporal evolution of the lateral force. Braille-pins are raised at $t = 0$. Force curves are averaged over 20 trials starting from trial number: 1 (black), 30 (red), 50 (blue), and 100 (green).

Figure 4.1(c) shows lateral force signals obtained for one subject, where each force curve reflects the average of 20 consecutive trials chosen over the course of the measurements. This figure demonstrates that the deflection of the friction-step

changed during the experiment. Apparently, after trial 30 there is a change from a positive to negative step in the lateral force, which is caused by an enhanced contact-strength between the fingertip and the Braille-display. The subject started the experiment with a light contact-strength but involuntary lowered the finger into contact in the course of the 180 trials. To check if this was the case for all subjects, i.e., if subjects tend to start measurements with a light contact-strength while to the end show a more firm one, an single trial analysis of the force-steps was performed. We compared mean values of the respective portions of the force signals, i.e., the pre-stimulus and post-stimulus interval. Trials showing smaller values for the pre-stimulus interval were assigned to a positive deflection in force-step suggesting a initially light contact-strength. In contrast, trials with higher values for the pre-stimulus interval, i.e., a enhanced contact-strength resulted in a negative deflection in force-step due to the reduction in contact-area.

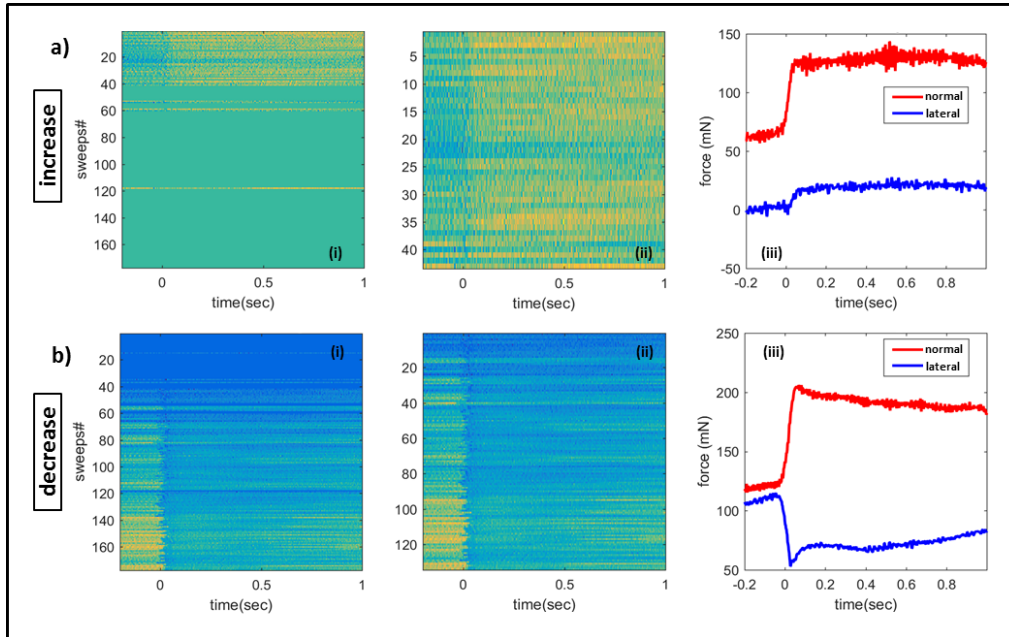


Figure 4.2: Single trial analysis of the friction step upon a positive (increasing, see panel (a)) or negative (decreasing, see panel (b)) deflection. i) Occurrence of increased (upper) and decreased (lower) step deflection across 180 trials. ii) Accordingly extracted trials from (i). iii) Time-domain averages of extracted lateral and normal force trials. Note that lateral force is showing a opposite step-deflection, comparing (a) (b) while normal forces always show a increase in step.

Figure 4.2 shows this analysis where trials with positive steps (see panel (a)) and

trials with negative steps (see panel (b)) are extracted and arranged in sub-matrices. Out of the 180 trials observed during the measurement it is noticeable that at the beginning (until approximately trial 40) contact strength is light (see figure 4.2 (a-i)) while during the time-course of the experiment becoming more firm (see figure 4.2 (b-i)). In figure 4.2 (ii) the respective trials are extracted and arranged in sub-matrices. For this subject it turns out that 43 trials show a step-increase and 137 trials a step-decrease. Considering the averaged waveforms depicted in figure 4.2 (iii), lateral forces (blue curves in (a) and (b)) clearly show the difference in step change.

When considering all measured force-signals for the subjects included in the study, 3293 single-trials of friction forces were collected, of which 63% show a positive and 38% a negative step-deflection. Despite the higher amount of trials with positive force-steps, the averaged time domain signals show a decrease in lateral force after stimulus onset (see figure 3.14 case (i)). This effect can be explained by the larger contrast (relative change) between baseline and step of the lateral force sequences for the trials with negative steps.

As mentioned, the Braille-display was adjusted in height such that there was light contact with the fingertip when pins were lowered, whereas the raising of pins brought them into pronounced contact with the fingertip. This setting, ideally maintained during measurement, resulted in an increase in friction in every single trial when pins are switched from the lowered to the raised state. Although participants were explicitly asked to stay passive, they unconsciously adjusted their fingertip-Braille contact strength. The resulting stronger contact led to a inverted step of the friction force (Özgün et al., 2018b). If subjects would not counteract and regulate the contact, cortical activity could dynamically adapt to the stimulation (temporal desensitization effects) and thus would lead to a suppression and decrease in somatosensory responses due to decrease in mechanoreception (Chung et al., 2015).

Friction of Skin on the Braille-display

Friction arises when the fingertip moves relative to a surface (or vice versa). Since signal-characteristics are attributed to multi-scale and nonlinear physics during sliding, friction is very complex and often chaotic (Wiertlewski et al., 2011). Many groups have studied the tribology of skin in terms of identifying the underlying fundamental mechanisms. Adams et al. considered Bowden's and Tabor's two-term

model as the basis for their analysis on friction (Adams et al., 2007). The model describes two terms which contribute to the friction, where one is adhesive interfacial shear and the other the viscoelastic deformation of the skin. By performing experiments comparing the friction of a sliding and rolling sphere on glabrous skin, they found that viscoelasticity of the skin played rather a subordinate role in friction. In lubricated sliding on skin, viscoelastic effects may still lead to a significant shift in the velocity dependence as predicted by so called Stribeck-curves, representing friction regimes categorized into solid, mixed, and fluid friction (Persson et al., 2013; Stribeck, 1902).

In a study by Darden and Schwartz (Darden and Schwartz, 2015), finger friction was studied by using Braille dots embossed into paper. Experiments were conducted by sliding the fingertip over the papers, traversing the dots. For this transitional fingertip-sliding, they found an increase in the coefficient of friction whenever the finger crossed the dots. With reference to Bowden and Tabor, the authors attributed this increase to the hysteretic deformation of soft skin rather than the adhesive shear, which they explained to become more important for probes of smaller radii. However, since the dots and the surface were made from the same material, adhesive friction was also expected to be rather small when fingertip crossed dots.

In the study presented in this thesis, the raising of Braille-pins into fingertip contact caused a decrease in the coefficient of friction. Bearing in mind the higher friction coefficient between fingertip and Braille-display, the difference between the materials of Braille-surface and pins, and the larger stroke height of our pins, we can say with confidence that our results are still in line with Darden's and Schwartz's analysis. Raising the dots efficiently decreased the interaction with the surface and led to a friction coefficient which approached that reported by Darden and Schwartz. Subsequently the tribology of the Braille-display can be elucidated as follows. Due to the indentation of Braille-pins into the fingertip-skin the normal force shows an increase, i.e., a positive intensity step when pins are raised. The expected force for one dot can be approximated by Hertz contact mechanics as

$$F = \frac{4}{3}E^*R^{\frac{1}{2}}d^{\frac{3}{2}} = 23\text{mN}$$

with the radius $R = 0.6\text{mm}$ and an indentation depth of $d = 0.6\text{mm}$. The elastic modulus for 1mm indentation depth has been determined by indentation with a comparable probe radius to be $E \approx 12\text{kPa}$ (Pailler-Mattei et al., 2008) and $E^* = E/(1 - 0.5)^2$. When Braille-pins are switched to the raised state, about

4.1 Tribology of Fingertip

four pins (equidistant from center-to-center; 2.5mm) are in contact with the fingertip. Considering the observed step in normal force, which is about 50mN (see figure 3.6 (a)), the step is less than four times the expected value for one dot. This observation can be attributed to the fact that skin deformations of adjacent pins overlap. When Braille-pins are raised, two terms contribute to the step in lateral force and its signal-characteristics. The first is the decrease of adhesive shear between fingertip and the Braille-display, while the second the increase in friction during fingertip Braille-pins interaction. Note that the latter may have components of adhesive shear and of viscoelastic deformation. If the contact-strength between fingertip and Braille-display is light, the first contribution can be ignored which results in a positive deflection of the step in lateral force. If contact strength is more firm, the decrease of adhesive shear friction dominates. The decrease in adhesive shear between the fingertip and the surface of the Braille-display follows the raising time of the Braille-pins of 40ms. The increase in friction during the interaction of fingertip and raised Braille-pins, however, shows a characteristic time constant of 35 ± 10 ms. We believe that this time constant is the duration for the viscoelastic deformation of the skin to adapt its shape to that of the raised Braille dots. On the other hand when Braille-pins are lowered, skin requires longer times for the relaxation. Thus, the full relaxation to the conformal contact with the surface of the Braille display takes 156 ± 70 ms. The observed characteristic time scales are deduced from the coefficient of friction, where the temporal development was quite similar over all subjects (see figure 3.10). Crichton et al. reported on indentation measurements at a smaller length scale in studying the viscoelastic relaxation of skin (Crichton et al., 2013). They found a fast relaxation with a time constant of 300ms and a slow component with a time constant of 2.5s. In terms of viscoelastic conformation the the time constant for the fast relaxation supports our interpretation in terms of viscoelastic conformation.

Reviewing the difference between subjects with a either positive or negative step in the lateral force (see figure 3.7 (a)), a doubling between one line and three or five lines of pins raised, as can be seen for the normal force (see figure 3.6), became apparent. In contrast, when steps exhibit a negative deflection no significant differences are observed. This observation may result from the fact that the raising of one line of pins is enough to reduce the contact with the Braille-surface, resulting in a decrease in lateral force. The raising of more than one Braille-line, however, clearly shows a increase in friction with the number of lines raised.

The three and five lines of stimulation showed quite similar forces acting between the fingertip and the Braille-pins. Considering figure 3.6 (b), however, it is noticeable that when five lines of pins are raised, the outermost lines do not interact significantly with the fingertip. This was also observed by Louis Braille, who decided to use only three lines for the Braille-print (Hatwell and Gentaz, 2008).

Friction as Key-Parameter in Tactile Perception

It has been claimed that the friction force plays a key-role in tactile perception (Skedung et al., 2013; Darden and Schwartz, 2015). Based on the results illustrated in figure 3.14, the following observations could be made concerning relations between exogenous stimuli profiles and the respective neural correlates.

Considering case (i), significant differences between the one line and three lines of stimulation were found only for the normal forces. Even a doubling in step intensity (from 45mN to 90mN) is not enough to induce significantly different ERPs, neither in amplitude nor latency (see figure 3.14). If we now assume that the normal force is not the key parameter in tactile perception, in case(ii) a clear difference is observed in the friction force intensities and respective amplitudes of averaged ERPs. Both stimulation patterns show a larger step in friction intensity when pins are raised, compared to the lowering of pins. For the one line stimulation the step is four times higher (20mN/5mN) and for the three lines stimulation three times higher (30mN/10mN). The observed N50-P100 peak-to-peak amplitudes show larger values for the larger frictional step when raising and smaller values for the smaller frictional step when lowering the pins ($1.4\mu\text{V}/0.6\mu\text{V}$ for one line pattern and $1.6\mu\text{V}/0.8\mu\text{V}$ for the three line pattern). ERPs, in general, are believed to reflect the summed activity of postsynaptic potentials of similarly oriented cortical pyramidal neurons, which fire in synchrony during information processing (Sur and Sinha, 2009). Larger ERP-amplitudes might therefore arise from the involvement of a larger amount of pyramidal neurons and indicate a better neurophysiological-performance to the respective stimuli or a higher synchrony. The results suggest that larger step intensities in friction result in larger ERP amplitudes, assuming that the absolute height of positive and negative step intensities is the relevant parameter. Our results then support the assumption that friction is the driving force in tactility.

4.2 Neurological Responses

The frictional stimuli supplied by the sliding Braille-display caused ERPs of similar prominent waves (N50, P100) among 15 of 20 subjects. In contrast, later peaks such as the N140 and P200 waves showed more variation across subjects, which might be due to higher cognitive process involvement. Considering the signal-characteristics of ERPs reported by Hashimoto (Hashimoto et al., 1988) and Forster (Forster and Eimer, 2004), where the authors focused on early tactile processing, the ERP-structure of our results show good agreement. In the study of Hashimoto et al., the authors investigated early ERPs as function of the stimulus intensity by applying short air-puff stimuli to the sole of feet. They found that ERP-amplitudes (most pronounced for the N60 component) increased with stimulus intensity, and that the latency of peaks decreased. In the work by Forster and Eimer, the main focus was on the influence of spatial attention on tactile perception. They found that the latency of later ERP peaks (from 80ms and higher) depended on the gaze of the subjects, i.e., on whether or not the test subjects looked at the finger. The stimulus was employed by the raising of a rod against the fingertip, where in the case when the subjects focused on the rod latencies decreased.

In the light of our initial observations in Part A we could not find significant coherences between stimulus-intensity and ERP-latency. Note that in Part A we did not consider different stimuli, i.e., the stimulus was the same over the course of the experiment. Thus, we expected that for the well defined and varying stimuli used in Part B, coherences would appear. This was not the case. As in case(i), even a doubling in the stimulus force offered by the Braille display (one vs. three lines of dots raised) showed no significant differences in amplitude and latency of ERPs (see figure 3.14). For a more detailed analysis we further split the subjects in two groups, one with light and one with firm contact between fingertip and Braille display (positive and negative lateral force-steps in figure 3.7 (a)), but none of the sub groups exhibited the expected effect. Normal and lateral forces showed variations in step-intensities across trials. We, thus, also took advantage of this variability by sorting the trials in ascending order with respect to the step-height. Figure 4.3 shows this procedure for one subject, as example. As can be seen the correlation between the sorted data, i.e., between the sorted step-intensity profile (see a) iiiii) and the P100-trace track (see b) iiiii) shows an antiproportional behaviour, where with increasing step height the P100-latency decreases. The correlation with the

accordingly sorted ERP-trials upon either latency or amplitude, however, did not show expected consistency over subjects.

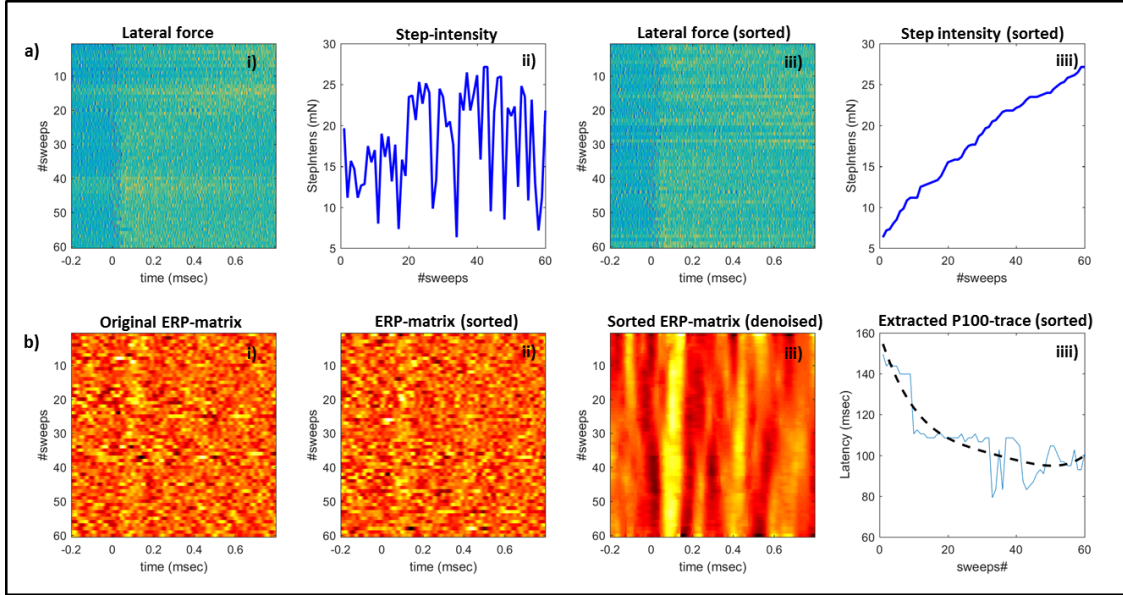


Figure 4.3: Sorting of single ERP-trials in dependence on the step-heights of single-trial lateral forces. a) Single trial lateral forces in matrix representation (i). Step-height profile of lateral forces over trials (ii). Sorted version of lateral force matrix (iii). Sorted step-height profile of lateral forces (iiii). b) Original ERP-matrix (i). Sorted version of ERP-matrix (ii). Denoised version of sorted ERP-matrix (iii). Extracted P100-trace track with polynomial fit of degree 9 (iiii).

Similar to our study, Genna et al. (Genna et al., 2017) reported on event related potentials evoked by a reciprocal sliding of a parallelepiped surface along the lateral direction of the human fingertip. The fingertip rested on the surface while the start of the sliding was the event. They found contralateral C3 ERPs which consisted of prominent P100-N140 and P240 waveforms. Lateralization was observed for the P100 and N140 component with smaller amplitudes and delayed latencies in the ipsilateral side. Considering the signal-characteristics of ERPs upon the raising of Braille-pins, our results are in good agreement with the study of Genna et al. However, our results also indicate a long latency N50 component consistent over all subjects. We assume that the raising of Braille-pins results in larger stimulus intensities as compared to the sliding of a static surface implemented in Genna et al. The larger intensity may then activate a larger amount of synchronized afferents and thus may lead to the distinct N50 peak in our study. In respect to lateralization, we

could also observe smaller amplitudes and delayed latencies for ipsilateral ERPs, e.g. for the C4 electrode position. Furthermore, Genna et al. observed a post-stimulus positive peak (150-200ms) in the central region of the brain, which they assigned to the cognitive process of reflecting the end of the tactile stimuli. In our study, the end of stimulation was characterized by the lowering of Braille-pins. Considering the respective portion of the EEG-signals, we could not observe such a positive waveform. However, our EEG-protocol did not include electrode spots at central regions. In contrast to the study by Genna et al., our design mimicking a Braille-reading scenario had the fingertip always staying in contact with the Braille-display and thus there was no actual end of the frictional movement.

Phase Synchrony of Brain Signals

Amplitudes of single ERP-trials are fragile and have high variance from trial to trial (Kolev and Yordanova, 1997). It is difficult to access information on synchronization measures even with robust amplitude detection techniques, such as the shift-invariant time scale entropy introduced in (Strauss et al., 2004), is difficult to access. Thus, we suggested a time-scale measure based on instantaneous phase characteristics of single ERP-sequences, which in contrast to time domain averaging show more consistent differences over larger time intervals.

The synchronization stability measure observed for the case(i) (see figure 3.15) showed main positive differences between patterns at around 300ms. The observation of the grand average ERPs for both patterns revealed a negative peak around 330ms more pronounced and with a earlier occurrence for the three lines stimulation. In respect to tactile perception this component is not yet investigated for our electrode configuration. For this time range only the prominent P300 wave has been recognized in studies on tactile perception with focus on attentional processes (see (Forster and Eimer, 2004)). ERP waveforms basically depend on exogenous and endogenous factors where the latter also include preparatory potentials known as the contingent negative variation (CNV) (Fonaryova Key et al., 2005), and readiness potentials (Scherer et al., 2009). The above mentioned N300-peak, which we observed may then be explained as follows. In our experiments procedure, the raising of Braille pins into contact is followed by a lowering of pins out of contact after a sustained stimulation time (longest 2 sec). Subjects may have had a readiness or a preparatory attitude for the second stimuli, i.e., they were expecting a subsequent lowering of pins after stimulation (raising of pins). In contrast, for the conditions when pins are lowered (see red curves in figure 3.14 case (ii)), this N300 wave can

hardly be found in the averaged ERP sequences.

From auditory studies it is known that the use of identical paired stimuli (usually a conditioning and a test stimulus) with inter-stimulus intervals larger than 500ms, typically result in a suppression of the amplitudes of middle latency auditory evoked ERPs to the second stimulus (see (Retz et al., 2012) and references therein). This is believed to happen due to intracortical inhibition processes. In our experiments ISIs between the two stimuli (i.e., raising and lowering of pins) are in the order of seconds. The reduction in amplitudes of the ERP-responses to the lowering of pins might, therefore, result from inhibitory processes. The analysis of the mean WPSS in case (ii), shown in figure 3.17 (a) and (b), revealed major differences in the time interval [0-400]ms. Within this time interval synchronization is higher for the condition when pins are raised (blue curves), which indicates that instantaneous phases of ERPs are less synchronized when the frictional stimulus is smaller (see respective friction forces in Fig. 3). Comparing either the raising or lowering between both stimulations, the three lines of stimulation showed much larger synchronization stability. Thus we hypothesize that the larger the friction the larger the instantaneous phase coherency.

4.3 Physical Stimuli and Neural Correlates

From the research field of auditory ERPs it is known that there exists a correlation between the stimulus-intensity and the latency of neural responses. A antiproportional relation, i.e, a consistent trend of decreased peak-latency towards the stimulus onset occurs with increased signal-intensity (Wolfe et al., 1978; Corona-Strauss et al., 2009). In the work by Corona-Strauss et al. (2009), the authors used chirps, i.e, short sharp high-pitched sound with varying intensity levels (20,30,40 dB nHL) over varying frequencies for stimulation purposes. Their results indicated a shift in latency of the wave V auditory brainstem response (ABR) towards the stimulus onset when intensity was increased.

In the framework of tactile perception there is little to no information regarding amplitude dependence of latency. To our knowledge there is only the work of Hashimoto et al., which directly relates physical forces (intensities) to physiological EEG correlates by means of intensity-latency relations (Hashimoto, 1987; Hashimoto et al., 1992). However, while the air puff technology of Hashimoto et al.

4.3 Physical Stimuli and Neural Correlates

provides well-defined reproducible stimuli, they differ significantly from the typical skin strain related to the perception of materials by touch. Thus, it remains a challenge in designing experiments with well-defined frictional stimulus events which resemble the strains experienced in tactile exploration. In the following, we discuss some of the results obtained in this study for neural correlates of fingertip friction which is comparable to tactile exploration.

Figure 4.4 shows the results for the analysis of latency-intensity relations from one selected subject after tactile stimulation of the fingertip using the machined block (Part A).

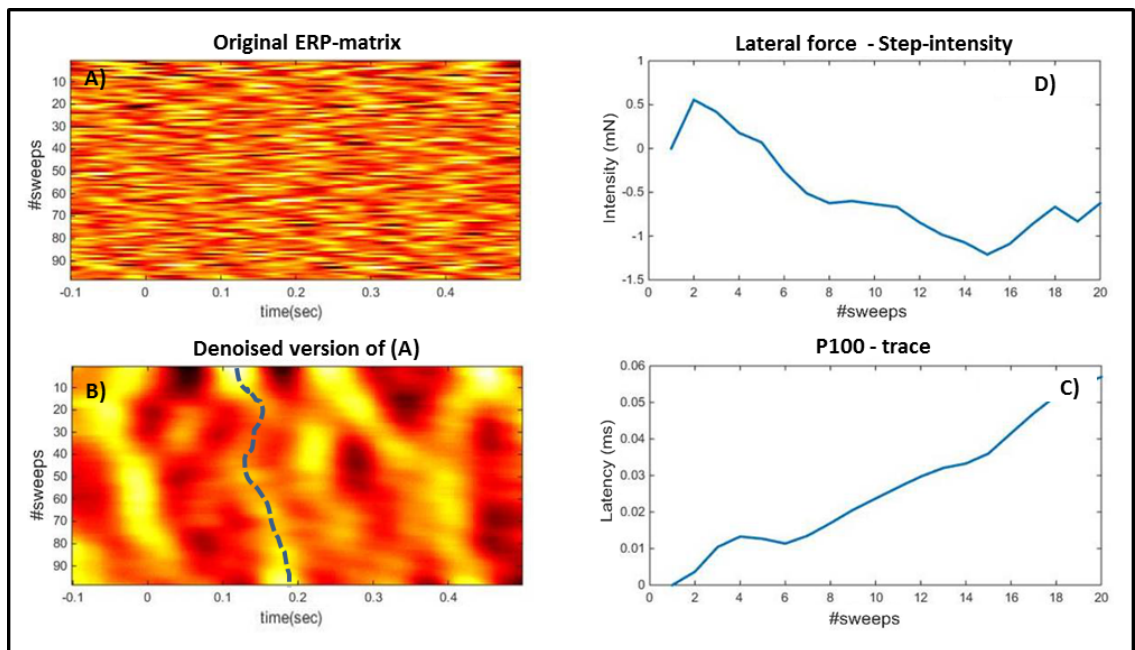


Figure 4.4: Individual results of latency-intensity relations obtained for the study in Part A. After applying the denoising scheme on the original ERP-trial matrix (A), traces became apparent (see the potential P100-trace track indicated by the blue dashed line in (B)). C) P100-trace extracted from (B). D) Step intensity of single friction forces. Note that the values in (C) and (D) are normalized to the very first trial (see (Öezgün et al., 2015)).

The top left image (A) depicts the contralateral C3 ERP-image as a function of time. ERP-images usually provide information on similarities in repeated stimulations visible as traces across trials. However, EEG signals mostly have a poor signal-to-noise ratio (SNR), where magnitude of transient ERPs differs often by several factors from the magnitude of the background EEG (Hu et al., 2010). For

the ERP-matrix obtained in figure 4.4 (A) no clear traces can be seen. In order to enhance the SNR by using both denoising algorithms (see section 2.4.4), traces became apparent as demonstrated in the lower left figure (B). The matrix exhibits a trace (from top to bottom) in a shifted manner, ranging from about 120ms to 180ms (highlighted by the dashed blue line), which we associated with the P100 trace over the course of the measurement.

It is believed that transient ERP-fluctuations reflect the change of slow postsynaptic potentials of similarly oriented cortical pyramidal neurons (Sur and Sinha, 2009). However, taken each trial in isolation it is not unreasonable to conclude that the unique combination of exogenous (e.g., time-dependent viscoelastic deformations and temperature fluctuations in skin, variability in the amount of activated mechanoreceptors, variability in conduction velocity resulting in differences in the spatial summation at central synapses) and endogenous cognitive processes (e.g., degree in vigilance and attention) (see (Hu et al., 2011) and references therein) may explain the great variability in latency over the course of the measurement (see figure 4.4 (B) dashed line).

Due to the shifted arrangement of the P100-trace track across trials, the extraction was computationally difficult to handle. We, thus, decided to take every fifth point by hand following the trace. The step-intensities were calculated as described in section 2.4.2 and downsampled to fit the length of the extracted support points of the trace-path. Thus, out of 150 trials we considered 30 support points for calculating the Pearson's correlation coefficient between the extracted intensity and latency profiles. However, apart from the fact that five out of ten subjects showed similar coefficients (mean: -0.7654; std: 0.0704) no conclusive evidence was found, to indicate a correlation of the traces with the step-intensities.

To evaluate whether a change in stimulus intensity may lead to pronounced jittering in latencies, subsequent measurements were performed. Different weights (intermediate (100g)/heavy (200g)) were applied from top onto the finger using a stemp (see red arrow in figure 4.5 c)). As a reference no weight was used, i.e., just the stamp weighting 30mg was in contact. Even for clearly different friction forces (see forces in the case of maximal weight used in figure 4.5 (b)) due to the use of different weights did not result in latency-shifts. For this experimental procedure subjects reported after measurements that during the course of the experiment they felt uncomfortable, and that the applied weights caused a feeling of numbness and pain in their fingertips, which likely occurred due to the compression of the fingertip

4.3 Physical Stimuli and Neural Correlates

towards the circular opening. Tactile hypaesthesia or numbness is known to result from nociceptive stimulation suggesting a mechanism involving central plasticity (Geber et al., 2008). We believe that the application of weights onto the finger activated nociceptive nerve endings, where pain-level seemed to be same for the different weights.

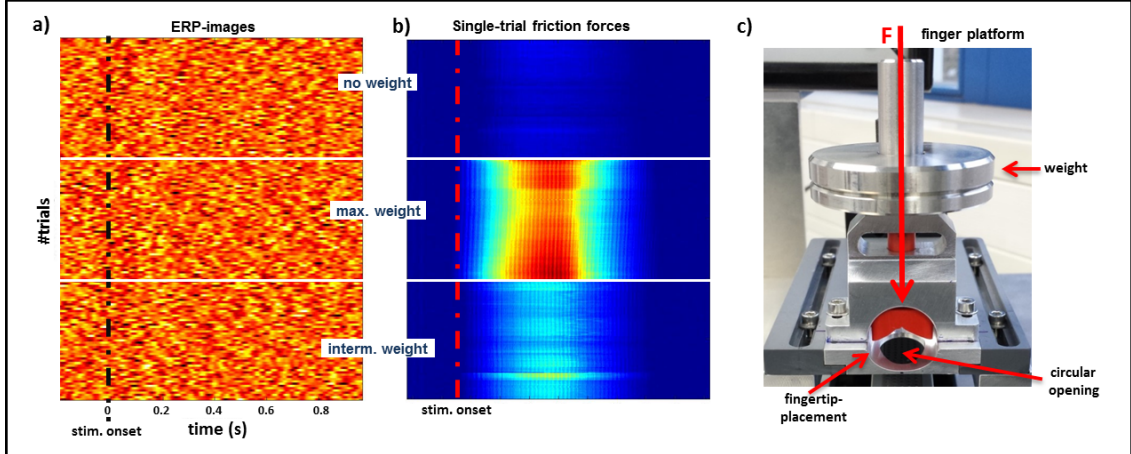


Figure 4.5: Individual results of latency-intensity relations obtained for the preliminary study in Part A after applying different weights onto the finger. a) Concatenated ERP-images obtained for the different weights: no weight (top) - intermediate weight (bottom; one ring weight of 100g) and maximal weight (middle; two ring weights). b) Concatenated friction forces obtained for the different weights. c) Finger holding platform with stamp (red part) for applying weights from top (red arrow).

Part B:

In contrast to the study in Part A, the change of the intensity was in the (external) stimulus itself. We used a Braille-display with programmable lines of pins, where the variation in stimulus-intensity was realized by different numbers of lines of pins raised or lowered. Figure 4.6 shows the results for one participant included in this study, where (a) depicts the original ERP-image, and (b) the denoised version of (a). The original ERP-images for the different numbers of lines show prominent traces over trials, approximately 100ms after stimulus onset which are enhanced in the denoised version. Although the denoised version shows a shift in P100-trace towards stimulus onset (over trials), no clear trend can be seen for the extracted trace shown in figure 4.6 (c). For the step-intensity-profile of the friction force in figure 4.6 (d), a increase is observed over trials (approximately from 20-30mN). For this subject the correlation coefficient calculated between the polynomial fits

(dashed black lines) of the P100-trace track and the intensity-profile of the friction force is negative, indicating that the P100-latency decreases with increase in force intensity. However, unfortunately out of the 15 subjects included in this study, only this subject showed a antiproportional relation between stimulus intensity and P100-latency.

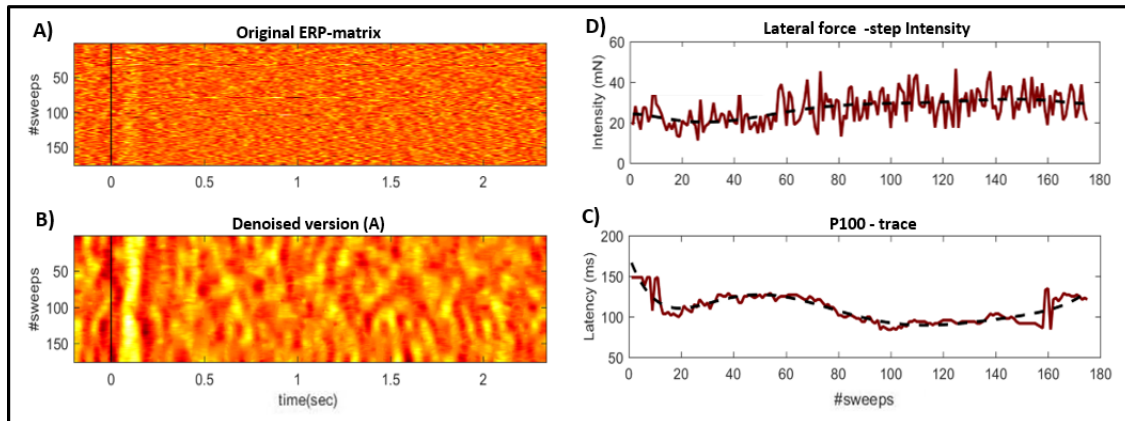


Figure 4.6: Individual results for the observation of the intensity-latency relation for the Braille-display. A) Original ERP sweep matrix. B) Denoised version of (A). C) P100-trace track extracted from (B). D) Friction steps over trials. Black solid vertical lines represent the stimulus onset, whereas black dashed lines the polynomial fit to the respective data.

Despite our efforts using a number of different approaches, no significant tendency was found for the relations between ERP-latency and force-intensity.

It is of great importance for the investigation of perception in general, to know the exact physical representation of the stimuli, as for example in the auditory framework the sound pressure level (SpL) and its perceptual correlate of loudness (Hatzfeld and Kern, 2016). As described in Hatzfeld and Kern there exist different physical representations of stimuli in tactile perception, either force F or kinematic measures (e.g., acceleration, velocity or deflection), whereby forces may be easier to handle in terms of measuring and describing, since they are single valued over the time course of the measurement. However, beyond those representations perception is also dependent on the mechanical characteristics of the skin and thus the distribution of mechanical stresses in the skin which are difficult to model (see (Hatzfeld and Kern, 2016) and references therein). The approaches in Part A and Part B may lead to different distribution of mechanical energy in the skin. The two approaches basically follow the same experimental procedure, but may lead to different kind of

perceptual features when considering the pre-stimulus interval. On the one hand the stimulation in Part A has a lead phase where no contact is established at all, whereas in the study in Part B there is a light contact with the Braille-display before pins are raised for stimulation purposes. Thus, we can distinguish between a sudden onset of stimulus, i.e., when the edge of the stimulation-block slid against fingertip (Part A) and a transitional stimulation (Part B) of the fingertip, where for sure the latter one involves influences that relay on distributional effects of the mechanical energy and stresses even before stimulus set on. Stimuli, which obviously differ in intensity (as was observed in Part B by changing the amount of Braille-lines), may therefore not be perceived appropriately, i.e., may distort sensory judgement and thus not reflect the possible intensity-latency relations.

In order to distinguish between ERP amplitudes or latencies, ERP studies reported a logarithmic dependence on the stimulus intensity. Aside the different frictional stimuli resulting from the different lines of Braille-pins, it seems that a factor of two may not be sufficient in causing significant effects. However, a dynamic force range of a factor of 25, as was used in Hashimoto's work (Hashimoto et al., 1992) to elicit early ERP responses of significant differences in amplitudes and latencies, is difficult to realize for a frictional stimulus between detection limit and pain level.

4.4 Limitations and Future Work

Setup and Stimulus

To collect data sets for a statistical evaluation of the ERPs due to standard averaging, stimulus has to be applied several tens of times during experiment (Woodman, 2010). The identification of the respective signal-portions is based on trigger signals. Facing the problem of an electrical cross-talk reported in section 2.4.1, we virtually detected the stimulus onsets using a threshold-procedure considering the single trial force steps, which indicated the very first contact with the stimulus material. However, another possibility in detecting the event in studies on passive surface structures could integrate a photoelectric sensor. Figure 4.7 (a) depicts a schematically view of the photoelectric sensor (transmitter and receiver) for triggering the contact between fingertip and surface. The sensor itself is mounted on the moving stage, where each time when the finger passes the beam a trigger signal is released.

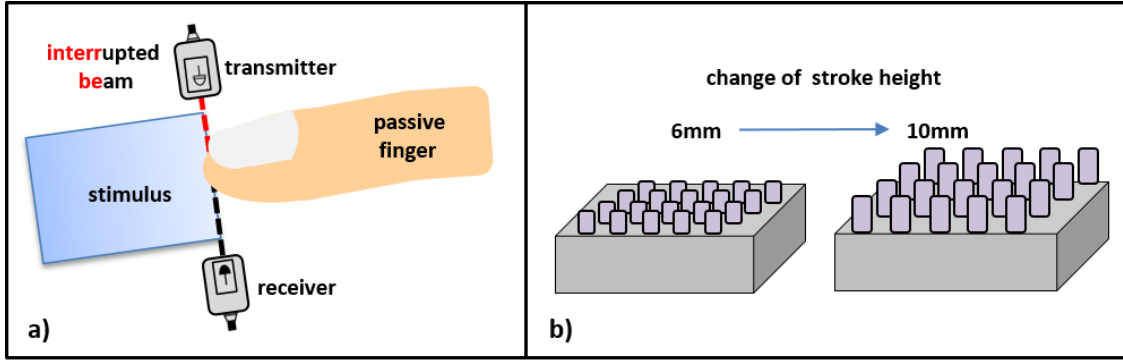


Figure 4.7: a) Photoelectric sensor for triggering the contact between fingertip and surface. b) Modification of the stroke height of Braille-pins.

Despite the pronounced differences in normal and lateral forces obtained for the different stimuli, the induced ERPs did not show the expected differences in amplitude and latency. We observed two distinct types of signal-characteristics for the lateral force which we identified to originate in the change in contact-strength (see figure 4.1) between fingertip and Braille-display during measurements. To mimic and match an appropriate Braille-reading scenario, we adjusted the Braille-display in height such that initially there was a light contact with the fingertip, when pins were in lowered-state. Although the stimulus resulted in pronounced ERPs, the light contact as adjusted clearly influenced our tribological and potentially also our ERP results. The stroke-height of Braille-pins from the lowered to the raised-state was 0.6mm. We observed that the height change of the fingertip over the course of 180 trials was of the same order than the stroke height. Thus, for further experiments we suggest a modification of the Braille-display itself, i.e., an enlargement of the pin-displacement (for instance up to 4mm) to check whether an initially not contacted state of lowered pins might result in distinguishable ERP amplitudes and latencies for different intensities (see figure 4.7 (b)).

Robust Trace-Extraction

The denoising of single trial ERP matrices introduced in section 2.4.4 showed a reliable way in enhancing the signal-to-noise-ratio (SNR). This SNR-enhancement may also help to improve the ability in extracting latency-information of prominent ERP-components occurring over trials. Having the matrices denoised, it turned out that the extraction, against expectations, was not trivial. Traces shifted across trials, exhibited large variations in amplitude and event interruptions. Algorithms for trace extraction facing this behaviour are not easy to implement. Thus, for

investigations on possible P100-latency force-intensity relations, we searched for a certain amount of sample-points within each trial, which correspond to the largest amplitude-values. We considered the portion of the signal surrounding the P100-trace across trials. The trial-wise averaging of those detected time-points then reflect the latency-track of the P100-trace. It turned out that within the considered time-range concurrent traces may be present, either across all or just some trials. This led to miscalculations where obtained latencies might not represent the visible trace-track. Unfortunately, the extraction of trace-tracks as done in this work, can only give a trend but is not accurate enough. One promising approach that might be used in reliable extracting event related information, such as latency information in ERP-images, is based on edge detection and structure preservation methods. We have now started to solve this problem in collaboration with mathematicians and computer scientists.

This work characterized the exogenous, i.e. stimulus driven component of the P100 wave. Thus further Future work which focuses on the variation of endogenous states by, e.g., selective attention (see (Forster and Eimer, 2004)) can be based on the presented results. It has been demonstrated in the auditory modality that instantaneous phase coherency measures are highly sensitive to endogenous attention (Low and Strauss, 2011). Thus the experimental setup and the analysis scheme may be appropriate to quantify endogenous attention in the somatosensory domain, too.

5 Conclusions

We have investigated the tactile perception of the human being and contributed to the understanding of the causal chain from the contact of the skin with materials to the brain dynamics representing recognition of and reaction to those materials. We successfully combined two experiments from two usually not connected research areas, namely tribology and neuroscience. A tribometer for the measurement of sliding friction between the fingertip and different lines of Braille-pins, and a setup for electroencephalographic (EEG) measurements for studying brain activity were combined. We have performed unique simultaneous measurements in which significant event-related potentials (ERPs) were detected for frictional stimuli applied to the fingertip by raising or lowering different amount of lines of Braille-pins. For the analysis of the signals we have established a well defined data processing pipeline dedicated to the purposes of the work in this thesis. In the light of all these efforts, we can draw the following conclusions.

Standard across-trial averaging of the EEG-data, due to the raising and lowering of Braille-pins, revealed noticeable ERP-components (N50-P100) consistent over all subjects. Considering the corresponding forces, distinct signal characteristics were obtained, which can be mapped to the different stimuli: The evaluation of amplitude and latency of the respective ERPs, however, did not reveal the expected variations as stimulus intensity varied. Even with forces doubled, ERPs could not be distinguished with significance. In contrast, the lowering of pins revealed smaller amplitudes but same latencies. It is concluded that the dynamic range of friction force stimuli provided by a Braille display may be too small or the definition of timing too blurred by viscoelastic delay of the skin to allow distinction between the neural correlates expressed in the N50 and P100 waves. Two components contribute to the friction on Braille-displays. One is the decrease in friction between fingertip and Braille-display while the other the increase in frictional interaction with the raised Braille-pins. We found that the friction coefficient is a unifying concept to describe the two components of the frictional stimulus. Steady-state friction is reached only after viscoelastic conformation of the skin to the raised dots and to the substrate, respectively. The former process has a characteristic time constant of (35 ± 10) ms, the latter of (156 ± 70) ms across the subjects.

Apart from standard across-trial averaging, we have applied for the first time the

wavelet-phase stability (WPS) measure in observing differences between neural correlates of tactile perception. The outcome reveals that the phase measure outperforms the standard averaging, because it shows more consistency in differences over larger time intervals. Thus, we conclude that the phase stability measure provides a more robust objective quantification in extracting differences in cognitive processes upon different tactile stimuli. It is finally concluded that friction is the driving force in tactility and that friction induces phase coherency. The larger the friction the larger the phase coherency, i.e., the raising of pins induces more phase coherency, than the lowering of pins.

This thesis reports on unique simultaneous measurements of friction forces acting on the human fingertip and of correlated EEG signals. The conclusions described above have shown that the newly constructed measurement setup and the implemented data processing pipeline are successful in studying the tactile perception in humans. To reach this, several challenges have been encountered during the work which helped in understanding, since we asked ourselves at the onset of this thesis, why literature does not provided more information on perception and cognitive processes during tactile exploration. Friction is an essential parameter to sensory functions of the hand, where mechanoreceptors are activated by induced vibrations propagating in the finger allowing for tactile judgment and perception. However, the perpetual change in skin deformation during contact gives rise to the complexity and difficulty of implementing well defined frictional stimuli. The result of our work contribute to the understanding of finger-friction signals and to the extraction of single ERP-components which can be attributed to the physical factors involved in tactile perception.

Bibliography

- Abraira, V. E. and Ginty, D. D. (2013). The sensory neurons of touch. *Neuron*, 79(4):618–639.
- Adams, M. J., Briscoe, B. J., and Johnson, S. A. (2007). Friction and lubrication of human skin. *Tribology letters*, 26(3):239–253.
- Agache, P. and Humbert, P. (2004). *Measuring the skin*. Springer Science & Business Media.
- Agache, P., Monneur, C., Leveque, J., and Rigal, J. D. (1980). Mechanical properties and young’s modulus of human skin in vivo. *Archives of dermatological research*, 269(3):221–232.
- Aguiar, L. and Soares, M. (2011). The continuous wavelet transform: A primer. NIPE Working Papers 16/2011, NIPE - Universidade do Minho.
- Avilés, J. M. R., Muñoz, F. M., Kleinböhl, D., Sebastián, M., and Jiménez, S. B. (2010). A new device to present textured stimuli to touch with simultaneous EEG recording. *Behavior research methods*, 42(2):547–555.
- Awate, S. P. and Whitaker, R. T. (2006). Unsupervised, information-theoretic, adaptive image filtering for image restoration. *IEEE Transactions on pattern analysis and machine intelligence*, 28(3):364–376.
- Ayres, A. J. and Robbins, J. (2005). *Sensory integration and the child: Understanding hidden sensory challenges*. Western Psychological Services.
- Barnes, C. J., Childs, T., Henson, B., and Southee, C. (2004). Surface finish and touch - a case study in a new human factors tribology. *Wear*, 257(7):740–750.
- Bergmann, R., Laus, F., Steidl, G., and Weinmann, A. (2014). Second order differences of cyclic data and applications in variational denoising. *SIAM J. Imaging Sci.*
- Bernarding, C., Strauss, D. J., Hannemann, R., Seidler, H., and Corona-Strauss, F. I. (2013). Neural correlates of listening effort related factors: Influence of age and hearing impairment. *Brain Res Bull.*, 91:21–30.
- Bethea, B. T., Okamura, A. M., Kitagawa, M., Fitton, T. P., Cattaneo, S. M., Gott, V. L., Baumgartner, W. A., and Yuh, D. D. (2004). Application of haptic feedback to robotic surgery. *Journal of Laparoendoscopic & Advanced Surgical Techniques*, 14(3):191–195.
- Bhushan, B. (2013). *Introduction to tribology*. John Wiley & Sons.

Bibliography

- Blackwood, D. H. and Muir, W. J. (1990). Cognitive brain potentials and their application. *The British Journal of Psychiatry*.
- Boada, M. D., Houle, T. T., Eisenach, J. C., and Ririe, D. G. (2010). Differing neurophysiologic mechanosensory input from glabrous and hairy skin in juvenile rats. *Journal of neurophysiology*, 104(6):3568–3575.
- Bourane, S., Garces, A., Venteo, S., Pattyn, A., Hubert, T., Fichard, A., Puech, S., Boukhaddaoui, H., Baudet, C., Takahashi, S., et al. (2009). Low-threshold mechanoreceptor subtypes selectively express mafa and are specified by ret signaling. *Neuron*, 64(6):857–870.
- Boyer, G., Laquière, L., Le Bot, A., Laquière, S., and Zahouani, H. (2009). Dynamic indentation on human skin in vivo: ageing effects. *Skin Research and Technology*, 15(1):55–67.
- Bradley, A. P. and Wilson, W. J. (2004). On wavelet analysis of auditory evoked potentials. *Clinical Neurophysiology*, 115(5):1114–1128.
- Bronzino, J. D. (1999). *Biomedical engineering handbook*, volume 2. CRC press.
- Buades, A., Coll, B., and Morel, J.-M. (2005). A review of image denoising algorithms, with a new one. *Multiscale Modeling & Simulation*, 4(2):490–530.
- Burdea, G. (1999). Haptic feedback for virtual reality, keynote address of proceedings of international workshop on virtual prototyping. *Laval: France*.
- Carter, T., Seah, S. A., Long, B., Drinkwater, B., and Subramanian, S. (2013). Ultrahaptics: multi-point mid-air haptic feedback for touch surfaces. In *Proceedings of the 26th annual ACM symposium on User interface software and technology*, pages 505–514. ACM.
- Caruso, G. (1995). S-4-3 mechanical versus electrical stimulation of peripheral nerves. *Electroencephalography and Clinical Neurophysiology/Electromyography and Motor Control*, 97(4):S11.
- Chung, Y. G., Han, S. W., Kim, H. S., Chung, S. C., Park, J. Y., Wallraven, C., and Kim, S. P. (2015). Adaptation of cortical activity to sustained pressure stimulation on the fingertip. *BMC Neuroscience*, 16(1):71.
- Corona-Strauss, F. I., Delb, W., Schick, B., and Strauss, D. J. (2009). Phase stability analysis of chirp evoked auditory brainstem responses by gabor frame operators. *IEEE Transactions on Neural Systems and Rehabilitation Engineering*, 17(6):530–536.
- Crichton, M. L., Chen, X. F., Huang, H., and Kendall, M. A. F. (2013). Elastic modulus and viscoelastic properties of full thickness skin characterised at micro scales. *Biomaterials*, 34(8):2087–2097.

Bibliography

- Cruccu, G., Aminoff, M., Curio, G., Guerit, J., Kakigi, R., Mauguiere, F., Rossini, P., Treede, R.-D., and Garcia-Larrea, L. (2008). Recommendations for the clinical use of somatosensory-evoked potentials. *Clinical neurophysiology*, 119(8):1705–1719.
- Darden, M. and Schwartz, C. (2015). Skin tribology phenomena associated with reading braille print: The influence of cell patterns and skin behavior on coefficient of friction. *Wear*, 332:734–741.
- Daubechies, I. (1992). *Ten Lectures on Wavelets*. SIAM, Philadelphia, PA.
- Derler, S., Gerhardt, L.-C., Lenz, A., Bertaux, E., and Hadad, M. (2009). Friction of human skin against smooth and rough glass as a function of the contact pressure. *Tribology International*, 42(11):1565–1574.
- Derler, S., Schrade, U., and Gerhardt, L.-C. (2007). Tribology of human skin and mechanical skin equivalents in contact with textiles. *Wear*, 263(7):1112–1116.
- Dictionary, O. E. (2008). Haptic. *Retrieved on February*, 10:2008.
- Dinc, O., Ettles, C., Calabrese, S., and Scarton, H. (1991). Some parameters affecting tactile friction. *Journal of tribology*, 113(3):512–517.
- Everett, J. S. and Sommers, M. S. (2013). Skin viscoelasticity: physiologic mechanisms, measurement issues, and application to nursing science. *Biological research for nursing*, 15(3):338–346.
- Fagiani, R., Massi, F., Chatelet, E., Berthier, Y., and Akay, A. (2011). Tactile perception by friction induced vibrations. *Tribology International*, 44(10):1100–1110.
- Farage, M. A., Miller, K. W., Berardesca, E., and Maibach, H. I. (2009). Clinical implications of aging skin: cutaneous disorders in the elderly. *American journal of clinical dermatology*, 10(2):73.
- Fonaryova Key, A., Dove, G., and M.J., M. (2005). Linking brainwaves to the brain: An ERP primer. *Developmental Neuropsychology*, 27:183–215.
- Forster, B. and Eimer, M. (2004). The attentional selection of spatial and non-spatial attributes in touch: ERP evidence for parallel and independent processes. *Biological psychology*, 66(1):1–20.
- Forster, B. and Eimer, M. (2005). Vision and gaze direction modulate tactile processing in somatosensory cortex: evidence from event-related brain potentials. *Experimental brain research*, 165(1):8–18.
- Gaetz, W., Jurkiewicz, M. T., Kessler, S. K., Blaskey, L., Schwartz, E. S., and Roberts, T. P. L. (2017). Neuromagnetic responses to tactile stimulation of the fingers: Evidence for reduced cortical inhibition for children with autism spectrum disorder and children with epilepsy. *NeuroImage: Clinical*, 16:624–633.

Bibliography

- Gallace, A. and Spence, C. (2010). Touch and the body: The role of the somatosensory cortex in tactile awareness. *Psyche: An Interdisciplinary Journal of Research on Consciousness*.
- Geber, C., Magerl, W., Fondel, R., Fechir, M., Rolke, R., Vogt, T., Treede, R.-D., and Birklein, F. (2008). Numbness in clinical and experimental pain—a cross-sectional study exploring the mechanisms of reduced tactile function. *Pain*, 139(1):73–81.
- Gellis, M. and Pool, R. (1977). Two-point discrimination distances in the normal hand and forearm: application to various methods of fingertip reconstruction. *Plastic and reconstructive surgery*, 59(1):57–63.
- Genna, C., Oddo, C. M., Fanciullacci, C., Chisari, C., Jorntell, H., Artoni, F., and Micera, S. (2017). Spatiotemporal dynamics of the cortical responses induced by a prolonged tactile stimulation of the human fingertips. *Brain Topography*, 30(4):473–485.
- Gerhardt, L. C., Strässle, V., Lenz, A., Spencer, N. D., and Derler, S. (2008). Influence of epidermal hydration on the friction of human skin against textiles. *Journal of The Royal Society Interface*, 5(28):1317–1328.
- Glaser, E. (2012). *Principles of neurobiological signal analysis*. Elsevier.
- Goldreich, D. and Kanics, I. M. (2003). Tactile acuity is enhanced in blindness. *Journal of Neuroscience*, 23(8):3439–3445.
- Hashimoto, I. (1987). Somatosensory evoked potentials elicited by air-puff stimuli generated by a new high-speed air control system. *Electroencephalography and clinical neurophysiology*, 67(3):231–237.
- Hashimoto, I., Gatayama, T., Yoshikawa, K., and Sasaki, M. (1992). Somatosensory evoked potential correlates of psychophysical magnitude estimations for air-puff stimulation of the foot in man. *Experimental brain research*, 92(2):318–325.
- Hashimoto, I., Yoshikawa, K., and Sasaki, M. (1988). Somatosensory evoked potential correlates of psychophysical magnitude estimations for tactile air-puff stimulation in man. *Experimental brain research*, 73(3):459–469.
- Hatwell, Y. and Gentaz, E. (2008). Early psychological studies on touch in France. In Grunwald, M., editor, *Human Haptic Perception*, pages 55–66, Basel. Birkhäuser.
- Hatzfeld, C. and Kern, T. (2016). *Engineering Haptic Devices*. Springer.
- Hu, L., Liang, M., Mouraux, A., Wise, R. G., Hu, Y., and Iannetti, G. D. (2011). Taking into account latency, amplitude, and morphology: improved estimation of single-trial erps by wavelet filtering and multiple linear regression. *Journal of Neurophysiology*, 106(6):3216–3229.

Bibliography

- Hu, L., Mouraux, A., Hu, Y., and Iannetti, G. (2010). A novel approach for enhancing the signal-to-noise ratio and detecting automatically event-related potentials (erps) in single trials. *Neuroimage*, 50(1):99–111.
- Johansson, R. S. and Vallbo, Å. B. (1979). Tactile sensibility in the human hand: relative and absolute densities of four types of mechanoreceptive units in glabrous skin. *The Journal of physiology*, 286(1):283–300.
- Johnson, S., Gorman, D., Adams, M., and Briscoe, B. (1993). The friction and lubrication of human stratum corneum. In *Tribology Series*, volume 25, pages 663–672. Elsevier.
- Jones, L. A. and Lederman, S. J. (2006). *Human hand function*. Oxford University Press.
- Jor, J. W., Nash, M. P., Nielsen, P. M., and Hunter, P. J. (2011). Estimating material parameters of a structurally based constitutive relation for skin mechanics. *Biomechanics and modeling in mechanobiology*, 10(5):767–778.
- Kalra, A., Lowe, A., and Al-Jumaily, A. (2016). Mechanical behaviour of skin: A review. *J Material Sci Eng*, 5(254):2169–0022.
- Kandel, E. R., Schwartz, J. H., Jessell, T. M., Siegelbaum, S. A., Hudspeth, A. J., et al. (2000). *Principles of neural science*, volume 4. McGraw-hill New York.
- Kapoor, S., Arora, P., Kapoor, V., Jayachandran, M., and Tiwari, M. (2014). Haptics–touchfeedback technology widening the horizon of medicine. *Journal of clinical and diagnostic research: JCDR*, 8(3):294.
- Kern, T. A. (2009). *Engineering haptic devices: a beginner’s guide for engineers*. Springer Publishing Company, Incorporated.
- Kim, S., Hong, J.-H., Li, K. A., Forlizzi, J., and Dey, A. K. (2012). Route guidance modality for elder driver navigation. In *International Conference on Pervasive Computing*, pages 179–196. Springer.
- Klein, A., Sauer, T., Jedynek, A., and Skrandies, W. (2006). Conventional and wavelet coherence applied to sensory-evoked electrical brain activity. *IEEE transactions on biomedical engineering*, 53(2):266–272.
- Klöcker, A., Arnould, C., Penta, M., and Thonnard, J.-L. (2012). Rasch-built measure of pleasant touch through active fingertip exploration. *Frontiers in neurobotics*, 6.
- Kolarik, A. J., Cirstea, S., and Pardhan, S. (2013). Evidence for enhanced discrimination of virtual auditory distance among blind listeners using level and direct-to-reverberant cues. *Experimental brain research*, 224(4):623–633.
- Kolev, V. and Yordanova, J. (1997). Analysis of phase-locking is informative for studying event-related EEG activity. *Biological Cybernetics*, 76(3):229–235.

Bibliography

- Korondi, P., Szemes, P., and Hashimoto, H. (2005). The industrial information technology handbook.
- LeConte, J. (1885). The evidence of the senses. *The North American Review*, 140(338):85–96.
- Lessard, N., Pare, M., Lepore, F., and Lassonde, M. (1998). Early-blind human subjects localize sound sources better than sighted subjects. *Nature*, 395(6699):278–280.
- Loomis, J. M. and Lederman, S. J. (1986). Tactual perception. *Handbook of perception and human performances*, 2:2.
- Low, Y. F., Corona-Strauss, F. I., Adam, P., and Strauss, D. J. (2007). Extraction of auditory attention correlates in single sweeps of cortical potentials by maximum entropy paradigms and its application. In *Proceedings of the 3rd Int. IEEE EMBS Conference on Neural Engineering*, pages 469–472, Kohala Coast, HI, USA.
- Low, Y. F. and Strauss, D. J. (2011). A performance study of the wavelet-phase stability measure in auditory selective attention. *Brain Res Bull*, 86:110–117.
- Lumpkin, E. A., Marshall, K. L., and Nelson, A. M. (2010). The cell biology of touch. *The Journal of cell biology*, 191(2):237–248.
- Manfredi, L. R., Saal, H. P., Brown, K. J., Zielinski, M. C., Dammann, J. F., Polashock, V. S., and Bensmaia, S. J. (2014). Natural scenes in tactile texture. *Journal of neurophysiology*, 111(9):1792–1802.
- Mao, Y. T. and Pallas, S. L. (2013). Cross-modal plasticity results in increased inhibition in primary auditory cortical areas. *Neural plasticity*, 2013.
- McGlone, F., Vallbo, A. B., Olausson, H., Loken, L., and Wessberg, J. (2007). Discriminative touch and emotional touch. *Canadian Journal of Experimental Psychology/Revue canadienne de psychologie expérimentale*, 61(3):173.
- McGlone, F., Wessberg, J., and Olausson, H. (2014). Discriminative and affective touch: sensing and feeling. *Neuron*, 82(4):737–755.
- Moronkeji, K. and Akhtar, R. (2015). Mechanical properties of aging human skin. In *Mechanical Properties of Aging Soft Tissues*, pages 237–263. Springer.
- Mustaffa, I., Trenado, C., Schwerdtfeger, K., and Strauss, D. (2010). Denoising of single-trial matrix representations using 2d nonlinear diffusion filtering. *Journal of neuroscience methods*, 185(2):284–292.
- Nakazawa, N., Ikeura, R., and Inooka, H. (2000). Characteristics of human fingertips in the shearing direction. *Biological Cybernetics*, 82(3):207–214.
- Nitsch, V. and Färber, B. (2013). A meta-analysis of the effects of haptic interfaces on task performance with teleoperation systems. *IEEE transactions on haptics*, 6(4):387–398.

Bibliography

- Norén, J. (2008). Warning systems design in a glass cockpit environment.
- Norman, J. F. and Bartholomew, A. N. (2011). Blindness enhances tactile acuity and haptic 3-D shape discrimination. *Attention, Perception, & Psychophysics*, 73(7):2323–2331.
- Özgül, N., Schubert, K. J., Bergmann, R., Bennewitz, R., and Strauss, D. J. (2015). Relating tribological stimuli to somatosensory electroencephalographic responses. In *Engineering in Medicine and Biology Society (EMBC), 2015 37th Annual International Conference of the IEEE*, pages 8115–8118. IEEE.
- Olausson, H., Wessberg, J., McGlone, F., and Vallbo, Å. (2010). The neurophysiology of unmyelinated tactile afferents. *Neuroscience & Biobehavioral Reviews*, 34(2):185–191.
- Ouyang, G., Herzmann, G., Zhou, C., and Sommer, W. (2011). Residue iteration decomposition (ride): a new method to separate erp components on the basis of latency variability in single trials. *Psychophysiology*, 48(12):1631–1647.
- Özgül, N., Bennewitz, R., and Strauss, D. J. (2018a). Friction in passive tactile perception induces phase coherency in late somatosensory single trial sequences. *IEEE Transactions on Neural Systems and Rehabilitation Engineering submitted*.
- Özgül, N., Strauss, D. J., and Bennewitz, R. (2018b). Tribology of a braille display and EEG correlates. *Tribology Letters*, 66(1):16.
- Pailler-Mattei, C., Bec, S., and Zahouani, H. (2008). In vivo measurements of the elastic mechanical properties of human skin by indentation tests. *Medical Engineering & Physics*, 30(5):599–606.
- Parikh, N. I. and Boyd, S. (2014). Proximal algorithms. *Foundations and Trends® in Optimization*, 1(3):127–239.
- Pawlaczyk, M., Lelonkiewicz, M., and Wieczorowski, M. (2013). Age-dependent biomechanical properties of the skin. *Advances in Dermatology and Allergology/Postępy Dermatologii i Alergologii*, 30(5):302.
- Persson, B. N. J., Kovalev, A., and Gorb, S. N. (2013). Contact mechanics and friction on dry and wet human skin. *Tribology Letters*, 50(1):17–30.
- Pfurtscheller, G., Krausz, G., and Neuper, C. (2001). Mechanical stimulation of the fingertip can induce bursts of β oscillations in sensorimotor areas. *Journal of clinical neurophysiology*, 18(6):559–564.
- Picton, T. W. (2010). *Human auditory evoked potentials*. Plural Publishing.
- Pleger, B. and Villringer, A. (2013). The human somatosensory system: from perception to decision making. *Progress in neurobiology*, 103:76–97.

Bibliography

- Prevost, A., Scheibert, J., and Debrégeas, G. (2009). Effect of fingerprints orientation on skin vibrations during tactile exploration of textured surfaces. *Communicative & integrative biology*, 2(5):422–424.
- Purves, D., Cabeza, R., Huettel, S. A., LaBar, K. S., Platt, M. L., Woldorff, M. G., and Brannon, E. M. (2008). *Cognitive Neuroscience*. Sunderland: Sinauer Associates, Inc.
- Retz, W., González-Trejo, E., Römer, K. D., Philipp-Wiegmann, F., Reinert, P., Low, Y. F., Bouregghda, S., Rösler, M., and Strauss, D. J. (2012). Assessment of post-excitatory long-interval cortical inhibition in adult attention-deficit/hyperactivity disorder. *European archives of psychiatry and clinical neuroscience*, 262(6):507–517.
- Robles-De-La-Torre, G. (2006). The importance of the sense of touch in virtual and real environments. *Ieee Multimedia*, 13(3):24–30.
- Roudaut, Y., Lonigro, A., Coste, B., Hao, J., Delmas, P., and Crest, M. (2012). Touch sense: functional organization and molecular determinants of mechanosensitive receptors. *Channels*, 6(4):234–245.
- Sadava, D., Heller, H. C., Orians, G. H., Purves, W. K., and Hillis, D. M. (2008). *Life, the science of biology*, volume 8th ed. Sinauer Associates; Sunderland, MA.
- Sagardia, M., Hulin, T., Hertkorn, K., Kremer, P., and Schätzle, S. (2016). A platform for bimanual virtual assembly training with haptic feedback in large multi-object environments. In *Proceedings of the 22nd ACM Conference on Virtual Reality Software and Technology*, pages 153–162. ACM.
- Savescu, A. V., Latash, M. L., and Zatsiorsky, V. M. (2008). A technique to determine friction at the fingertips. *Journal of Applied Biomechanics*, 24(1):43–50.
- Scheibert, J., Leurent, S., Prevost, A., and Debrégeas, G. (2009). The role of fingerprints in the coding of tactile information probed with a biomimetic sensor. *Science*, 323(5920):1503–1506.
- Scherer, M. J. (2002). The change in emphasis from people to person: introduction to the special issue on assistive technology. *Disability and rehabilitation*, 24(1-3):1–4.
- Scherer, R., Müller-Putz, G. R., and Pfurtscheller, G. (2009). Flexibility and practicality: Graz brain–computer interface approach. *International review of neurobiology*, 86:119–131.
- Schubert, J. K. (2016). A comparative study of phase-denoising techniques for evoked and event-related potentials. Technical report, Systems Neuroscience & Neurotechnology Unit (SNN-Unit), Homburg/Saar, Germany, Report No. 2016/1.

Bibliography

- Shaout, A., Colella, D., and Awad, S. (2011). Advanced driver assistance systems—past, present and future. In *Computer Engineering Conference (ICENCO), 2011 Seventh International*, pages 72–82. IEEE.
- Shepherd, G. M. (2009). 16 new perspectives on olfactory processing and human smell. *The neurobiology of olfaction*, page 395.
- Shevchenko, R. V., James, S. L., and James, S. E. (2009). A review of tissue-engineered skin bioconstructs available for skin reconstruction. *Journal of the Royal Society Interface*, page rsif20090403.
- Siewe, Y. J. (2004). *Understanding the Effects of Aging on the Sensory System*. Division of Agricultural Sciences and Natural Resources, Oklahoma State University.
- Sivamani, R. K., Goodman, J., Gitis, N. V., and Maibach, H. I. (2003). Coefficient of friction: tribological studies in man—an overview. *Skin Research and Technology*, 9(3):227–234.
- Skedung, L., Arvidsson, M., Chung, J. Y., Stafford, C. M., Berglund, B., and Rutland, M. W. (2013). Feeling small: Exploring the tactile perception limits. *Scientific reports*, 3.
- Soto-Faraco, S. and Azañón, E. (2013). Electrophysiological correlates of tactile remapping. *Neuropsychologia*, 51(8):1584–1594.
- Spence, C. (2015). Leading the consumer by the nose: on the commercialization of olfactory design for the food and beverage sector. *Flavour*, 4(1):31.
- Spies, R., Hamberger, W., Blattner, A., Bubbs, H., and Bengler, K. (2010). Adaptive haptic touchpad for infotainment interaction in cars—how many information is the driver able to feel. In *AHFE International—Applied Human Factors and Ergonomics Conference*.
- Spies, R., Peters, A., Toussaint, C., and Bubbs, H. (2009). Touchpad mit adaptiv haptisch veränderlicher oberfläche zur fahrzeuginfotainmentbedienung. In Brau, H., Diefenbach, S., Hassenzahl, M., Kohler, K., Koller, F., Peissner, M., Petrovic, K., Thielsch, M., Ullrich, D., and Zimmermann, D., editors, *Usability Professionals 2009*, pages 74–78. Fraunhofer Verlag, Stuttgart.
- Strauss, D. J., Delb, W., D’Amelio, R., and Falkai, P. (2005). Neural synchronization stability in the tinnitus decompensation. In *Proceedings of the 2st Int. IEEE EMBS Conference on Neural Engineering*, pages 186–189, Arlington, VA, USA.
- Strauss, D. J., Delb, W., D’Amelio, R., Low, Y. F., and Falkai, P. (2008). Objective quantification of the tinnitus decompensation by measures of auditory evoked single sweeps. *IEEE Trans Neural Syst Rehabil Eng.*, pages 74–81.
- Strauss, D. J., Delb, W., and Plinkert, P. K. (2004). Analysis and detection of binaural interaction in auditory evoked brainstem responses by time-scale representations. *Computers in biology and medicine*, 34(6):461–477.

Bibliography

- Strauss, D. J., Teuber, T., Steidl, G., and Corona-Strauss, F. I. (2013). Exploiting the self-similarity in erp images by nonlocal means for single-trial denoising. *IEEE Transactions on Neural Systems and Rehabilitation Engineering*, 21(4):576–583.
- Stribeck, R. (1902). Die wesentlichen eigenschaften der gleit-und rollenlager. *Zeitschrift des Vereines Deutscher Ingenieure*, 46:1341–1348.
- Striem-Amit, E., Bubic, A., and Amedi, A. (2012). Neurophysiological mechanisms underlying plastic changes and rehabilitation following sensory loss in blindness and deafness.
- Subramanian, S., Seah, S. A., Shinoda, H., Hoggan, E., and Corenthy, L. (2016). Mid-air haptics and displays: Systems for un-instrumented mid-air interactions. In *Proceedings of the 2016 CHI Conference Extended Abstracts on Human Factors in Computing Systems*, pages 3446–3452. ACM.
- Sur, S. and Sinha, V. K. (2009). Event-related potential: An overview. *Industrial psychiatry journal*, 18(1):70.
- Tholey, G., Desai, J. P., and Castellanos, A. E. (2005). Force feedback plays a significant role in minimally invasive surgery: results and analysis. *Annals of surgery*, 241(1):102–109.
- Tzanakis, I., Hadfield, M., Thomas, B., Noya, S., Henshaw, I., and Austen, S. (2012). Future perspectives on sustainable tribology. *Renewable and Sustainable Energy Reviews*, 16(6):4126–4140.
- Urribarri, A. C. R., van der Heide, E., Zeng, X., and de Rooij, M. B. (2016). Modelling the static contact between a fingertip and a rigid wavy surface. *Tribology international*, 102:114–124.
- Van Der Heide, E., Zeng, X., and Masen, M. A. (2013). Skin tribology: Science friction? *Friction*, 1(2):130–142.
- van Kuilenburg, J., Masen, M. A., and van der Heide, E. (2013). The role of the skin microrelief in the contact behaviour of human skin: Contact between the human finger and regular surface textures. *Tribology international*, 65:81–90.
- van Kuilenburg, J., Masen, M. A., and van der Heide, E. (2015). A review of fingerpad contact mechanics and friction and how this affects tactile perception. *Proceedings of the Institution of Mechanical Engineers, Part J: Journal of Engineering Tribology*, 229(3):243–258.
- Wagner, C., Stylopoulos, N., and Howe, R. (2002). Force feedback in surgery: Analysis of blunt dissection. In *Proceedings of the 10th symposium on haptic interfaces for virtual environment and teleoperator systems*.
- Wandersman, E., Candelier, R., Debrégeas, G., and Prevost, A. (2011). Texture-induced modulations of friction force: the fingerprint effect. *Physical review letters*, 107(16):164301.

Bibliography

- Weinstein, G. D. and Boucek, R. J. (1960). Collagen and elastin of human dermis. from the divisions of dermatology and cardiology of the department of medicine, university of miami school of medicine and howard hughes medical institute, miami, florida. this investigation was supported in part by grants a-2586 and 2g-224, from the nih, us public health service. *Journal of Investigative Dermatology*, 35(4):227–229.
- Wiertlewski, M. and Hayward, V. (2012). Mechanical behavior of the fingertip in the range of frequencies and displacements relevant to touch. *Journal of Biomechanics*, 45(11):1869–1874.
- Wiertlewski, M., Hudin, C., and Hayward, V. (2011). On the 1/f noise and non-integer harmonic decay of the interaction of a finger sliding on flat and sinusoidal surfaces. In *World Haptics Conference (WHC), 2011 IEEE*, pages 25–30. IEEE.
- Wolfe, C. T. (2009). Early modern epistemologies of the senses: From the nobility of sight to the materialism of touch. *University of Sydney*.
- Wolfe, J., Skinner, P., and Burns, J. (1978). Relation between sound intensity and the latency and amplitude of the brainstem auditory evoked response. *J Speech Hear Res*, 21(2):401–407.
- Woodman, G. F. (2010). A brief introduction to the use of event-related potentials in studies of perception and attention. *Attention, Perception, & Psychophysics*, 72(8):2031–2046.
- Yuan, B. and Folmer, E. (2008). Blind hero: enabling guitar hero for the visually impaired. In *Proceedings of the 10th international ACM SIGACCESS conference on Computers and accessibility*, pages 169–176. ACM.

Own Publications

Journal Papers

N. Özgün, D. J. Strauss , and R. Bennewitz. Tribology of a Braille display and EEG correlates. *Tribology Letters*, 66(1):16, 2018.

N. Özgün, R. Bennewitz, and D. J. Strauss. Friction in passive tactile perception induces phase coherency in late somatosensory single trial sequences, *IEEE Transactions on Neural Systems and Rehabilitation Engineering*, 2018, submitted.

Papers in Proceedings and other Contributions

N. Özgün, K. Schubert, R. Bergmann, R. Bennewitz, and D. J. Strauss. Relating tribological stimuli to somatosensory electroencephalographic responses, *In Proceedings of the Annual International Conference of the IEEE Engineering in Medicine and Biology Society, EMBS*, pp. 8115–8118, 2015.

N. Özgün, R. Bennewitz, and D. J. Strauss. Relating tribological stimuli to single-trial somatosensory electroencephalographic responses: A pilot study, *7th International IEEE/EMBS Conference on Neural Engineering (NER)*, Late breaking paper, 2015.

Acknowledgements

First of all, I would like to thank my doctoral advisor Prof. Dr. Dr. Daniel J. Strauss not only for offering me the opportunity to pursue my doctoral studies in his research group but also for his excellent support, numerous discussions, and consistent encouragement I received throughout the research work.

This work would not have been possible without the cooperation with the Leibniz Institute for New Materials (INM). In particular, I owe my deep gratitude to Prof. Dr. Roland Bennewitz, the head of the Nanotribology group, for his unconditional support and the fruitful discussions whenever i was approaching him. I could not have imagined having a better cooperation partner.

I would also like to thank Prof. Dr. Eduard Arzt, the scientific director and CEO of the INM, for the continuous support.

I would like to give my deep thanks to all the members of the *Systems Neuroscience and Neurotechnology Unit (SNN)* for the pleasant and constructive working atmosphere. In particular, I would like to thank Dr. Corinna Bernarding and Dr. Lars Haab from the SNN-Unit for not only proofreading my thesis but also for very helpful suggestions and discussions with respect to analysis. My research would have been impossible without the aid and support of other wonderful colleagues. I am also profoundly grateful to J. Kristof Schubert, Ernesto González Trejo, and Dr. Farah I. Corona-Strauss for her great assistance and help in introducing me to the EEG-measurement technique.

I also hereby acknowledge the member of the *Nanotribology-group* at the INM for their open and friendly nature when getting in touch with them. Thanks to Dr. Felix Wällisch, Dr. Arnaud Caron, Dr. Johanna Blass and Kai T. Rittgen.

Many thanks to all participants for supporting of this research, without their help this study would not have been possible. In this regard I would like to thank Andre Richter who helped to conduct experiments and acquire the data.

I owe my deepest gratitude towards my parents, Guli and Hasan, who have sacrificed a lot to ensure a better and easier future for their children than they have had. It is impossible to put this in words, but I would not be here without your support, guidance and love. Many thanks for my sister Elisa and brothers Daham, Hauran

and Deniz for their love and support. They were always there through the ups and downs of my journey.

My heart felt regard goes to my parents in law for their role in encouraging me to believe in myself and to not loose the objective in rewarding myself for the hard work. I also would like to thank my sisters and brothers-in-law for their love and moral support. I am very happy to be part of this great family.

I am grateful to my aunt Xanim and uncle Fikret who morally supported me and regarded me as their own son. They were not blessed with children, but *your* son did it.

Above all I would like to thank my greatest treasures, my daughters Aliyah and Mira, and my beloved wife Resmiye, to whom I dedicate this work. Thank you for your perseverance, patience, support and understanding during my pursuit of Ph.D degree. Without you, I would not have been able to complete much of what I have done and to become who I am. Thank you for always being there whenever I needed you. Be sure, I will stay at your side. Together we will master everything.